C.P. No. 451
(20,572)
A.R.C. Technical Report

C.P. No. 451
(20,572)
A.R.C. Technical Report

MINISTRY OF SUPPLY

AERONAUTICAL RESEARCH COUNCIL

CURRENT PAPERS

Effects of Interaction between Boundary Layers and External Stream and of Incidence on Boundary- Layer Drag at Supersonic Speeds

by

A. D. Young,
Queen Mary College, London

and

S. Kirkby,
College of Aeronautics, Cranfield

LONDON: HER MAJESTY'S STATIONERY OFFICE
1959

NINE SHILLINGS NET

C O R R I G E N D A

p.2 and Table 2 (p.27).	For ΔC_{Dp_2} read ΔC_{Dp_1}.
p.6. 9 lines from bottom.	Delete 'quadratic' and after 'x' on the next line add 'of the form $ax - bx^3$'.
p.8. 8 lines from bottom.	For C_{Dp} read C_{DB}.
p.15. 1st line.	Delete minus sign in front of last term.
p.16. 2 lines below equation A.17.	For Δn on left hand side read Δu.
p.18. Equation A.24.	Delete second plus sign and replace by multiplication sign.
p.22. Last line.	For 0.005 read 0.001.
Fig. 7 and 8.	For C_{D_β} read C_{D_B}.
Fig.22.	Ordinate should read $\rho_1 u_1^2/\rho_0 u_0^2$.
Fig.31.	Top ordinate should be 1.4.

C.P. No.451

Effects of Interaction between Boundary Layers and External Stream and of Incidence on Boundary-Layer Drag at Supersonic Speeds

- By -
A. D. Young,
Queen Mary College, London
and
S. Hirsby,
College of Aeronautics, Cranfield

21st November, 1958

SUMMARY

This paper completes a series dealing with the determination of the boundary-layer drag of biconvex wing sections at supersonic speeds with zero heat transfer for a range of thickness-chord ratio (up to 0·1), mainstream Mach number (up to 5·0), Reynolds number ($10^3 \sim 10^8$) and transition position. Previous results have been extended and improved by allowing for the interaction of boundary layer and external stream, insofar as the resulting changes in the external pressure distribution modify the skin friction distribution (Fig. 1). Calculations have also been made of the effect of incidence (up to 10°) on the boundary-layer drag of a flat plate. The discussion includes an analysis in physical terms of the effects on skin friction and boundary-layer pressure drag distributions of the main parameters investigated and in particular of the changes that accompany increase in Mach number. These changes are shown to be readily related to the changes in local free stream Mach number distribution and the associated changes in local free stream density × velocity^2 ($\rho_1 u_1^2$). Tables 1-4 present the detailed results and Figs. 9 and 27 summarise the effects of thickness-chord ratio and incidence on boundary-layer drag.

Notation

x	distance measured along the surface
$\bar{x}$	distance measured parallel to the chord
y	distance measured normal to the surface
y_s	ordinate of wing section
ρ	density
μ	coefficient of viscosity
T	temperature

ω/

ω exponent in the viscosity-temperature relation (i.e., $\mu \propto T^{\omega}$)

u velocity component in x direction

k coefficient of heat conduction

c_p coefficient of specific heat at constant pressure

c_v coefficient of specific heat at constant volume

γ c_p/c_v

σ $\mu c_p/k$ (Prandtl number)

M Mach number

R Reynolds number

θ momentum thickness $= \int_0^{\delta} \frac{\rho u}{\rho_1 u_1}\left(1 - \frac{u}{u_1}\right) dy$

δ^* displacement thickness $= \int_0^{\delta} \left(1 - \frac{\rho u}{\rho_1 u_1}\right) dy$

δ boundary-layer thickness

h δ^*/θ

c_f skin friction coefficient, $2\tau_w/\rho_0 u_0^2$

c_{fa} $c_f \cdot \rho_0 u_0^2/\rho_a u_a^2 = 2\tau_w/\rho_a u_a^2$

C_F overall skin friction coefficient, $\frac{1}{c}\int_0^c c_f \cdot dx$

ΔC_p change in pressure coefficient due to the boundary layer

t wing thickness

c wing chord

α wing incidence

τ frictional stress

Δp change in pressure from that in inviscid flow due to presence of the boundary layer

ΔC_{Dp_ℓ} boundary-layer pressure drag coefficient, excluding contribution due to discontinuity in δ^* at the transition point

ΔC_{DpT} contribution to boundary-layer pressure drag coefficient arising from discontinuity in δ^* at the transition point

ΔC_{Dp} boundary-layer pressure drag coefficient $= \Delta C_{Dp_\ell} + \Delta C_{DpT}$

C_{F_1}/

C_{F_1} first stage value of C_F calculated on basis of inviscid flow pressure distribution

C_{F_2} second stage value of C_F calculated on basis of inviscid flow pressure distribution corrected for presence of boundary layer

ΔC_F $C_{F_2} - C_{F_1}$

C_{D_B} boundary-layer drag coefficient = $C_{F_2} + \Delta C_{D_p}$.

Unless otherwise specified suffix 1 refers to quantities measured at the outer edge of the boundary layer (local free stream), suffix w to quantities at the surface, suffix a to quantities at the leading edge just aft of the leading-edge shock (if any), suffix 0 to quantities in the undisturbed stream, suffix T to the transition point, suffix ℓ to the laminar boundary layer, suffix t to the turbulent boundary layer.

It should be noted that in the Appendix suffix 0 generally denotes quantities obtained in the first stage calculation (i.e., zero pressure gradient). For consistency with the main text, however, the overall skin friction coefficients for first and second stages remain, as shown above, C_{F_1} and C_{F_2}.

Other symbols are defined in the text.

1. Introduction

This paper completes a series arising out of a programme of work, the object of which has been the determination of the boundary-layer drag of biconvex wings at supersonic speeds with zero heat transfer. Previous papers relevant to this topic are listed as Refs. 1-5.

The term 'boundary-layer drag' is here used instead of 'profile drag' as in the previous papers, in conformity with the definitions of drag components listed in Ref. 6. It denotes the drag arising directly from the viscosity of the medium and is the sum of the skin friction drag and the boundary-layer pressure drag. The latter (previously referred to as 'form drag') is here defined as the change in the wave drag, relative to that in inviscid flow, due to the effective modification of the wing or body shape caused by the boundary layer. The total drag is then the sum of the inviscid flow wave drag and the boundary-layer drag.

In the previous papers the method of calculation adopted was described[1,2] and the results were presented on its application to biconvex wing sections at zero incidence and with zero heat transfer for the following values of the main variables[4,5]:-

Thickness chord ratio (t/c)	0, 0·05, 0·1
Mach number (M_0)	1·5, 2·5, 5·0
Reynolds number (R_0)	10^6, 10^7, 10^8
Transition positions (x_T)	0, 0·1c, 0·3c, 0·5c, 1·0c.

The value of the Prandtl number (σ) was assumed to be 0·72, and it was also assumed that the relation between viscosity (μ) and absolute temperature (T) was of the form $\mu = \text{const } T^\omega$, where the exponent ω was taken as 0·5. These values of σ and ω were chosen as representative

of/

of air for a wide range of conditions of practical interest, but it may be noted that the method of calculation adopted would permit of other values of σ and ω being chosen if required.

The results so far presented have been determined by what might be termed first stage calculations, i.e., the skin friction drag calculated was that appropriate to the inviscid flow pressure distribution in each case. The interaction of boundary layer and external flow becomes more profound, however, with increase of Mach number, and a few check calculations in the more extreme cases of high Mach number and low Reynolds number indicated that the effect of this interaction on skin friction drag could not always be left out of account. Accordingly, a selected number of key second stage calculations have been made in which in each case the skin friction drag was recalculated using the pressure distribution determined by adding to the initial inviscid flow distribution the pressure increments associated with the boundary-layer displacement thickness distribution given by the first stage calculation. In addition an approximate theoretical treatment of this second stage correction to the skin friction drag for the flat plate has been developed and this is described in the Appendix. With the formulae resulting from the latter as a guide it has been readily possible to expand the results of the second stage calculations to cover all the cases considered. The final results in the form of tables and figures, together with a discussion of some of the more interesting trends demonstrated, are presented in Sections 3.1 and 3.2.

Since incidence was likely to prove a variable of some significance, a comprehensive series of first stage calculations as well as a few second stage calculations have also been made for the flat plate at incidences of 5° and 10°, covering the ranges of Mach number, Reynolds number and transition position given above. These results are presented and discussed in Sections 4.1 and 4.2.

2. Summary of Main Formulae Involved

The main details of the analysis underlying the method of calculation have been described in Ref. 2 and further points of detail have been elaborated in Refs. 4 and 5. For the sake of ease of reference, however, the main formulae are reproduced here.

2.1 Laminar layer

The momentum thickness of the boundary layer, θ, when the layer is laminar is given at any station x_1 by

$$[\rho_1^2 \theta^2]_{x_1} = \frac{4\mu_a}{f\, u_1^g} \int_0^{x_1} \rho_1 u_1^{g-1}\, dx, \qquad \ldots(1)$$

where x is the distance measured along the surface from the leading edge, ρ_1 and u_1 are local values of the density and velocity, respectively, just outside the boundary layer, f and g are functions of a reference Mach number M_a taken at the leading edge just aft of the leading-edge shock (if any), f and g being given by

$$\left.\begin{aligned} f &= 9{\cdot}072\,[1 + 0{\cdot}365\,(\gamma-1)\,\sigma^{\frac{1}{2}} M_a^2]^{1-\omega}, \\ g &= 9{\cdot}10 + 1{\cdot}43\,M_a^2 - \frac{f}{3}\left[1 + \frac{(\gamma-1)}{2}\,\sigma^{\frac{1}{2}} M_a^2\right]^{\omega}, \end{aligned}\right\} \qquad \ldots(2)$$

μ_a is the viscosity corresponding to the leading-edge reference conditions, and γ is the ratio of the specific heats which is taken as 1·40 for air.

The/

The skin friction coefficient, $c_{fa} = 2\tau_w/\rho_a u_a^2$, where τ_w is the local intensity of skin friction, is given by

$$c_{fa} = \frac{(\Lambda+12)}{3R_a \cdot f} \cdot \frac{u_1}{u_a} \cdot \frac{c}{\theta}, \qquad \ldots(3)$$

where

$$\Lambda = R_a \left(\frac{du_1}{dx} \cdot \frac{\theta^2 f^2}{u_a \cdot c} \cdot \frac{\rho_1}{\rho_a} \cdot \frac{\mu_w}{\mu_a} \right), \qquad \ldots(4)$$

c is the wing chord, used as a reference length, $R_a = \frac{u_a \cdot c\rho_a}{\mu_a}$, i.e., the Reynolds number based on conditions at the leading edge and aft of the leading-edge shock (if any), and μ_w = value of μ at the surface and is given by

$$\frac{\mu_w}{\mu_a} = \left\{ 1 + \frac{(\gamma-1)}{2} M_a^2 \left[1 + \frac{u_1^2}{u_a^2} (\sigma^{\frac{1}{2}}-1) \right] \right\}^{\omega}. \qquad \ldots(5)$$

From the standard formulae relating quantities on either side of a plane shock wave, quantities are finally referred to reference conditions in the undisturbed stream (suffix 0) ahead of the wing, e.g., the skin friction coefficient is

$$c_f = 2\tau_w/\rho_0 u_0^2 .$$

The displacement thickness, δ^*, of the boundary layer is obtained from θ by means of the formula

$$\frac{\delta^*}{\theta} = H_a = 2{\cdot}59\ (1 + 0{\cdot}277\ M_a^2). \qquad \ldots(6)$$

2.2 Turbulent layer

As in incompressible flow, θ is assumed to be continuous at the transition point. The momentum thickness at any station x_1 when the layer is turbulent is given by

$$[\theta/c]_{x_1}^{n/(n-1)} \left[\exp \cdot \int_T^{x_1} F(x) \cdot \frac{n}{n-1} \cdot \frac{dx}{c} \right] - [\theta/c]_T^{n/(n-1)}$$

$$= \frac{n}{n-1} \cdot C\, R_a^{-1/(n-1)} \int_T^{x_1} G(x) \cdot \exp \cdot \left[\int_T^{x} F(x) \cdot \frac{n}{n-1} \cdot \frac{dx}{c} \right] \cdot \frac{dx}{c}, \qquad \ldots(7)$$

where suffix T refers to the transition point, and

$$F(x) = \frac{du_1}{dx} \cdot \frac{c}{u_a} \{(H_1+2) - M_1^2\}, \qquad \ldots(8)$$

$$G(x) = \left(\frac{u_1}{u_a} \cdot \frac{\nu_a}{\nu_1} \right)^{-1/(n-1)} \left\{ t_1 \left[\frac{\log R_\theta}{\log R_\theta + (2+\omega) \log t_1} \right]^{2{\cdot}5\omega} \right\}^{n/(n-1)} \qquad \ldots(9)$$

$$t_1 = \left[1 + \frac{(\gamma-1)}{2} M_1^2\, \sigma^{\frac{1}{2}} \right]^{-1} .$$

Appropriate/

Appropriate to the range of Reynolds number considered

$$\left.\begin{aligned} n &= 6 \\ C &= 0{\cdot}00878 \end{aligned}\right\}. \qquad \ldots(10)$$

The relation between H_1 and M_1 is taken to be the same as for the boundary layer on a flat plate at zero incidence with a one-ninth power velocity profile (see, for example, Fig. 3 of Ref. 2).

The skin friction distribution is determined from the distribution of θ by the formula

$$c_f = \frac{2\tau_w}{\rho_0 u_0^2} = 2C \left(\frac{u_1\theta}{\nu_1}\right)^{\frac{1}{(n-1)}} \left(\frac{\rho_1 u_1^2}{\rho_0 u_0^2}\right) \left\{ t_1 \left[\frac{\log R_0}{\log R_0 + (2+\alpha)t_1} \right]^{2\cdot58} \right\}^{\frac{n}{n-1}}. \qquad \ldots(11)$$

Again, the displacement thickness is related to the momentum thickness by

$$\delta^* = \theta \cdot H_1 \qquad \ldots(12)$$

2.3 Boundary-layer pressure drag

On the assumption that the effect of the boundary layer on the external pressure distribution is small, it can be shown (see Ref. 2) that it is equivalent to a change of surface slope $d\delta^*/dx$, and if the flow outside the boundary layer is regarded as a simple wave flow this yields to the first order a change in local pressure

$$\Delta p = \frac{\rho_1 u_1^2}{(M_1^2-1)^{\frac{1}{2}}} \cdot \frac{d\delta^*}{dx}. \qquad \ldots(13)$$

Equation (13) can be integrated to give the boundary-layer pressure drag subject to certain limitations. We may note that for M_1 very close to unity this equation becomes invalid and the complete simple wave relation between p and M_1 must then be used to take account of the change of M_1 with Δp. For the range of M_1 covered by these calculations, however, the equation is generally applicable. Further in the region of the leading edge, as x tends to zero the value of $d\delta^*/dx$ given by equation (13) tends to infinity, and hence equation (13) ceases to apply there as in fact do the basic assumptions of classical boundary layer. The procedure that has been adopted here is to assume equation (13) is applicable for values of x/c beyond $0{\cdot}04$ (the reasons for this are given in Refs. 4 and 5). For $x < 0{\cdot}04c$, Δp was assumed to vary linearly with x with the same slope as at $0{\cdot}04c$. This assumption was thought to be somewhat more acceptable than that made earlier (see Refs. 4 and 5) when Δp was assumed to be constant for $0 < x \leq 0{\cdot}04c$. It may be noted that a linear variation of Δp with x is consistent with a quadratic variation of boundary-layer thickness with x. There are at present theories of the laminar boundary layer in the region of the leading edge of a flat plate at high Mach numbers which attempt to take some account of the effect of the shock there (e.g., see Refs. 7 and 8) and these yield power law variations of boundary-layer thickness with x of a higher exponent than the classical $x^{\frac{1}{2}}$ law.* None of these theories can be regarded as completely acceptable but it would seem in the light of them that the above assumption is not grossly at variance with theoretically predicted trends

nor,/

*Kuo[8] for example quotes a rate of growth of boundary-layer thickness proportional to $x^{3/2}$.

nor, in any case, is it likely to lead to significant errors as far as the resulting drag estimates are concerned.

A contribution to the pressure drag coefficient is also provided by the discontinuity in δ^* at the transition point, due to the change in H there, and this is given for each surface by

$$\Delta C_{D_{pT}} = \pm \frac{2\rho_1 u_1^2}{\rho_0 u_0^2} \frac{dy_s}{dx} \frac{(\delta^*_{tT} - \delta^*_{\ell T})}{c} \cdot \frac{1}{\sqrt{M_1^2 - 1}} \qquad \ldots(14)$$

where y_s is the ordinate of the surface measured relative to the undisturbed stream direction and the plus sign refers to the upper surface whilst the minus sign refers to the lower surface, δ^*_{tT} and $\delta^*_{\ell T}$ are the values of δ^* at the transition point for the turbulent and laminar boundary layers, respectively.

3. Results and Discussion for Biconvex Wings at Zero Incidence

3.1 Results

As already remarked the second stage calculations were made in only a selected number of cases, so as to keep the time and effort involved to a minimum. These cases were as follows:-

t/c	M_0	R_0	Mean Transition Positions
0	1·5, 2·5	10^6, 10^7	0, 1c
0	5	10^5	0, 0·1c, 0·3c, 0·5c, 1c
0	5	10^7	0
0	5	10^8	0, 1c
0·05	5	10^6	0, 0·1c, 0·3c, 0·5c, 1c
0·10	1·5, 2·5	10^6	0
	5	10^6	0, 0·1c, 0·3c, 0·5c, 1c

An analysis of the difference in each case between the overall skin friction drag values given by the first and second stage calculations as a ratio of the value given by the first stage calculation ($\Delta C_F/C_{F_1}$) showed that the form of its variation with Mach number was sensibly independent of Reynolds number, transition position and thickness-chord ratio. The approximate analysis for the case of the flat plate at zero incidence described in the Appendix supports this conclusion as far as the effects of Reynolds number and transition position are concerned. The effect of Reynolds number on $\Delta C_F/C_{F_1}$ is clearly a function of transition position, however, but transpired to be independent in form of thickness-chord ratio, and again consistency was found between the results of the numerical calculations and the trends predicted by the approximate theory given in the Appendix. The remaining effect of thickness-chord ratio is also, not surprisingly, a function of transition position. As a result of the analysis, therefore, it was finally found possible to express the ratio $\Delta C_F/C_{F_1}$ in the form

$\Delta C_F/C_{F_1}$ /

$$\Delta C_F/C_{F_1} = k(M_o) \cdot \ell\left(\frac{\bar{x}_T}{c}, \frac{t}{c}\right) \cdot m\left(\frac{x_T}{c}, R_o\right) \qquad \ldots(15)$$

where $\bar{x}_T$ denotes the transition position aft of the nose measured parallel to the chord line. The functions k, ℓ and m are shown in Fig. 1.

From equation (15) and Fig. 1 the correction to C_{F_1} to give the second stage overall skin friction value was determined for all the cases considered and Table 1* lists the values of C_{F_1}, ΔC_F and C_{F_2} whilst the values of C_{F_2} for the flat plate and the two biconvex wings are shown plotted in Figs. 2, 3 and 4.

The boundary-layer pressure drag coefficients, ΔC_{Dp}, for the two biconvex wings are similarly given in Table 2 and Figs. 5 and 6, whilst the final boundary-layer drag coefficients ($C_{DB} = C_{F_2} + \Delta C_{Dp}$) are given in Table 3 and Figs. 7 and 8. A crossplot of some of the main results illustrating the variation of C_{F_2} and C_{DB} with thickness-chord ratio for $R_o = 10^6$ and 10^8 is given in Fig. 9.

Because of their intrinsic interest and their value in illustrating some of the points in the discussion that follows specimen chordwise distributions are also presented of pressure increment (Figs. 10, 11 and 12), skin friction (Figs. 13, 14 and 15), skin friction increment (Figs. 16, 17 and 18), Mach number (Figs. 19, 20), kinetic pressure ratio, $\rho_1 u_1^2/\rho_o u_o^2$ (Figs. 21, 22), and momentum thickness (Fig. 23).

3.2 Discussion

It has already been noted in Refs. 4 and 5 when discussing the first stage results that there is a marked decrease in the overall effect of rearward movement of transition on skin friction and total boundary-layer drag with increase of Mach number, increase of wing thickness and decrease of Reynolds number. This is still very evident in the second stage results (see Figs. 2, 3, 4, 7 and 8), although the effect of the correction for displacement thickness has been to increase slightly the effect of transition shift, as is otherwise clear from the shape of the curves $\ell(\bar{x}_T/c, t/c)$ of Fig. 1. Thus, in the case of the flat plate at $R_o = 10^6$ the boundary-layer drag is reduced by about 65 percent at $M_o = 1{\cdot}5$ with a shift of transition from the leading edge to the trailing edge, the corresponding reduction at $M_o = 5{\cdot}0$ is about 52 percent (Fig. 2), whilst for the 10 percent thick wing these reductions are about 49 percent and 38 percent respectively (Fig. 8).

Various factors contribute to this result as well as to the peculiarities of shape of the curve of C_{Dp} against transition position for the biconvex wings at $M_o = 5{\cdot}0$. First and foremost is the fact that the basic flat plate skin friction in the turbulent boundary layer decreases much more rapidly with Mach number than does the skin friction in the laminar boundary layer (see Fig. 2, Ref. 1 and Fig. 2, Ref. 2). This factor is also illustrated in Fig. 13. The effect of section thickness is manifest in three ways. Firstly, it introduces a negative pressure gradient over both surfaces and this tends to increase the skin

friction/

*A few minor errors that appeared in the original tables of C_{F_1} in Refs. 4 and 5 have been here corrected.

friction but much more markedly when the boundary layer is laminar (through the term Λ of equation (3)) than when it is turbulent (cf., Figs. 13, 14 and 15). Secondly, it results in a local stream Mach number which is lower than the mainstream Mach number at the front and higher over the rear of the section (Figs. 19 and 20). This results in an increase in the skin friction over the front and a decrease over the rear, as compared with the flat plate case, particularly when the boundary layer is turbulent. This effect is strongly augmented by the fact that associated with a local Mach number distribution that increases from front to rear we may expect the product $\rho_1 u_1^2$ to decrease provided the Mach number is everywhere greater than $\sqrt{2}$ (see Figs. 21 and 22). This follows from the fact that in isentropic flow $\rho_1 u_1^2$ reaches a maximum when $M_1 = \sqrt{2}$, and we find that

$$\frac{d}{dM_1}\left(\frac{\rho_1 u_1^2}{\rho_0 u_0^2}\right)_{M_1=M_0} = \frac{2 - M_0^2}{M_0\left[1 + \frac{\gamma-1}{2} M_0^2\right]}. \qquad \ldots(16)$$

The right-hand side of equation (16) is plotted in Fig. 24, and we see that between $M_0 = 2{\cdot}5$ and $M_0 = 5{\cdot}0$ it is very nearly constant and equal to $-0{\cdot}8$, approximately. The skin friction is almost directly proportional to $\rho_1 u_1^2$ so that again we may expect a greater part of the skin friction with a laminar or turbulent boundary layer to be contributed from the front of the wing and a smaller part from the rear with increase of Mach number and thickness-chord ratio (cf., Figs. 13, 14 and 15). As against this we note that on a wing section the Reynolds number based on local free stream velocity and kinematic viscosity is somewhat higher near the nose than in the undisturbed stream and this will tend to reduce the friction particularly when the boundary layer is laminar. Finally, we may remark that although the laminar boundary layer has smaller values of the momentum thickness over most of a wing surface than does the turbulent boundary layer, this is not necessarily so very near the nose at the lowest Reynolds numbers considered, whilst the value of H for the laminar layer is generally larger than for the turbulent layer. In consequence, the displacement thickness and its rate of growth near the nose can, at these Reynolds numbers, be greater when the boundary layer is laminar than when it is turbulent. Thus we find in these cases (see Figs. 10, 11 and 12) that the associated pressure increments are greater near the nose for the laminar boundary layer than for the turbulent boundary layer and hence a rearward movement of transition near the nose can result in an increase of the pressure drag. We may also note that the effects of the discontinuity of displacement thickness at transition tends in general to reduce slightly the effects of rearward movement of transition on boundary-layer drag (see Table 2).

The net result of these various factors is that in the extreme case of $M_0 = 5{\cdot}0$ and $R_0 = 10^6$ a rearward movement of transition from the nose of the biconvex wings has at first little effect on the boundary-layer drag because of the relatively high skin friction with the boundary layer laminar very close to the nose, the effect then becomes more marked as the transition traverses the forward region of high turbulent boundary-layer friction and then becomes less marked as the transition moves over the rear half of the wing where both the overall drag contribution and the difference between laminar and turbulent skin friction are small.

We come now to consider in more detail the magnitude and character of the second stage correction. As will be clear from Fig. 1 (or Table 1), in the extreme case considered of $R_0 = 10^6$ and $M_0 = 5{\cdot}0$ this correction to overall skin friction drag is about 7% for a flat plate with a fully turbulent boundary layer, whilst for the

5 and 10 percent thick wings it is about $11\frac{1}{2}$ percent and 14 percent respectively. With the boundary layer fully laminar the corresponding values for the correction in the three cases are about 6 percent, $4\frac{1}{2}$ percent and 4 percent, respectively, so that the effect of section thickness on the ratio $\Delta C_F/C_{F_1}$ is reversed as the transition position moves back from the leading edge to the trailing edge. The correction appears to vary almost as M_0^2; with a fully turbulent boundary layer it varies with Reynolds number approximately as $R_0^{-1/6}$, with the boundary layer laminar the variation with Reynolds number is as $R_0^{-1/2}$, and intermediate negative powers of R_0 apply for intermediate positions of transition.

It will be appreciated that the increase in skin friction associated with the second stage correction is due mainly to the fact that the positive pressure increment induced by the boundary layer implies a reduction of local Mach number everywhere and for Mach numbers greater than about 1·4 this results in an increase of $\rho_1 u_1^2$ and therefore c_f (see Figs. 21 and 22). It will be noted that the pressure increments and the corresponding changes in $\rho_1 u_1^2$ and c_f increase markedly towards the rear with wing thickness (see Figs. 10, 11, 12, 21 and 22). A study of Fig. 23 will demonstrate that these effects are intimately bound up with the rapid increase of θ and $d\theta/dx$ over the section rear with wing thickness, and this in turn can be ascribed to the momentum defect in the boundary layer being spread over a greater thickness because of the low local value of $\rho_1 u_1^2$. Further the high local Mach number, M_1, implies a large value of H and therefore of δ^*. Since the turbulent boundary layer is generally much thicker than the laminar boundary layer these effects are to that extent more marked when the boundary layer is turbulent than when it is laminar.

Finally, referring to Fig. 9, it will be seen that up to a thickness-chord ratio of 0·05 the effect of this ratio on skin friction drag is small with the boundary layer fully turbulent but its effect is quite significant with the boundary layer laminar. However, the effect of the thickness-chord ratio on the boundary-layer drag is somewhat more marked in all cases.

4. Results and Discussion for Flat Plate at Incidence

4.1 Results

The first stage calculations for the flat plate at incidence covered the following cases:-

α	M_0	R_0	Mean Transition Positions ($\bar{x}_T$)
5°	1·5, 2·5, 5·0	10^6, 10^7, 10^8	0, 0·1c, 0·3c, 0·5c, 1c
10°	1·5, 2·5, 5·0	10^6, 10^8	0, 0·1c, 0·3c, 0·5c, 1c

Second stage calculations were, however, made only for the following cases:-

α	M_0	R_0	Mean Transition Positions ($\bar{x}_T$)
5°	5·0	10^6	0, 0·5c, 1c
10°	5·0	10^6	0, 0·5c, 1c

The/

The resulting values of the ratio $\Delta C_F/C_{F_1}$ for these cases were found to be as follows:-

α	Mean Transition Position	$\Delta C_F/C_{F_1}$
5°	0	6·3%
	0·5c	6·3%
	1c	7·2%
10°	0	5·7%
	0·5c	5·7%
	1c	6·8%

These values are within about 1 percent of the corresponding values predicted from Fig. 1 for a flat plate at zero incidence. Thus, in spite of the very significant differences in the drag characteristics of the two surfaces of a plate at incidence (to be discussed in more detail later) the overall magnitude of the second stage correction ratio in these cases is much the same as for a plate at zero incidence. These cases involve the largest values of the second stage correction for the ranges of the main variables considered and also the largest differences between the frictional characteristics of the upper and lower surfaces. It seems reasonable, therefore, to assume that in all cases the overall second stage correction ratio can be reliably taken to be the same as for a flat plate at zero incidence as given by Fig. 1. This assumption was therefore applied in general to determine the values of C_{F_2} from the calculated values of C_{F_1}.

To illustrate the separate contributions of the two surfaces values of C_{F_1} are shown in Fig. 25 for both surfaces for $R_o = 10^6$ and 10^8 and the two incidences considered. In Fig. 26 the overall second stage skin friction coefficient, C_{F_2}, is shown as a function of incidence for $\bar{x}_T/c = 0$, 0·5, and 1·0, $M_o = 1·5$, 2·5 and 5·0, and $R_o = 10^6$. Similarly in Fig. 27, the overall boundary-layer drag coefficient, C_{DB}, is shown as a function of incidence for $R_o = 10^6$, and it is likewise presented in Fig. 28 for $R_o = 10^8$. The results are also given in Table 4 which presents the values of C_{F_1}, ΔC_F, C_{F_2}, ΔC_{Dp} and C_{DB}.

4.2 Discussion

Considering first Fig. 25 we see that in almost all cases the skin friction drag of the lower surface is greater than that of the upper surface, and the difference between the skin friction drags of the two surfaces increases with incidence, Mach number and with forward movement of the transition position. Thus, in the extreme case of $\alpha = 10°$, $M_o = 5·0$, and with transition at the leading edge the skin friction drag of the upper surface is only about 22 percent of that of the lower surface. Further, we note that there is a tendency for the reduction of frictional drag with Mach number, characteristic of the flat plate at zero incidence, to be reversed for the lower surface of the plate at incidence.

These/

These results can be readily explained by essentially the same arguments as those of Section 3.2, as there are clearly close parallels between the effects of thickness and the effects of incidence. For the flat plate at incidence the effective Mach number of the flow past the lower surface is less than that of the undisturbed stream, whilst that of the flow past the upper surface is greater than that of the undisturbed stream. This is illustrated in Fig. 29 where the effective Mach number M_a for each surface is shown as a function of incidence for the three values of M_0 considered. By itself this change in effective Mach number would account for a small increase of frictional drag of the lower surface and a small decrease of that of the upper surface, and such effects would be more marked with a fully turbulent boundary layer than a fully laminar boundary layer. However, as in the case of thickness effects, the largest changes in drag with incidence result from the accompanying changes in $\rho_1 u_1^2$, and Fig. 30 shows the ratio $\rho_a u_a^2/\rho_0 u_0^2$ plotted as a function of incidence for both surfaces of the flat plate and the Mach numbers considered. It will be noted how rapidly this ratio increases for the lower surface and decreases for the upper surface with increase of Mach number (provided it is greater than about 1·4) and incidence. Thus in the extreme case of $M_0 = 5{\cdot}0$, and $\alpha = 10°$, the ratio $\rho_a u_a^2/\rho_0 u_0^2$ for the upper surface is barely one fifth of that for the lower surface. The only other factor of significance is the effective Reynolds number R_a, which is increased on the lower surface and decreased on the upper surface, as shown in Fig. 31. This has the effect of reducing somewhat the lower surface frictional drag and increasing that of the upper surface, and this effect is relatively greater with a boundary layer that is largely laminar than with one that is largely turbulent.

Consider now the overall second stage skin friction drag coefficient, C_{F_2}, and its variation with incidence, α, as illustrated in Fig. 26. We see that for $M_0 = 1{\cdot}5$ C_{F_2} falls somewhat with incidence, at $M_0 = 2{\cdot}5$ it changes only slightly with incidence, but at $M_0 = 5{\cdot}0$ it increases significantly with incidence particularly with far forward transition positions. Thus, with $\bar{x}_T/c = 0$, $M_0 = 5{\cdot}0$, C_{F_2} increases by about 5 percent as α increases from 0° to 5°, whilst for a change in α from 0° to 10° the corresponding increase in C_{F_2} is about 20 percent. With $\bar{x}_T/c = 1{\cdot}0$, on the other hand, there is very little change in C_{F_2} with α for α less than about 8°. If we now consider the total boundary-layer drag coefficient, $C_{DB} = C_{F_2} + \Delta C_{Dp}$, as illustrated in Fig. 27 for $R_0 = 10^6$ and Fig. 28 for $R_0 = 10^8$, it will be clear that the boundary-layer pressure drag contribution is generally important, as is otherwise apparent from Table 4. Its effect is to cause an increase of C_{DB} with incidence in all cases, and this increase is particularly marked with far forward transition positions and at the higher Mach numbers. We see that with $\bar{x}_T/c = 0$, $M_0 = 5{\cdot}0$ and $R_0 = 10^6$, C_{DB} increases by about 10 percent as α increases from 0° to 5°, and it increases by about 40 percent for a change in α from 0° to 10°. The corresponding percentage increases with $R_0 = 10^8$ are slightly larger but of the same order. However, we find that with $\bar{x}_T/c = 1{\cdot}0$ there is little significant change in C_{DB} with incidence for α less than about 5°. It can be inferred, therefore, that in general for a wing section significant boundary-layer drag changes with incidence will occur at Mach numbers of the order of 5·0 and incidence changes of the order of

5°/

5° unless the boundary layers are largely laminar. It is anticipated that the data presented in Figs. 27 and 28 and Table 4 can be used as a quantitative as well as a qualitative guide for wing sections.

5. Conclusions

The main object of this work has been the production of comprehensive data on the boundary-layer drag of wing sections for supersonic speeds up to a Mach number of 5·0 that can provide a basis for the estimation of boundary-layer drag in all cases where the application of two-dimensional sectional characteristics is valid. Apart from the limitation of the zero heat-transfer condition it is believed that this object has now been achieved. A separate investigation is currently in progress on the effect of heat transfer.

It has been shown that for Mach numbers of the order of 2·5 or higher, the secondary effects on boundary-layer drag of the changes in pressure distribution produced by the boundary layer are not negligible and must be taken into account. The resulting correction to the overall skin friction drag for the biconvex wing sections considered is presented in Fig. 1. The main effect is an increase in skin friction due to the increase in $\rho_1 u_1^2$ associated with the reduction of local free stream Mach number caused by the boundary layer.

More generally the analysis has demonstrated the important effects on chordwise skin friction distribution of the local free stream Mach number distribution and the associated distribution of $\rho_1 u_1^2$. In the light of these factors the main calculated effects of wing thickness and incidence with increasing mainstream Mach numbers on the skin friction distribution, the boundary-layer pressure drag and the overall boundary-layer drag can be readily explained. Notable points of interest are the reduction in the effects of shift of transition position with increase of Mach number, particularly at low Reynolds number, and the increase of the drag of the lower surface relative to that of the upper surface with increase of Mach number for a wing at incidence.

For thickness-chord ratios less than about 0·05 the effect of thickness on skin friction drag is very small with the boundary layer fully turbulent, but its effect is more significant if the boundary layer is fully laminar. However, the effect of thickness-chord ratio on boundary-layer drag is generally more marked in all cases (Fig. 9).

The boundary-layer drag of a flat plate at 5° incidence is significantly greater than at 0° incidence at the highest Mach number considered and with extensive turbulent boundary layers, but with a fully laminar boundary layer or a much lower Mach number the effect of incidence is small (Figs. 27 and 28). This result can be expected to apply more generally to wing sections.

APPENDIX/

APPENDIX I

Approximate Analysis of the Second Stage Correction to the Skin Friction Coefficient for a Flat Plate at Zero Incidence

We will in general denote quantities obtained in the first stage calculation, i.e., zero pressure gradient, by suffix 0, and increments of quantities between the first and second stages will be denoted by the prefix Δ. For consistency with the main text, however, we will continue to denote the overall skin friction coefficients for the first and second stages by C_{F_1} and C_{F_2}. Thus for the laminar boundary layer we have from equation (1)

$$\frac{\theta_0}{c} = \frac{2}{(R_0 f_0)^{\frac{1}{2}}} \cdot \left(\frac{x}{c}\right)^{\frac{1}{2}}, \qquad \ldots(A.1)$$

and at transition

$$\frac{\theta_{T_0}}{c} = \frac{2}{(R_0 f_0)^{\frac{1}{2}}} \cdot \left(\frac{x_T}{c}\right)^{\frac{1}{2}}. \qquad \ldots(A.2)$$

For the turbulent boundary layer (see equation (7))

$$\frac{\theta_0}{c} = \left[\frac{6}{5} C R_0^{-\frac{1}{5}} \cdot h_0 \cdot \left(\frac{x - x_T}{c}\right) + \left(\frac{\theta_T}{c}\right)^{\frac{6}{5}}\right]^{\frac{5}{6}}$$

where

$$h_0 = G(x)\left(\frac{u_1}{u_0} \cdot \frac{\nu_0}{\nu_1}\right)^{\frac{1}{5}} = \left\{ t_1 \left[\frac{\log R_0}{\log R_0 + (2+\omega)\log t_1}\right]^{2.5c}\right\}^{\frac{6}{5}}, \qquad \ldots(A.3)$$

and the overall skin friction coefficient up to station x is, for each surface,

$$C_{Fx_0} = \frac{1}{c}\int_0^x c_{f_0} \cdot dx = \frac{2\theta_0}{c}. \qquad \ldots(A.4)$$

For the second stage we have a pressure increment, for $\frac{x}{c} \geq 0{\cdot}04$,

$$\Delta p = \frac{\rho_0 u_0^2}{B_0} \frac{d\delta^*}{dx} = \frac{\rho_0 u_0^2}{B_0} \cdot H_0 \frac{d\theta_0}{dx}, \qquad \ldots(A.5)$$

where $B_0 = (M_0^2 - 1)^{\frac{1}{2}}$.

But, since Δp is assumed small, from Bernoulli's equation

$$\Delta p = -\rho_0 u_0 \cdot \Delta u, \quad \text{where } \Delta u = u_1 - u_0,$$

and therefore

$$\frac{\Delta u}{u_0} = \frac{u_1 - u_0}{u_0} = -\frac{H_0}{B_0} \cdot \frac{d\theta_0}{dx}, \qquad \ldots(A.6)$$

$$\frac{du_1}{dx} = -u_0 \cdot \frac{H_0}{B_0} \cdot \frac{d^2\theta_0}{dx^2}. \qquad \ldots(A.7)$$

Also/

Also $$\frac{\Delta\rho}{\rho_o} = \frac{\rho_1 - \rho_o}{\rho_o} = -M_o^2 \frac{\Delta u}{u_o} = -M_o^2 \frac{H_o}{E_o} \cdot \frac{d\theta_o}{dx}. \qquad \ldots(A.8)$$

No generality is lost by taking c (the chord length), u_o and ρ_o as quantities of unit magnitude, and length, velocities and densities respectively, will be measured in terms of them, the analysis will therefore now be continued in terms of such non-dimensional quantities. Increments between the first and second stage values of quantities will in all cases be assumed to be small and squares, products and higher order terms in the increments will be neglected.

The momentum equation is

$$\theta' + \theta\left[(H+2)\frac{u_1'}{u_1} + \frac{\rho_1'}{\rho_1}\right] = \frac{\tau_w}{\rho_1 u_1^2} = c_f/2\ \rho_1 u_1^2,$$

where dashes denote differentiation with respect to x, and this can be written

$$\frac{c_f}{2} \cdot u_1^H = \frac{d}{dx}[\rho_1 u_1^{H+2} \cdot \theta] - \rho_1 u_1^{H+2}\,\theta \cdot \log_e u_1 \cdot \frac{dH}{dx}.$$

But for the laminar boundary layer H is taken as constant and equal to H_o, whilst for the turbulent boundary layer, and to the first order, u_1 can be put equal to $u_o = 1$ in the last term and so we have

$$\frac{c_f}{2} \cdot u_1^H = \frac{d}{dx}[\rho_1 u_1^{H+2} \cdot \theta]. \qquad \ldots(A.9)$$

But
$$\begin{aligned}\rho_1 u_1^{H+2} \cdot \theta &= \theta_o[1 + \Delta\rho + (H_o+2)\Delta u] + \Delta\theta \\ &= \theta_o[1 + (H_o+2-M_o^2)\Delta u] + \Delta\theta,\end{aligned} \qquad \ldots(A.10)$$

and
$$\begin{aligned}\frac{c_f}{2} \cdot u_1^H &= \frac{d}{dx}[\rho_1 u_1^{H+2} \cdot \theta] \\ &= \frac{d\theta_o}{dx}[1 + (H_o+2-M_o^2)\Delta u] + \theta_o(H_o+2-M_o^2)\frac{du_1}{dx} \\ &\quad + \frac{d}{dx}(\Delta\theta).\end{aligned} \qquad \ldots(A.11)$$

Hence, using (A.6) and (A.7), for $x \geq 0{\cdot}04$

$$\rho_1 u_1^{H+2} \cdot \theta = \theta_o\left[1 - \frac{H_o}{E_o}(H_o+2-M_o^2)\frac{d\theta_o}{dx}\right] + \Delta\theta, \qquad \ldots(A.12)$$

and
$$\begin{aligned}\frac{c_f}{2} \cdot u_1^H &= \frac{c_f}{2} \cdot u_1^{H_o} \\ &= \frac{d\theta_o}{dx} + \frac{d}{dx}(\Delta\theta) - \frac{H_o}{E_o}(H_o+2-M_o^2)\left[\left(\frac{d\theta_o}{dx}\right)^2 + \theta_o\frac{d^2\theta_o}{dx^2}\right].\end{aligned} \qquad \ldots(A.13)$$

With/

With the assumption that the pressure increment Δp is linear with x for $x \leq 0{\cdot}04$, we have for those values of x

$$\Delta p = \frac{H_0}{B_0}\left[\left(\frac{d\theta_0}{dx}\right)_{0.04} + (x-0{\cdot}04)\left(\frac{d^2\theta_0}{dx^2}\right)_{0.04}\right] \qquad \ldots(A.14)$$

and hence

$$\Delta u = -\frac{H_0}{B_0}\left[\left(\frac{d\theta_0}{dx}\right)_{0.04} + (x-0{\cdot}04)\left(\frac{d^2\theta_0}{dx^2}\right)_{0.04}\right]. \qquad \ldots(A.15)$$

We now require to evaluate $\Delta\theta$. For the laminar boundary layer (equation (1)) we have

$$[\rho_1^2\theta^2]_x = \frac{4}{R_0 f_0 u_1^{\varepsilon}}\int_0^x \rho_1 u_1^{\varepsilon-1}\,.\,dx,$$

or, to the first order,

$$\theta^2 = \frac{4}{R_0 f_0}(1 + 2M_0^2\Delta u - \varepsilon\Delta u)\int_0^x [1 + (\varepsilon-1-M_0^2)\Delta u]dx. \qquad .(A.16)$$

But from (A.6) and (A.15), if $x > 0{\cdot}04$

$$\int_0^x [1 + (\varepsilon-1-M_0^2)\Delta u]\,.\,dx = \int_{0.04}^x \left[1 - \frac{H_0}{B_0}\,.\,\frac{d\theta_0}{dx}(\varepsilon-1-M_0^2)\right]dx$$

$$+ \int_0^{0.04}\left[1 - \frac{H_0}{B_0}(2+\beta x)(\varepsilon-1-M_0^2)\right]dx,$$

where

$$\alpha = \left(\frac{d\theta_0}{dx}\right)_{0.04} - 0{\cdot}04\left(\frac{d^2\theta_0}{dx^2}\right)_{0.04}, \quad \beta = \left(\frac{d^2\theta_0}{dx^2}\right)_{0.04}. \qquad \ldots(A.17)$$

This yields after some algebra, with the aid of (A.1)

$$\int_0^x [1 + (\varepsilon-1-M_0^2)\Delta n]dx = x - \frac{H_0}{B_0}\,\frac{(\varepsilon-1-M_0^2)}{(R_0 f_0)^{\frac{1}{2}}}[2x^{\frac{1}{2}} - 0{\cdot}15],$$

and hence (A.16) becomes

$$\theta_0^2\left[1 + \frac{2\Delta\theta}{\theta_0}\right] = \frac{4}{R_0 f_0}[1 + (2M_0^2-\varepsilon)\Delta u]\left[x - \frac{H_0}{B_0}\,\frac{(\varepsilon-1-M_0^2)}{(R_0 f_0)^{\frac{1}{2}}}(2x^{\frac{1}{2}} - 0{\cdot}15)\right]$$

$$= \theta_0^2\left\{1 - \frac{2H_0}{R_0 R_0 f_0 \theta_0}\left[\varepsilon - 2 - \frac{0{\cdot}15}{x^{\frac{1}{2}}}(\varepsilon - 1 - M_0^2)\right]\right\}.$$

Thus

$$\Delta\theta = -\frac{H_0}{R_0 R_0 f_0}\left[(\varepsilon-2) - \frac{0{\cdot}15}{x^{\frac{1}{2}}}(\varepsilon-1-M_0^2)\right] \qquad \ldots(A.18)$$

$$\frac{d}{dx}(\Delta\theta) = -\frac{0{\cdot}075\,H_0}{R_0(R_0 f_0)x^{3/2}}\,.\,(\varepsilon-1-M_0^2). \qquad \ldots(A.19)$$

But/

But from (A.1) $$\left(\frac{d\theta_o}{dx}\right)^2 + \theta_o \cdot \frac{d^2\theta_o}{dx^2} = 0.$$

and hence from (A.13)

$$\frac{c_f}{2} \cdot u_1^{H_o} = \frac{d\theta_o}{dx} + \frac{d}{dx}(\Delta\theta) = \frac{c_{f_o}}{2}\left[1 + \frac{d/dx(\Delta\theta)}{d\theta_o/dx}\right].$$

Specimen values for H_o, g and B_o substituted in (A.19) show that at the most, when $x = 0{\cdot}04$, $\frac{d}{dx}(\Delta\theta)\Big/\frac{d\theta_o}{dx}$ is about $0{\cdot}01$ and is generally very much less, so that we can deduce for the laminar boundary layer and $x > 0{\cdot}04$

$$\frac{c_f}{2} \cdot u_1^{H_o} = \frac{c_{f_o}}{2}$$

and hence $$c_f = c_{f_o}\left[1 + \frac{H_o^2}{B_o} \cdot \frac{d\theta_o}{dx}\right]. \qquad \ldots(A.20)$$

Similarly, we find that for $x < 0{\cdot}04$

$$\theta^2 = \theta_o^2\left[1 + \frac{H_o}{B_o}\alpha(1-M_o^2) + \text{terms in } \alpha x, \beta x, \text{ etc.,}\right],$$

so that we can write

$$\Delta\theta = \frac{H_o}{2B_o}\frac{(1-M_o^2)}{R_o f_o}\left(\frac{x}{0{\cdot}04}\right)^{\frac{1}{2}},$$

or $$\frac{\Delta\theta}{\theta_o} = -\frac{5\,H_o B_o}{4(R_o f_o)^{\frac{1}{2}}}. \qquad \ldots(A.21)$$

We shall not make direct use of this result, but we note that for $x < 0{\cdot}04$, it leads to

$$\theta = \text{const}\ \theta_o$$

and hence c_f like c_{f_o} must be proportional to $x^{-\frac{1}{2}}$. Therefore

$$\int_o^{0{\cdot}04} c_f dx = 0{\cdot}08\,(c_f)_{0{\cdot}04}$$

$$= 0{\cdot}08\left[c_{f_o}\left(1 + \frac{H_o^2}{B_o}\frac{d\theta_o}{dx}\right)\right]_{0{\cdot}04}. \qquad \ldots(A.22)$$

from (A.20). Further, from (A.20),

$$\int_{0{\cdot}04}^{x_T} c_f dx = \int_{0{\cdot}04}^{x_T} c_{f_o}\left[1 + \frac{H_o^2}{B_o}\frac{d\theta_o}{dx}\right] dx$$

or/

$$\text{or} \qquad [C_{F\ell}]_{0\cdot04}^{x_T} = [C_{F\ell_0}]_{0\cdot04}^{x_T} + \frac{2H_0^2}{R_0 R_0 f_0} \log_e \left(\frac{x_T}{0\cdot04} \right),$$

when suffix ℓ denotes the laminar boundary layer. But from (A.22) and (A.1)

$$[C_{F\ell}]_0^{0\cdot04} = [C_{F\ell_0}]_0^{0\cdot04} + \frac{4H_0^2}{B_0 R_0 f_0}.$$

Hence, we have finally

$$C_{F\ell} = C_{F\ell_0} + \frac{2H_0^2}{B_0 R_0 f_0} \left[2 + \log_e \left(\frac{x_T}{0\cdot04} \right) \right]. \qquad \ldots(A.23)$$

Here $C_{F\ell}$ denotes the contribution to C_F due to the skin friction in the laminar layer. For a fully laminar boundary layer $x_T = 1\cdot0$, and

$$C_{F\ell_0} = 4/(R_0 f_0)^{\frac{1}{2}}$$

and therefore

$$\frac{C_{F\ell}}{C_{F\ell_0}} = 1 + \frac{H_0^2}{2B_0 (R_0 f_0)^{\frac{1}{2}}} + [\log_e 25 + 2]$$

$$= 1 + \frac{2\cdot61\ H_0^2}{B_0 (R_0 f_0)^{\frac{1}{2}}}. \qquad \ldots(A.24)$$

We see that for this case $(\Delta C_F/C_{F_1})_\ell = \left(\frac{C_{F\ell}}{C_{F\ell_0}} - 1 \right)$ varies with Mach number as $H_0^2/B_0 f_0^{\frac{1}{2}}$ and it varies with Reynolds number as $R_0^{-\frac{1}{2}}$. A comparison of the results given by equation (A.24) and those given by the full calculations for $R_0 = 10^3$ is as follows:-

Values of $(\Delta C_F/C_{F_1})_\ell$ for fully laminar boundary layer

M_0	1·5	2·5	5·0
As given by full calculations	0·003	0·010	0·053
As given by equation (A.24)	0·013	0·018	0·069

Bearing in mind that the quoted result as given by the full calculations represents the small difference between two relatively large quantities, and that the numerical accuracy with which either quantity is calculated is unlikely to be better than ± half a percent, the agreement can be regarded as satisfactory. The full calculations were not made for the fully laminar boundary layer and $R_0 = 10^7$, but the result for 10^3 and $M_0 = 1\cdot5$ and $5\cdot0$ showed a negligible difference between the first and second stages for both Mach numbers which can be compared with the corresponding results predicted by equation (A.24), viz., 0·001 and 0·007 respectively.

Further,/

Further, from the point of view of producing a set of curves such as those of Fig. 1 for predicting the correction to the first stage calculation, an important conclusion from equation (A.24) is the fact that the Mach number and Reynolds number effects can be considered separately.

We come now to consider the turbulent boundary layer. Equations (A.6) to (A.10) apply, but we now have to evaluate $\Delta\theta$ from the relation (equation (7))

$$\left[\theta^{\frac{n}{n-1}}\right]_{x_1}\left[\exp\cdot\int_T^{x_1}F(x)\cdot\frac{n}{n-1}\cdot dx\right]-\theta_T^{\frac{n}{n-1}}$$

$$=\frac{n}{n-1}\cdot CR_o^{-\frac{1}{n-1}}\int_T^{x_1}G(x)\cdot\exp\cdot\left[\int_T^{x}F(x)\cdot\frac{n}{n-1}\cdot dx\right]\cdot dx.$$

But $$F(x)=\frac{u_1'}{u_1}\left[(H_o+2)-M_o^2\right]=-\frac{H_o}{R_o}\left(H_o+2-M_o^2\right)\cdot\frac{d^2\theta_o}{dx^2}$$

and hence we can write to the order of accuracy required

$$\exp\left[\int_T^{x}F(x)\cdot\frac{n}{n-1}\cdot dx\right]=1-\frac{n}{n-1}\frac{H_o}{R_o}\left(H_o+2-M_o^2\right)\left[\frac{d\theta_o}{dx}\right]_T^{x}. \qquad \ldots(A.25)$$

Similarly $$G(x)=\left(\frac{u_1}{\nu_1}\right)^{-\frac{1}{n-1}}\cdot h_o,$$

and this reduces to

$$G(x)=h_o\left\{1+\frac{H_o}{R_o(n-1)}\cdot\frac{d\theta_o}{dx}\left[1-M_o^2\left(1+\omega y-\omega\right)\right]\right\}. \qquad \ldots(A.26)$$

With the aid of (A.25) and (A.26) the above equation for $\theta^{\frac{n}{n-1}}$ finally yields

$$\theta^{\frac{n}{n-1}}=\theta_{T_o}^{\frac{n}{n-1}}\left[1+\alpha_1\right]+\frac{n}{n-1}\cdot CR_o^{-\frac{1}{n-1}}\cdot h_o(x-x_T)(1+\alpha_2),\quad\text{where}$$

$$\alpha_1=\frac{n}{n-1}\left\{\frac{H_o(2-g)}{2R_o(R_o f_o x_T)^{\frac{1}{2}}}+\frac{H_o\cdot 0{\cdot}075(g-1-M_o^2)}{R_o(R_o f_o)^{\frac{1}{2}}x_T}+\frac{H_o}{R_o}\left(H_o+2-M_o^2\right)\left[\frac{d\theta_o}{dx}\right]_T^{x}\right\}$$

and

$$\alpha_2=\frac{n}{n-1}\frac{H_o}{R_o}\left(H_o+2-M_o^2\right)\left(\frac{d\theta_o}{dx}\right)+\frac{H_o}{R_o(n-1)}\frac{(\theta_o-\theta_{o_T})}{(x-x_T)}\left[1-M_o^2\left(1+\omega y-\omega\right)-n\left(H_o+2-M_o^2\right)\right].$$

$$\ldots(A.27)$$

From/

From (A.27) it follows that

$$\frac{\Delta\theta}{\theta_o} = \frac{n-1}{n}\left[\alpha_2 + (\alpha_1-\alpha_2)\left(\frac{\theta_{T_o}}{\theta_o}\right)^{\frac{n}{n-1}}\right], \qquad \ldots(A.28)$$

and (A.12) eventually yields

$$\rho_1 u_1^{H+2}\theta = \theta_o\left\{1 + \frac{n-1}{n}\left[\alpha_3 + (\alpha_1-\alpha_2)\left(\frac{\theta_{T_o}}{\theta_o}\right)^{\frac{n}{n-1}}\right]\right\}$$

where $$\alpha_3 = \frac{H_o}{B_o(n-1)}\frac{(\theta_o-\theta_{T_o})}{(x-x_T)}\left[1 - M_o^2(1+\omega y-\omega) - n(H_o+2-M_o^2)\right]$$

$\ldots(A.29)$

The analysis now proceeds somewhat differently from that adopted for the laminar layer.

From equation (A.9)

$$\int_{x_T}^{1\cdot0}\frac{c_f}{2}\cdot u_1^{\bar{H}}\,dx = \left[\rho_1 u_1^{H+2}\cdot\theta\right]_{x_T}^{1\cdot0}$$

and hence the contribution to C_F from the turbulent layer is

$$C_{F_t} = \int_{x_T}^{1\cdot0} c_f\cdot dx = 2\left[\rho_1 u_1^{H+2}\cdot\theta\right]_{x_T}^{1\cdot0}\bar{u_1^{H}}, \qquad \ldots(A.30)$$

where $\bar{u_1^{H}}$ is some mean value of u_1^{H}.

From (A.29) and (A.30) we obtain finally

$$C_{F_t}\cdot\bar{u_1^{H}} = 2\theta_{c_o}\left\{1 + \frac{n-1}{n}\left[\alpha_3 + (\alpha_1-\alpha_2)\left(\frac{\theta_{T_o}}{\theta_{c_o}}\right)^{\frac{n}{n-1}}\right]\right\}_{x=1\cdot0} - 2\theta_{T_o}(1+\alpha_4)$$

$\ldots(A.31)$

where

$$\alpha_4 = \left[\frac{H_o(2-g)}{2B_o(R_o f_o x_T)^{\frac{1}{2}}} + \frac{0\cdot075\,H_o(g-1-M_o^2)}{B_o(R_o f_o)^{\frac{1}{2}}x_T} - \frac{H_o}{B_o}(H_o+2-M_o^2)\left(\frac{d\theta_o}{dx}\right)_T\right]$$

and θ_{c_o} is the value of θ_o at the trailing edge (where $x = c = 1\cdot0$).

The quantity u_1^{H} will in general change relatively little between the transition point and the trailing edge, it is therefore proposed that $\bar{u_1^{H}}$ can be taken as the arithmetic mean between the value of u_1^{H} at transition and at the trailing edge, i.e.,

$\bar{u_1^{H}}$/

$$\overline{u_1^H} = \frac{1}{2}\left[(u_1^H)_{x_T} + (u_1^H)_{1.0} \right] \qquad \ldots(A.32)$$

$$= 1 - \frac{H_o^2}{2B_o}\left[\left(\frac{d\theta_o}{dx} \right)_{x_T} + \left(\frac{d\theta_o}{dx} \right)_{1.0} \right].$$

Hence from (A.31)

$$C_{Ft} = 2\theta_{c_o}\left\{ 1 + \frac{n-1}{n}\left[\alpha_3 + (\alpha_1 - \alpha_2)\left(\frac{\theta_{T_o}}{\theta_{c_o}} \right)^{\frac{n}{n-1}} \right]_{x=1.0} + \frac{H_o^2}{2B_o}\left[\left(\frac{d\theta_o}{dx} \right)_{x_T} + \left(\frac{d\theta_o}{dx} \right)_{1.0} \right] \right\}$$

$$- 2\theta_{T_o}\left\{ 1 + \alpha_4 + \frac{H_o^2}{2B_o}\left[\left(\frac{d\theta_o}{dx} \right)_{x_T} + \left(\frac{d\theta_o}{dx} \right)_{1.0} \right] \right\}. \qquad \ldots(A.33)$$

We note that $C_{Ft_o} = 2\theta_{c_o} - 2\theta_{T_o}$

and hence

$$C_{Ft} - C_{Ft_o} = 2\theta_{c_o}\left\{ \frac{(n-1)}{n}\left[\alpha_3 + (\alpha_1 - \alpha_2)\left(\frac{\theta_{T_o}}{\theta_{c_o}} \right)^{\frac{n}{n-1}} \right]_{x=1.0} + \frac{H_o^2}{2B_o}\left[\left(\frac{d\theta_o}{dx} \right)_{x_T} + \left(\frac{d\theta_o}{dx} \right)_{1.0} \right] \right\}$$

$$- 2\theta_{T_o}\left\{ \alpha_4 + \frac{H_o^2}{2B_o}\left[\left(\frac{d\theta_o}{dx} \right)_{x_T} + \left(\frac{d\theta_o}{dx} \right)_{1.0} \right] \right\}. \qquad \ldots(A.34)$$

For a fully turbulent boundary layer this equation yields

$$C_{Ft} - C_{Ft_o} = 2\theta_{c_o}\left\{ \frac{n-1}{n}\cdot\alpha_3 + \frac{H_o^2}{2B_o}\left[\left(\frac{d\theta_o}{dx} \right)_{0} + \left(\frac{d\theta_o}{dx} \right)_{1.0} \right] \right\}$$

$$= 2\theta_{c_o}\left\{ \frac{n-1}{n}\cdot\alpha_3 + \frac{H_o^2}{2B_o}\left[\left(\frac{d\theta_o}{dx} \right)_{0.04} - 0.04\left(\frac{d^2\theta_o}{dx^2} \right)_{0.04} + \left(\frac{d\theta_o}{dx} \right)_{1.0} \right] \right\}$$

or

$$\frac{C_{Ft}}{C_{Ft_o}} = 1 + \frac{(n-1)}{n}\cdot\alpha_3 + \frac{H_o^2}{2B_o}\left[\left(\frac{d\theta_o}{dx} \right)_{0.04} - 0.04\left(\frac{d^2\theta_o}{dx^2} \right)_{0.04} + \left(\frac{d\theta_o}{dx} \right)_{1.0} \right], \qquad \ldots(A.35)$$

and/

and from (A.29)

$$\alpha_3 = \frac{H_o}{B_o(n-1)}\,\theta_{c_o}\,[1 - M_o^2\,(1+\omega\gamma-\omega) - n\,(H_o+2-M_o^2)]. \qquad \ldots(A.36)$$

Putting $n = 6$, $\omega = 0{\cdot}89$, $\gamma = 1{\cdot}4$, $\theta_o = \text{const}\ R_o^{-1/6} \cdot h_o^{5/6}\ x^{5/6}$, $\frac{d\theta_o}{dx} = \frac{5}{6}\frac{\theta_o}{x}$ and $\frac{d^2\theta_o}{dx^2} = -\frac{5}{36}\frac{\theta_o}{x^2}$, we get

$$\frac{C_{Ft}}{C_{Ft_o}} = 1 + \frac{H_o}{6B_o}\,\theta_{o_c}\,[1 - 1{\cdot}36\,M_o^2 - 6\,(H_c+2-M_o^2)]$$

$$+ \frac{H_o^2}{2B_o}\left[-\frac{5}{6}\theta_{c_o} + \frac{5}{6\cdot 0{\cdot}04}\theta_{o\cdot 04} + \frac{5}{36\cdot 0{\cdot}04}\cdot\theta_{o\cdot 04}\right]$$

$$= 1 + \frac{H_o}{B_o}\,\theta_{c_o}\,[0{\cdot}773\,M_o^2 - 0{\cdot}582\,H_o - 1{\cdot}833]$$

$$+ \frac{H_o^2}{B_o}\,\theta_{o\cdot 04}\cdot 12{\cdot}13. \qquad \ldots(A.37)$$

With $C = 0{\cdot}00878$, (A.3) gives for the fully turbulent boundary layer

$$\left.\begin{aligned} \theta_{c_o} &= 0{\cdot}0450\ R_o^{-1/6}\cdot h_o^{5/6} \\ \text{and}\qquad \theta_{o\cdot 04} &= 0{\cdot}00308\ R_o^{-1/6}\cdot h_o^{5/6} \end{aligned}\right\}. \qquad \ldots(A.38)$$

If we disregard the small variation of h_o with R_o (see Fig. 2, Ref. 2) then we see that $\left(\frac{C_{Ft}}{C_{Ft_o}} - 1\right)$ takes the form $R_o^{-1/6}$ times a function of Mach number. The following table compares the results given by equation (A.37) and the full calculations for

$$\left(\Delta C_F/C_{F_1}\right)_t = \frac{C_{Ft}}{C_{Ft_o}} - 1.$$

Values of $(\Delta C_F/C_{F_1})_t$ for fully turbulent boundary layer

M_o	R_o	Value given by (A.37)	Value given by full calculations
5·0	10^6	0·063	0·069
5·0	10^7	0·036	0·042
5·0	10^8	0·020	0·027
2·5	10^6	0·012	0·016
1·5	10^6	0·002	0·003
1·5	10^8	0·005	0·002

Again/

Again bearing in mind the limitations to the possible accuracy of the full calculations, we see that the agreement is in general good.

A plot of these values for $R_0 = 10^6$ as fractions of the corresponding values of $\left(\Delta C_F / C_{F_1} \right)_t$ at $M_0 = 5$ are shown in Fig. 32 against M_0 and similarly are shown the values of $\left(\Delta C_F / C_{F_1} \right)_l$ for a fully laminar boundary layer likewise reduced in terms of the value of $\left(\Delta C_F / C_{F_1} \right)_l$ at $M_0 = 5 \cdot 0$. For comparison the curve of $k(M_0)$ from Fig. 1 is also shown and it will be seen that with the exception of the value of the fully laminar boundary layer at $M_0 = 1 \cdot 5$ given by (A.24) the run of the points is reasonably well described by the curve. It will be appreciated that this method of plotting considerably magnifies the effects of small errors in the calculations, whilst the final results for C_F at the lower Mach numbers are relatively insensitive to quite large fractional changes in the value of the function k there since the correction is in any case small. It will be recalled that the method of calculation adopted in the full calculations as well as the method of this Appendix will both become invalid as $M_0 = 1 \cdot 0$, is approached from above as is made evident by the factor $(M_0^2 - 1)^{\frac{1}{2}}$ in the denominator of equation (13). In consequence both methods will yield points in Fig. 32 which with decreasing Mach number reach a minimum, somewhere a little above $M_0 = 1 \cdot 0$ and then increase rapidly to infinity as $M_0 = 1 \cdot 0$ is approached. However, it is clear that both methods must be discounted when the estimated pressure increment can no longer be regarded as a small quantity. The form of the curve $k(M_0)$ in Fig. 1 for M_0 less than $1 \cdot 5$ was therefore determined on the plausible assumption that it would in fact continue to decrease with decreasing Mach number. Having fixed the curve $k(M_0)$ and knowing the effect of Reynolds number on the value of $\Delta C_F / C_{F_1}$ for the fully laminar and fully turbulent boundary layers there was no difficulty in the light of the values calculated for the cases considered to determine the curves $\ell(\bar{x}_T/c, t/c)$ and $m(\bar{x}_T/c, R_0)$ shown in Fig. 1.

References/

References

No.	Author(s)	Title, etc.
1	A. D. Young	Skin friction in the laminar boundary layer in compressible flow. College of Aeronautics Report No. 20, July, 1948; also The Aeronautical Quarterly, Vol.1, Part 2, August, 1949, pp.137-164.
2	A. D. Young	The calculation of the profile drag of aerofoils and bodies of revolution at supersonic speeds. College of Aeronautics Report No. 73, April, 1953.
3	H. K. Zienkiewicz	An investigation of boundary-layer effects on two-dimensional supersonic aerofoils. College of Aeronautics Report No. 49, December, 1951.
4	A. D. Young and S. Kirkby	The profile drag of biconvex wing sections at supersonic speeds. '50 Jahre Grenzschichtforschung' edited by H. Görtler and W. Tollmien, pp.419-431. (Verlag. Friedr. Vieweg & Sohn, Braunschweig.) 1955.
5	A. D. Young and S. Kirkby	The profile drag of biconvex and double wedge wing sections at supersonic speeds. Boundary Effects in Aerodynamics. Symposium held at N.P.L., 31st March - 2nd April, 1955, pp.1-34. H.M.S.O. 1955.
6	-	Report of the Definitions Panel on definitions to be used in the description and analysis of drag. A.R.C. C.P. No.369. May, 1957.
7	L. Lees	On boundary-layer equations in hypersonic flow and their approximate solutions. Jour. Aero. Sciences, Vol. 20, No.2, pp.143-145, 1953.
8	Y. H. Kuo	Viscous flow along a flat plate moving at high supersonic speeds. Jour. Aero. Sciences, Vol. 23, No.2, pp.125-136, 1956.

Table 1/

Table 1

Table of $10^4 C_{F_1}$, $10^4 \Delta C_F$ and $10^4 C_{F_2}$, where $C_{F_2} = C_{F_1} + \Delta C_F$

ΔC_F = correction to C_F for displacement thickness effect

(a) Flat plate

		$M_o = 0$			$M_o = 1.5$			$M_o = 2.5$			$M_o = 5.0$		
x_T/c	R_o	C_{F_1}	ΔC_F	C_{F_2}	C_{F_1}	ΔC_F	C_{F_2}	C_{F_1}	ΔC_F	C_{F_2}	C_{F_1}	ΔC_F	C_{F_2}
0.0	10^6	90.0	0	90.0	77.8	0.2	78.0	66.1	1.0	67.1	51.1	3.5	54.6
	10^7	61.3	0	61.3	51.5	0.1	51.6	42.0	0.5	42.5	28.6	1.3	29.9
	10^8	41.8	0	41.8	34.4	0.1	34.5	27.3	0.2	26.5	17.0	0.5	17.5
0.1	10^6	86.9	0	86.9	75.5	0.2	75.7	65.0	1.0	66.0	51.2	3.5	54.7
	10^7	57.4	0	57.4	48.3	0.1	48.4	39.7	0.4	40.1	27.4	1.2	28.6
	10^8	38.6	0	38.6	31.7	0	31.7	25.3	0.2	25.5	15.7	0.4	16.1
0.3	10^6	75.7	0	75.7	66.5	0.2	66.7	58.0	0.9	58.9	46.9	3.1	50.0
	10^7	48.1	0	48.0	40.6	0.1	40.7	33.7	0.3	34.0	23.8	0.9	24.7
	10^8	31.7	0	31.7	26.1	0	26.1	20.9	0.1	21.1	13.3	0.3	13.6
0.5	10^6	63.1	0	63.1	56.2	0.2	56.4	49.8	0.7	50.5	41.2	2.7	43.9
	10^7	37.9	0	37.9	32.3	0.1	32.4	27.1	0.2	27.3	19.7	0.6	20.3
	10^8	24.4	0	24.4	20.2	0	20.2	16.3	0	16.3	10.5	0.2	10.7
1.0	10^6	26.6	0	26.6	26.2	0.1	26.3	25.7	0.3	26.0	24.6	1.4	26.0
	10^7	8.4	0	8.4	8.3	0	8.3	8.1	0	8.1	7.8	0.1	7.9
	10^8	2.7	0	2.7	2.6	0	2.6	2.6	0	2.6	2.5	0	2.5

(b) Biconvex Wing (t/c = 0.05)

		$M_o = 1.5$			$M_o = 2.5$			$M_o = 5.0$		
$\bar{x}_T/c$	R_o	C_{F_1}	C_F	C_{F_2}	C_{F_1}	C_F	C_{F_2}	C_{F_1}	C_F	C_{F_2}
0.0	10^6	78.4	0.5	78.9	66.6	1.8	68.4	51.9	6.0	57.9
	10^7	51.3	0.2	51.5	42.5	0.8	43.4	29.3	2.3	21.6
	10^8	34.9	0.1	35.0	27.7	0.3	28.0	17.6	0.9	18.6
0.1	10^6	76.0	0.4	76.4	64.8	1.7	66.5	51.7	5.9	57.6
	10^7	48.4	0.2	48.6	39.4	0.7	40.0	27.2	2.0	29.2
	10^8	31.8	0.1	31.9	25.1	0.3	25.4	15.7	0.7	16.4
0.3	10^6	67.8	0.3	68.2	57.6	1.4	59.0	46.5	5.0	51.5
	10^7	40.8	0.1	40.9	32.6	0.4	33.0	22.2	1.3	23.6
	10^8	25.5	0	25.5	19.7	0.1	19.9	12.3	0.4	12.7
0.5	10^6	58.8	0.3	59.1	50.0	1.1	51.0	41.8	3.8	45.6
	10^7	33.0	0.1	33.1	25.7	0.3	26.0	17.8	0.8	18.6
	10^8	19.7	0	19.7	14.7	0.1	14.8	8.8	0.2	9.0
1.0	10^6	34.0	0.1	34.1	32.3	0.3	32.7	33.3	1.6	34.9
	10^7	10.8	0	10.8	10.2	0	10.2	10.5	0.2	10.7
	10^8	3.4	0	3.4	3.2	0	3.2	3.3	0	3.3

continued/

Table 1 (contd)

(c) Biconvex Wing (t/c = 0·10)

		M_0 = 1·5			M_0 = 2·5			M_0 = 5·0		
$\bar{x}_T/c$	R_0	C_{F_1}	C_F	C_{F_2}	C_{F_1}	C_F	C_{F_2}	C_{F_1}	C_F	C_{F_2}
0·0	10^6	76·3	0·5	76·8	76·4	2·2	69·6	55·5	7·7	63·1
	10^7	50·3	0·2	50·5	43·2	0·9	44·1	31·9	3·0	34·9
	10^8	33·8	0·1	33·9	27·9	0·4	28·3	19·4	1·2	20·7
0·1	10^6	74·7	0·5	75·2	64·9	2·1	67·0	54·5	7·4	61·9
	10^7	47·5	0·2	47·7	39·2	0·8	40·0	28·5	2·5	31·0
	10^8	31·1	0·1	31·2	25·0	0·3	25·3	16·6	0·9	17·5
0·3	10^6	67·7	0·4	68·1	57·6	1·6	59·2	48·5	5·8	54·3
	10^7	40·1	0·1	40·2	31·7	0·5	32·2	22·1	1·5	23·6
	10^8	25·4	0	25·4	19·0	0·2	19·2	11·3	0·4	11·7
0·5	10^6	59·8	0·3	60·1	50·5	1·2	51·7	44·3	4·5	48·8
	10^7	32·3	0·1	32·4	24·8	0·3	25·1	17·8	0·9	18·7
	10^8	19·4	0	19·4	13·7	0·1	13·8	8·2	0·2	8·4
1·0	10^6	40·0	0·1	40·1	37·6	0·4	38·0	41·0	1·7	42·7
	10^7	12·6	0	12·6	11·9	0	11·9	13·0	0·2	13·2
	10^8	4·0	0	4·0	3·8	0	3·8	4·1	0	4·1

Table 2/

Table 2

Calculated Boundary-Layer Pressure Drag Coefficients × 10^4

ΔC_{Dp_ℓ} = direct contribution due to boundary-layer effect on external pressure distribution

ΔC_{pT} = contribution arising from change in δ^* at transition

			$M_o = 1.5$			$M_o = 2.5$			$M_o = 5.0$		
t/c	$\bar{x}_T/c$	R_o	ΔC_{Dp_ℓ}	ΔC_{DpT}	ΔC_{Dp}	ΔC_{Dp_ℓ}	ΔC_{DpT}	ΔC_{Dp}	ΔC_{Dp_ℓ}	ΔC_{DpT}	ΔC_{Dp}
0.05	0.0	10^6	2.17		2.2	1.15		1.1	1.01		1.0
		10^7	1.46		1.5	0.75		0.7	0.65		0.7
		10^8	0.99		1.0	0.51		0.5	0.42		0.4
	0.1	10^6	2.44	-1.29	1.1	1.40	-0.93	0.5	1.66	-1.19	0.5
		10^7	0.88	-0.41	0.5	0.36	-0.29	0.1	0.37	-0.38	0
		10^8	0.37	-0.13	0.2	0.07	-0.09	0	0.03	-0.12	-0.1
	0.3	10^6	1.47	-0.89	0.6	0.86	-0.68	0.2	1.37	-0.78	0.6
		10^7	-0.36	-0.29	-0.6	-0.43	-0.22	-0.6	-0.25	-0.25	-0.5
		10^8	-0.66	-0.09	-0.7	-0.59	-0.07	-0.7	-0.52	-0.08	-0.6
	0.5	10^6	0.90		0.9	0.60		0.6	1.33		1.3
		10^7	-0.94		-0.9	-0.72		-0.7	-0.34		-0.3
		10^8	-1.12		-1.1	-0.83		-0.8	-0.61		-0.6
	1.0	10^6	3.08	2.24	5.3	2.30	1.55	3.9	3.14	0.59	3.7
		10^7	0.98	0.70	1.7	0.73	0.49	1.2	0.99	0.19	1.2
		10^8	0.31	0.22	0.5	0.23	0.16	0.4	0.31	0.06	0.4
0.10	0.0	10^6	7.17		7.2	3.69		3.7	2.05		2.0
		10^7	4.87		4.9	2.55		2.5	1.49		1.5
		10^8	3.31		3.3	1.73		1.7	1.02		1.0
	0.1	10^6	7.79	-3.05	4.7	2.40	-1.93	0.5	4.99	-2.53	2.5
		10^7	3.06	-0.96	2.1	0.53	-0.61	-0.1	0.57	-0.80	-0.2
		10^8	1.40	-0.30	1.1	0.05	-0.19	-0.1	-0.09	-0.25	-0.3
	0.3	10^6	5.55	-1.51	4.0	-0.90	-1.16	-2.1	2.44	-1.26	1.2
		10^7	0.29	-0.48	-0.2	-2.48	-0.38	-2.9	-0.78	-0.40	-1.2
		10^8	-0.87	-0.15	-1.0	-1.23	-0.12	-2.3	-1.26	-0.13	-1.4
	0.5	10^6	4.47		4.5	-1.73		-1.7	2.61		2.6
		10^7	-0.80		-0.8	-3.27		-3.3	-0.64		-0.6
		10^8	-1.73		-1.7	-2.84		-2.8	-1.18		-1.2
	1.0	10^6	8.56	1.59	10.2	4.73	0.57	5.3	6.82	-3.27	3.6
		10^7	2.71	0.50	3.2	1.50	0.18	1.7	2.16	-1.03	1.1
		10^8	0.86	0.16	1.0	0.47	0.06	0.5	0.68	-0.33	0.4

Table 3/

Table 3

Calculated Boundary-Layer Drag Coefficients x 10^4

$$C_{DB} = C_{F_2} + \Delta C_{Dp}$$

Biconvex Wings

		t/c = 0·05			t/c = 0·10		
		M_o = 1·5	M_o = 2·5	M_o = 5·0	M_o = 1·5	M_o = 2·5	M_o = 5·0
$\bar{x}_T/c$	R_o	C_{DB}	C_{DB}	C_{DB}	C_{DB}	C_{DB}	C_{DB}
0·0	10^6	81·0	69·5	58·9	83·9	73·2	65·2
	10^7	53·0	44·1	32·3	55·4	46·7	36·3
	10^8	36·0	28·5	19·0	37·2	30·0	21·7
0·1	10^6	77·5	67·0	58·1	79·9	67·5	64·4
	10^7	49·0	40·1	29·2	49·8	39·9	30·7
	10^8	32·1	25·3	16·3	32·3	25·2	17·2
0·3	10^6	63·7	59·2	52·0	72·2	57·1	55·4
	10^7	40·2	32·4	23·0	40·0	29·4	22·4
	10^8	24·3	19·2	12·1	24·4	16·8	10·4
0·5	10^6	60·0	51·6	46·9	64·6	49·9	51·4
	10^7	32·1	25·3	18·3	31·6	21·8	18·1
	10^8	18·6	14·0	8·4	17·7	11·0	7·2
1·0	10^6	39·5	36·5	38·6	50·2	43·2	46·2
	10^7	12·5	11·5	11·9	15·9	13·6	14·2
	10^8	3·9	3·6	3·7	5·0	4·3	4·5

Table 4/

Table 4

Flat Plate at Incidence

Table of Values of $10^4 C_{F_1}$, $10^4 \Delta C_F$, $10^4 C_{F_2}$, $10^4 \Delta C_{Dp}$, $10^4 C_{DB}$

For (a) $\alpha = 5°$, (b) $\alpha = 10°$

(a) $\alpha = 5°$

R_o	M_o	$\bar{x}_T/c$	$10^4 C_{F_1}$	$10^4 \Delta C_F$	$10^4 C_{F_2}$	$10^4 \Delta C_{Dp}$	$10^4 C_{DB}$
10^6	1·5	0	76·43	0·23	76·66	2·77	79·43
		0·5	55·32	0·17	55·49	1·74	57·23
		1·0	25·73	0·08	25·81	0·54	26·35
	2·5	0	66·26	0·98	67·24	1·41	68·65
		0·5	49·82	0·74	50·56	0·95	51·51
		1·0	25·54	0·38	25·92	0·36	26·28
	5·0	0	53·79	3·70	57·49	2·47	59·96
		0·5	42·93	2·83	45·76	1·96	47·72
		1·0	24·99	1·50	25·49	1·07	26·56
10^7	1·5	0	50·65	0·12	50·77	1·88	52·65
		0·5	31·87	0·05	31·92	1·09	33·01
		1·0	8·14	0·01	8·15	0·17	8·32
	2·5	0	42·24	0·42	42·66	0·95	43·61
		0·5	27·23	0·20	27·43	0·57	28·00
		1·0	8·08	0·03	8·11	0·12	8·23
	5·0	0	30·40	1·43	31·83	1·52	33·35
		0·5	20·72	0·68	21·40	1·01	27·41
		1·0	7·90	0·14	8·04	0·33	8·37
10^8	1·5	0	33·82	0·05	33·87	1·27	35·14
		0·5	19·92	0·02	19·94	0·73	20·67
		1·0	2·57	0	2·57	0·05	2·62
	2·5	0	27·42	0·19	27·61	0·64	28·25
		0·5	16·36	0·06	16·42	0·37	16·79
		1·0	2·56	0	2·56	0·04	2·60
	5·0	0	18·17	0·62	18·79	0·95	19·74
		0·5	11·22	0·19	11·41	0·39	11·80
		1·0	2·50	0·01	2·51	0·10	2·61
(b)	$\alpha = 10°$						
10^6	1·5	0	71·10	0·24	71·34	13·79	85·13
		0·5	51·26	0·17	51·43	9·31	60·74
		1·0	23·65	0·08	23·73	3·48	27·21
	2·5	0	68·08	1·03	69·11	5·97	75·08
		0·5	50·40	0·75	51·15	3·93	55·08
		1·0	24·95	0·37	25·32	1·40	26·72
	5·0	0	61·94	4·26	66·20	9·42	75·62
		0·5	48·88	3·22	52·10	7·25	59·35
		1·0	27·84	1·62	29·46	3·76	33·22

Continued/

Table 4 (contd)

(b) $\alpha = 10^{\circ}$

R_0	M_0	$\bar{x}_T/c$	$10^4 C_{F_1}$	$10^4 \Delta C_F$	$10^4 C_{F_2}$	$10^4 \Delta C_{Dp}$	$10^4 C_{DB}$
10^8	1·5	0	31·46	0·05	31·51	6·38	37·89
		0·5	18·52	0·02	18·54	3·69	22·23
		1·0	2·37	0	2·37	0·35	2·72
	2·5	0	28·68	0·20	28·88	2·61	31·49
		0·5	17·03	0·06	17·09	1·50	18·59
		1·0	2·50	0	2·50	0·13	2·63
	5·0	0	21·78	0·74	22·52	3·72	26·24
		0·5	13·34	0·23	13·57	2·25	15·82
		1·0	2·78	0·01	2·79	0·38	3·17

FIG. 1.

$$\frac{\Delta C_F}{C_{F_1}} = k\,(M_0)\; l\left(\frac{\bar{x}_T}{c}, \frac{t}{c}\right) \cdot m\left(\frac{\bar{x}_T}{c}, R_0\right)$$

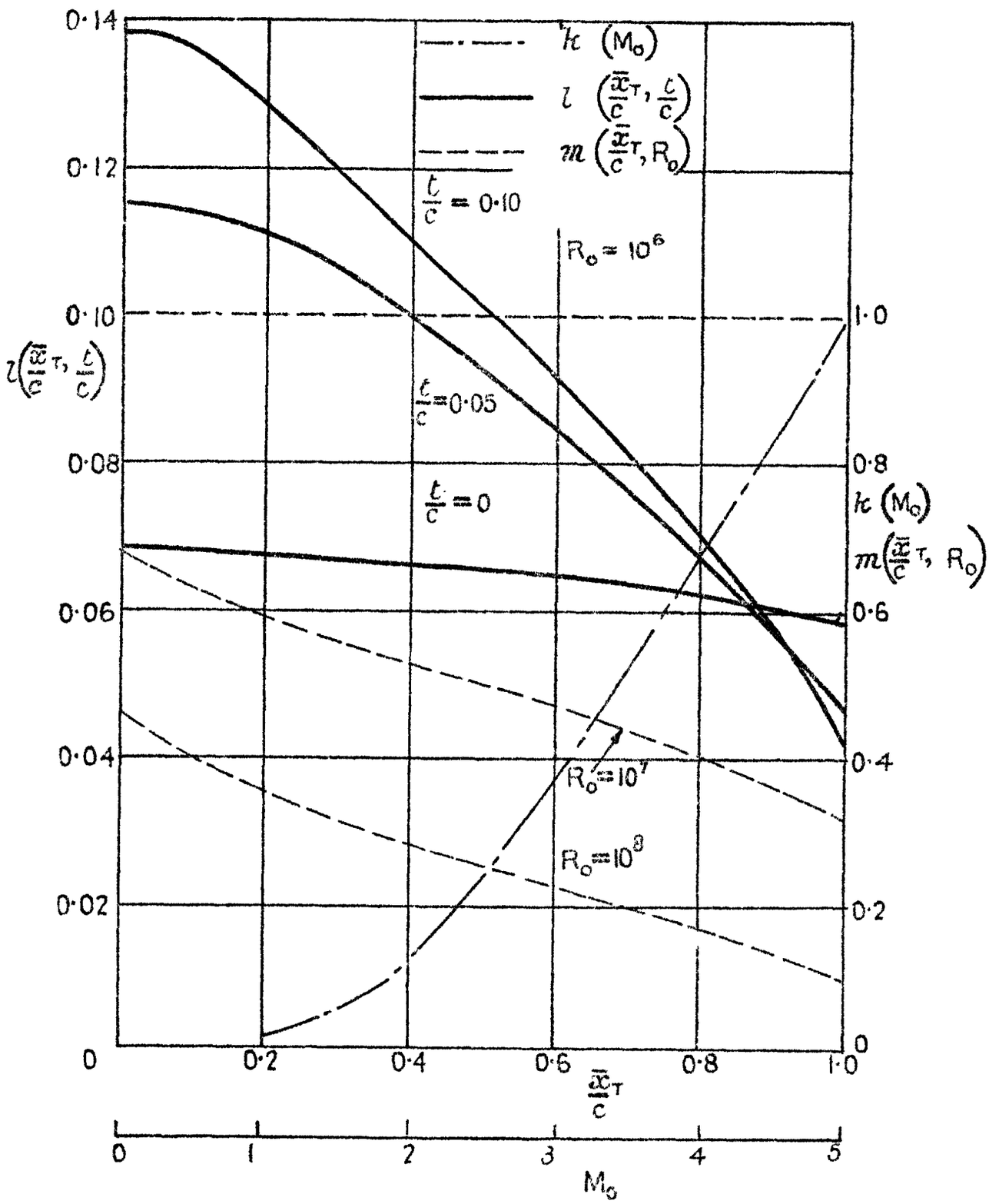

Second stage correction for skin friction on biconvex wings as function of Mach number, Reynolds number, transition position and thickness

Fig. 2.

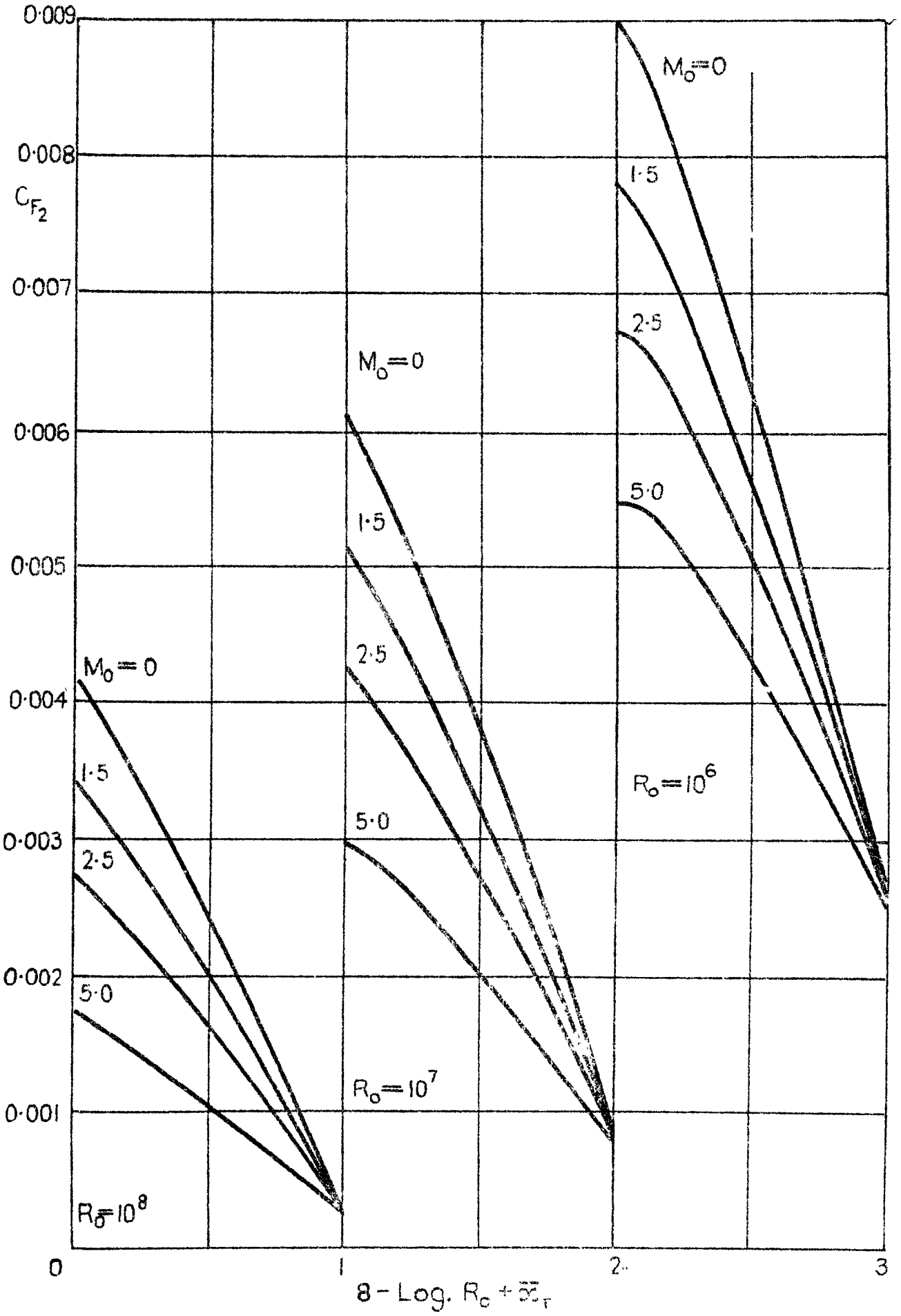

Skin friction coefficient for flat plate, corrected for displacement thickness effect

FIG. 3.

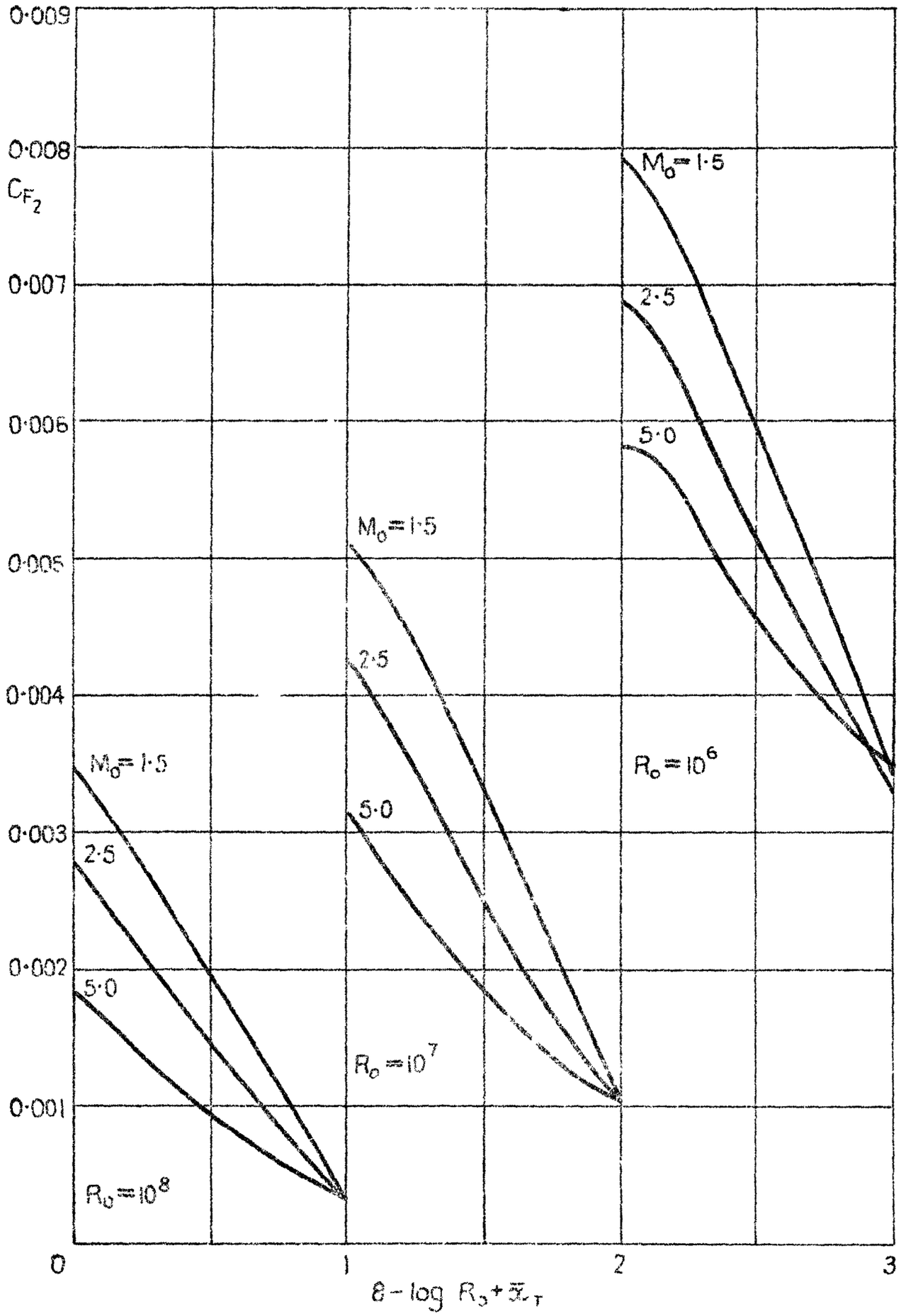

Skin friction coefficient for biconvex wings corrected for displaced thickness effect. $t/c = 0·05$.

FIG. 4.

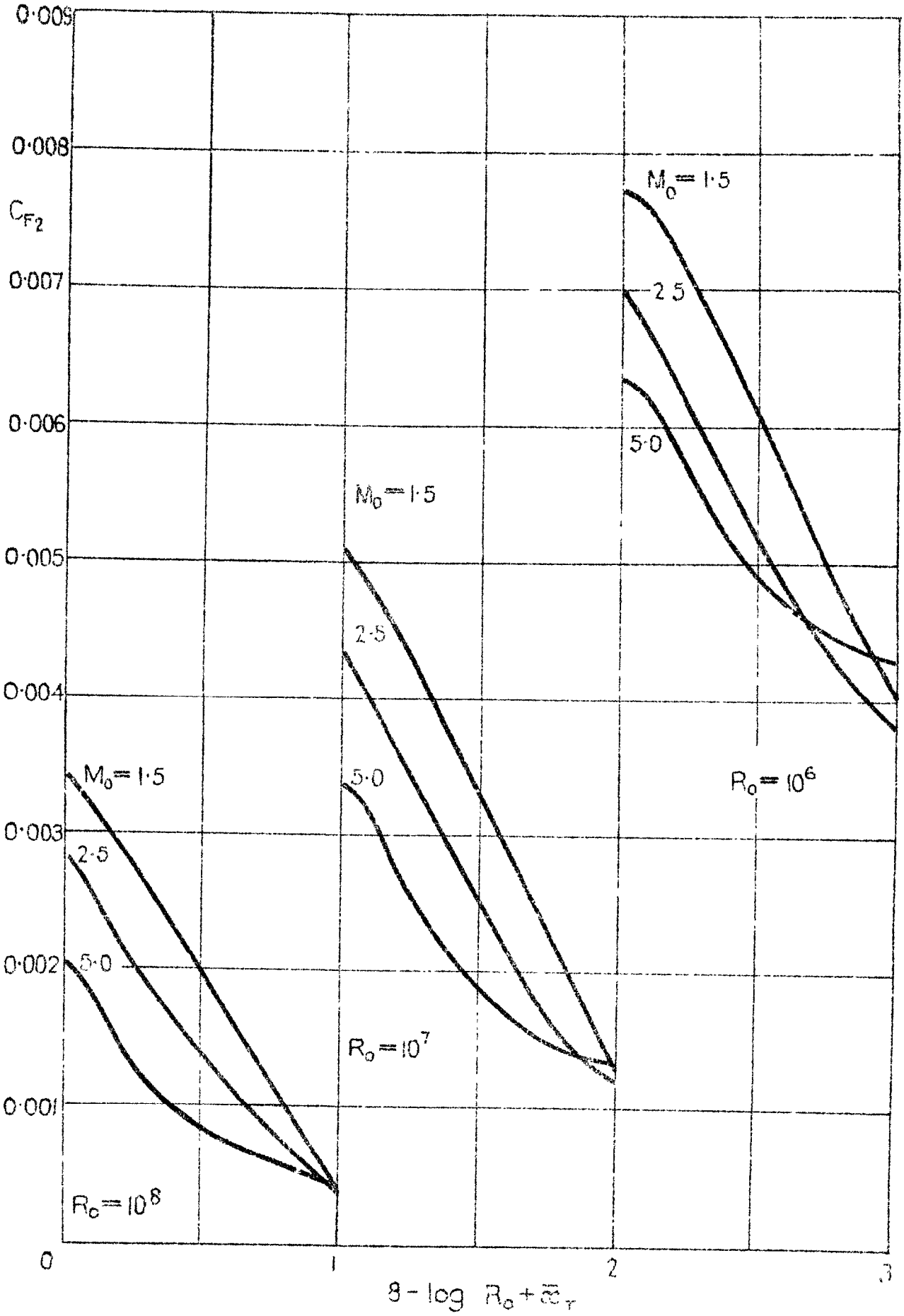

Skin friction coefficient for biconvex wings corrected for displacement thickness effect $t/c = 0·10$

FIG. 5.

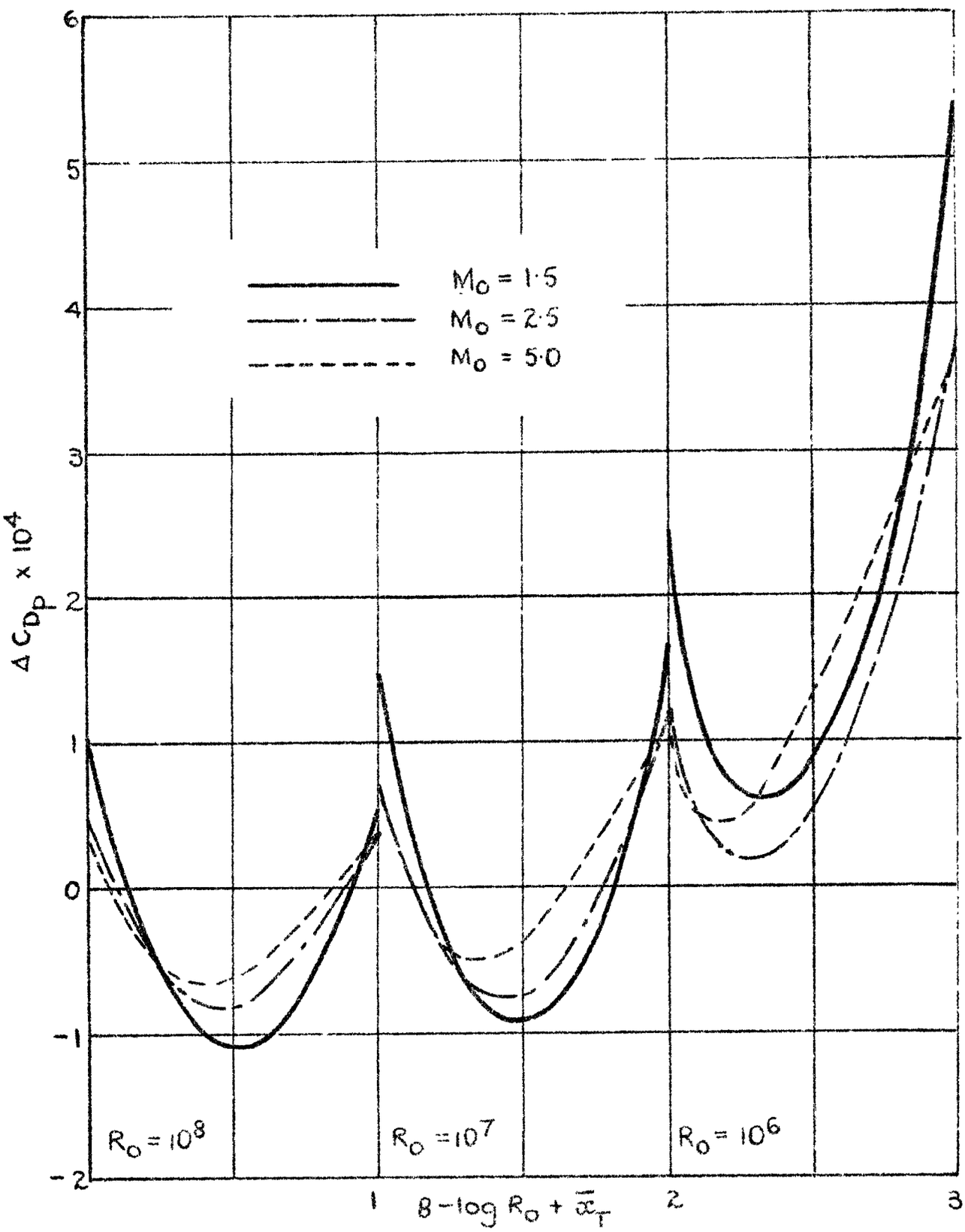

Boundary layer pressure drag coefficient for biconvex wings t/c = 0.05

FIG. 6.

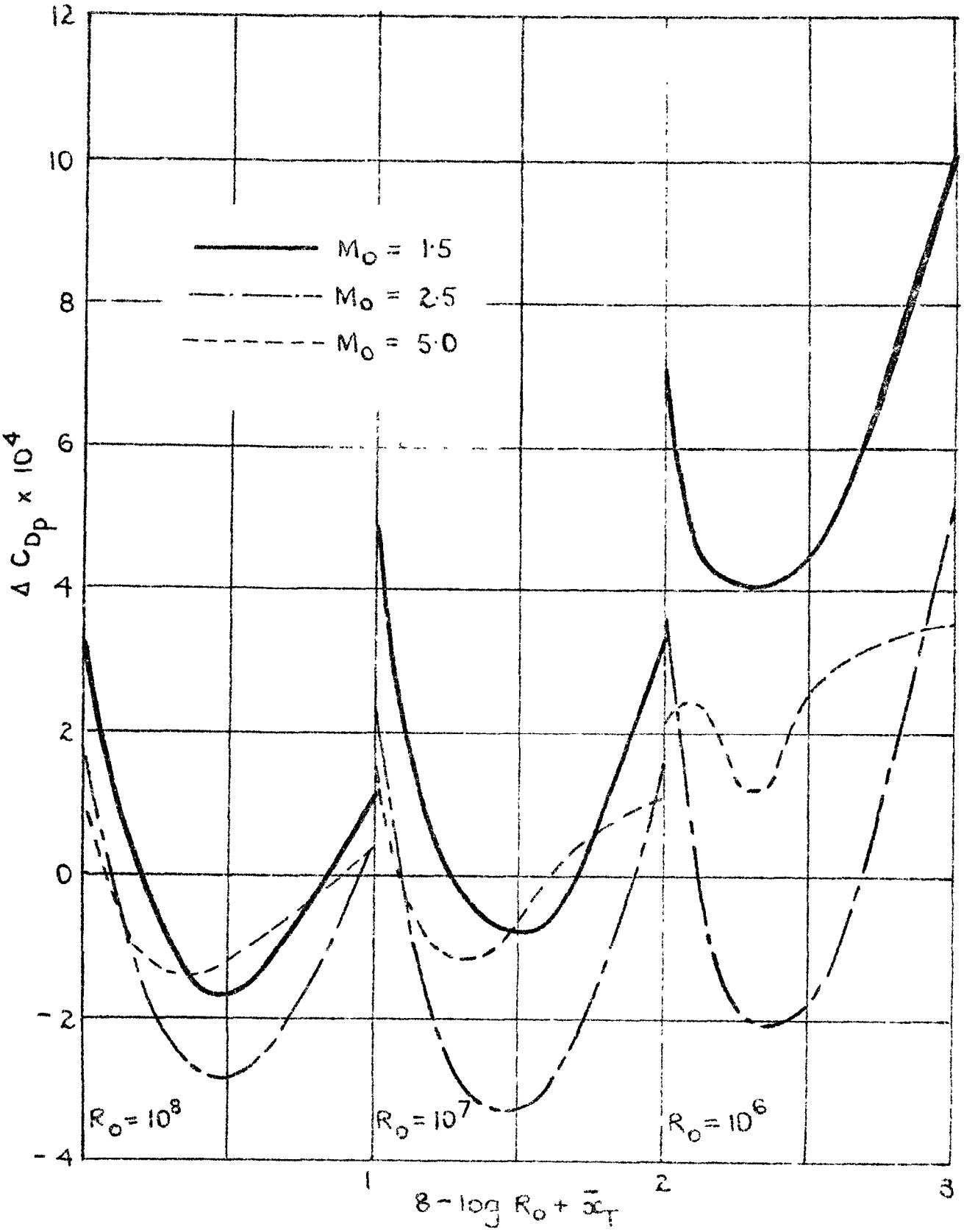

Boundary layer pressure drag coefficient for biconvex wings. $t/c = 0.10$

FIG. 7.

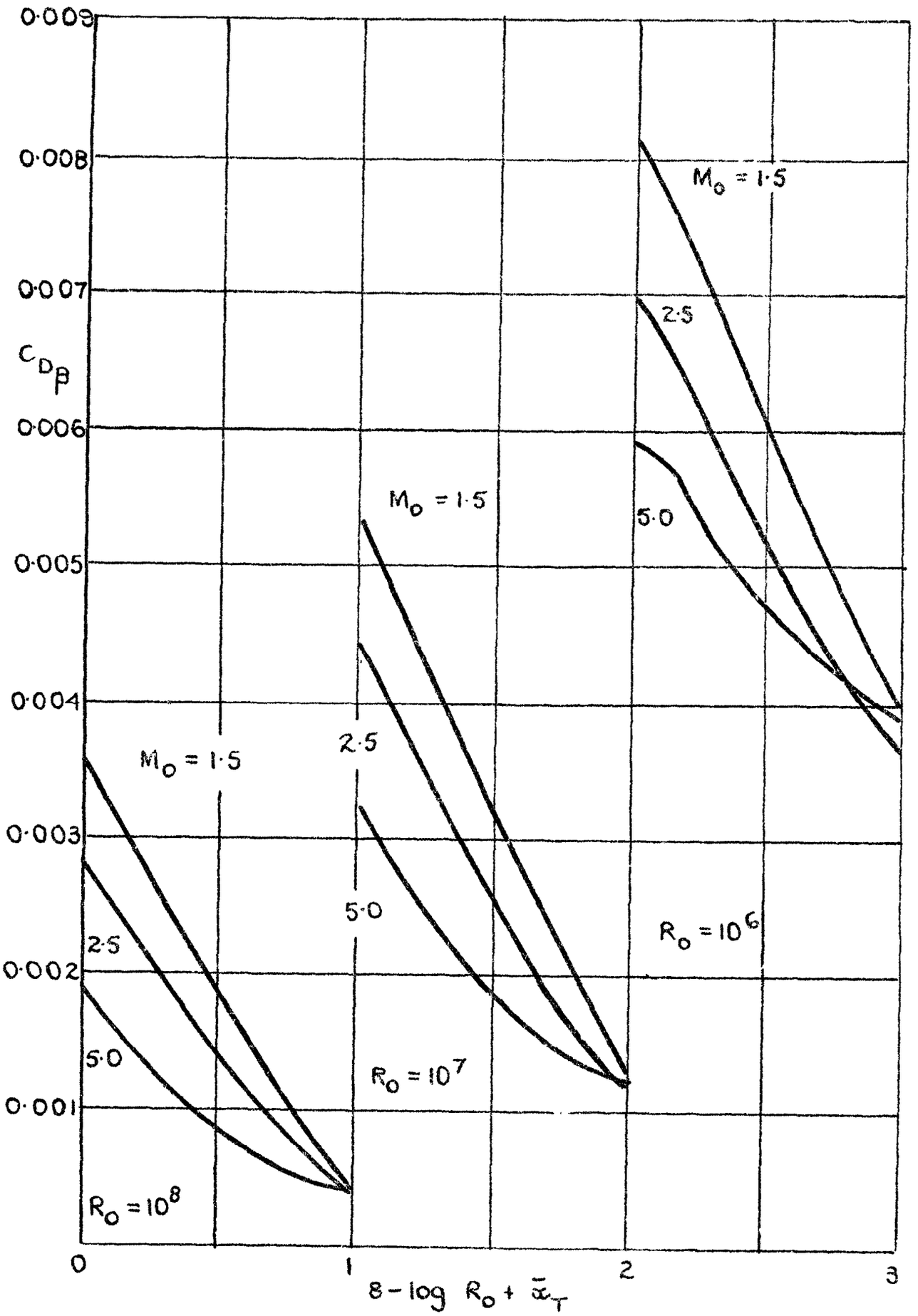

Total boundary layer drag of biconvex wing of t/c = 0·05.

FIG. 8.

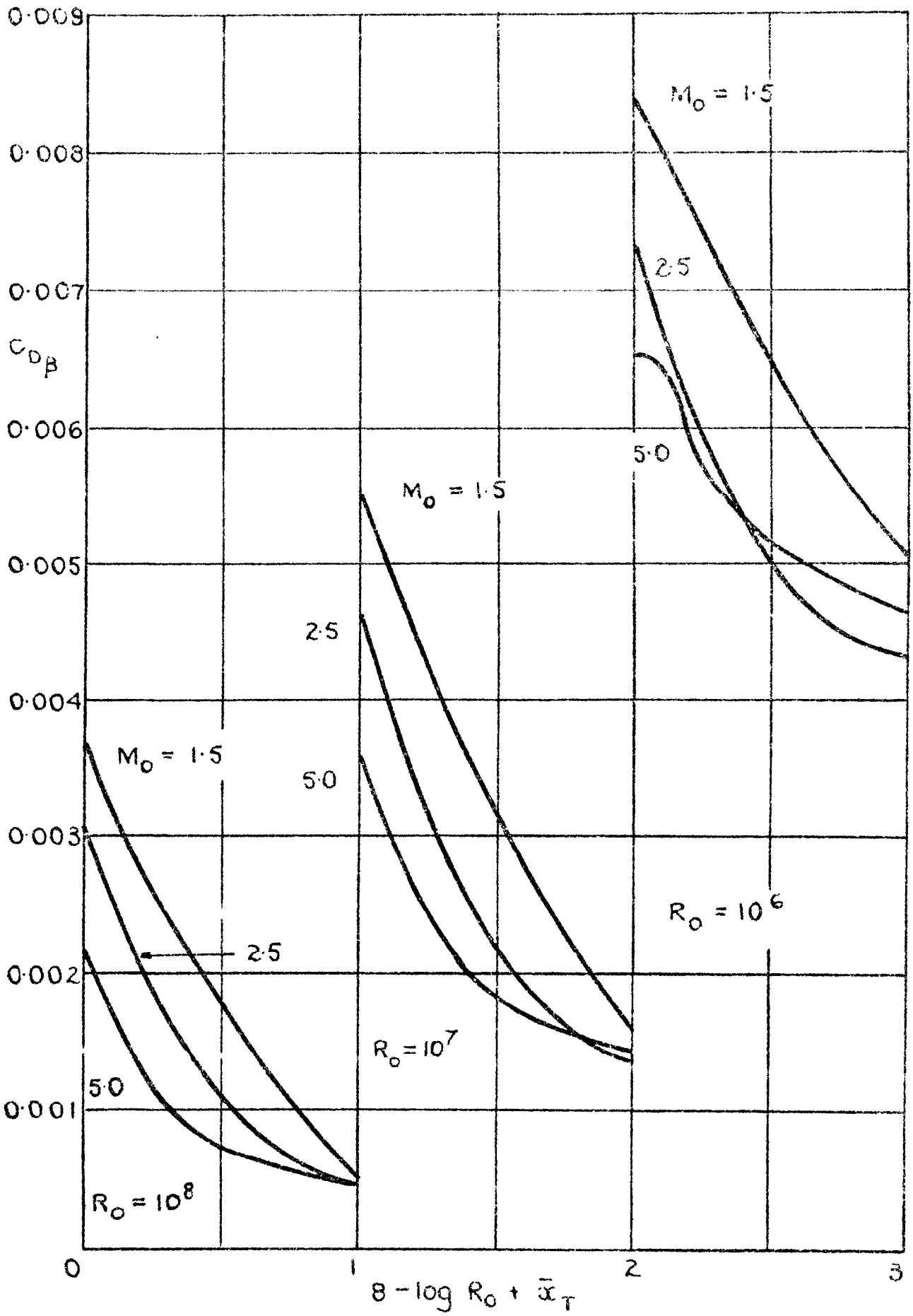

Total boundary layer drag of biconvex wing of t/c = 0·10

FIG 9.

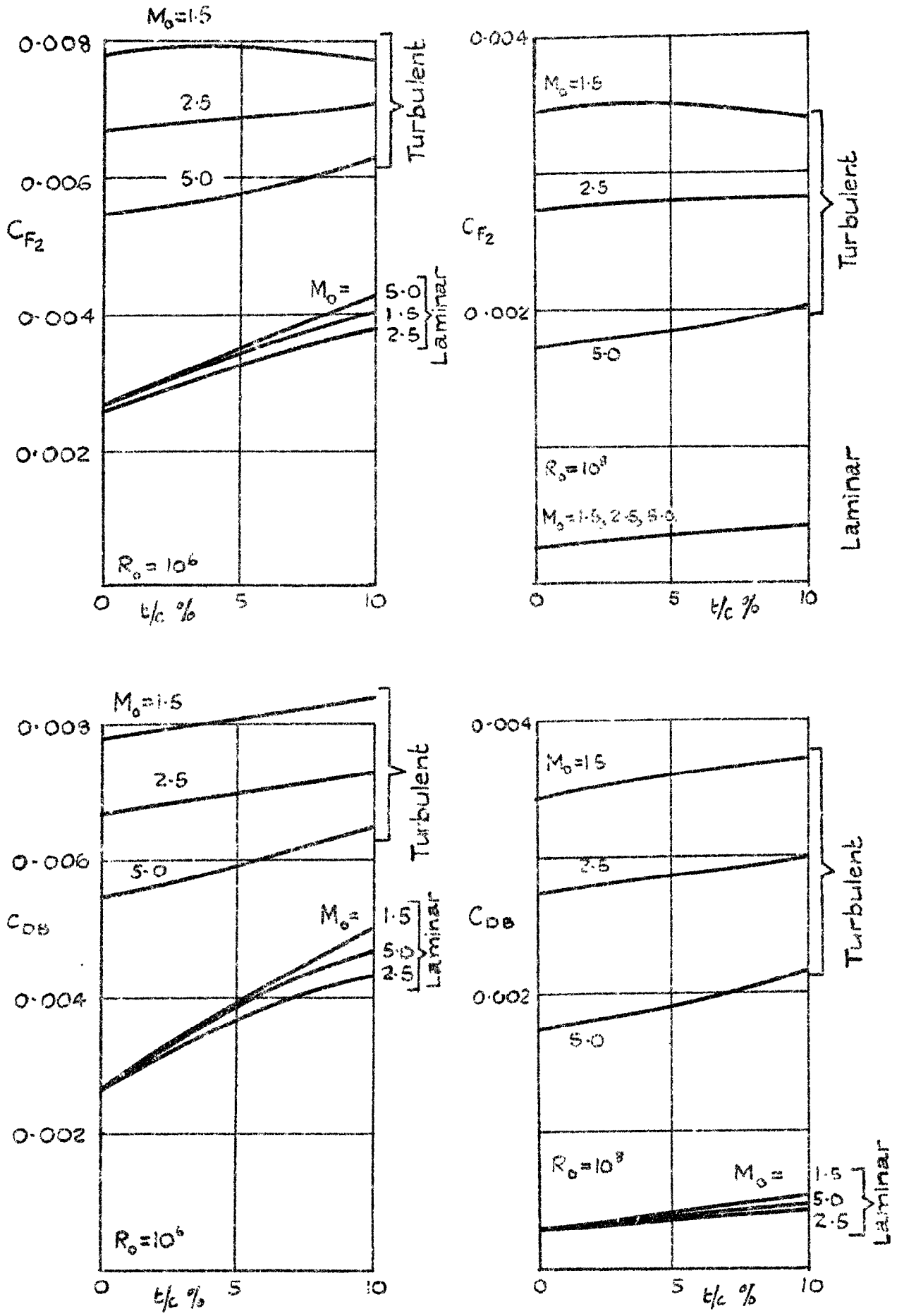

Skin friction and profile drag coefficients for biconvex wings as functions of thickness chord ratio. ($R_0 = 10^6$ and 10^8), corrected for displacement thickness effect.

FIG 10.

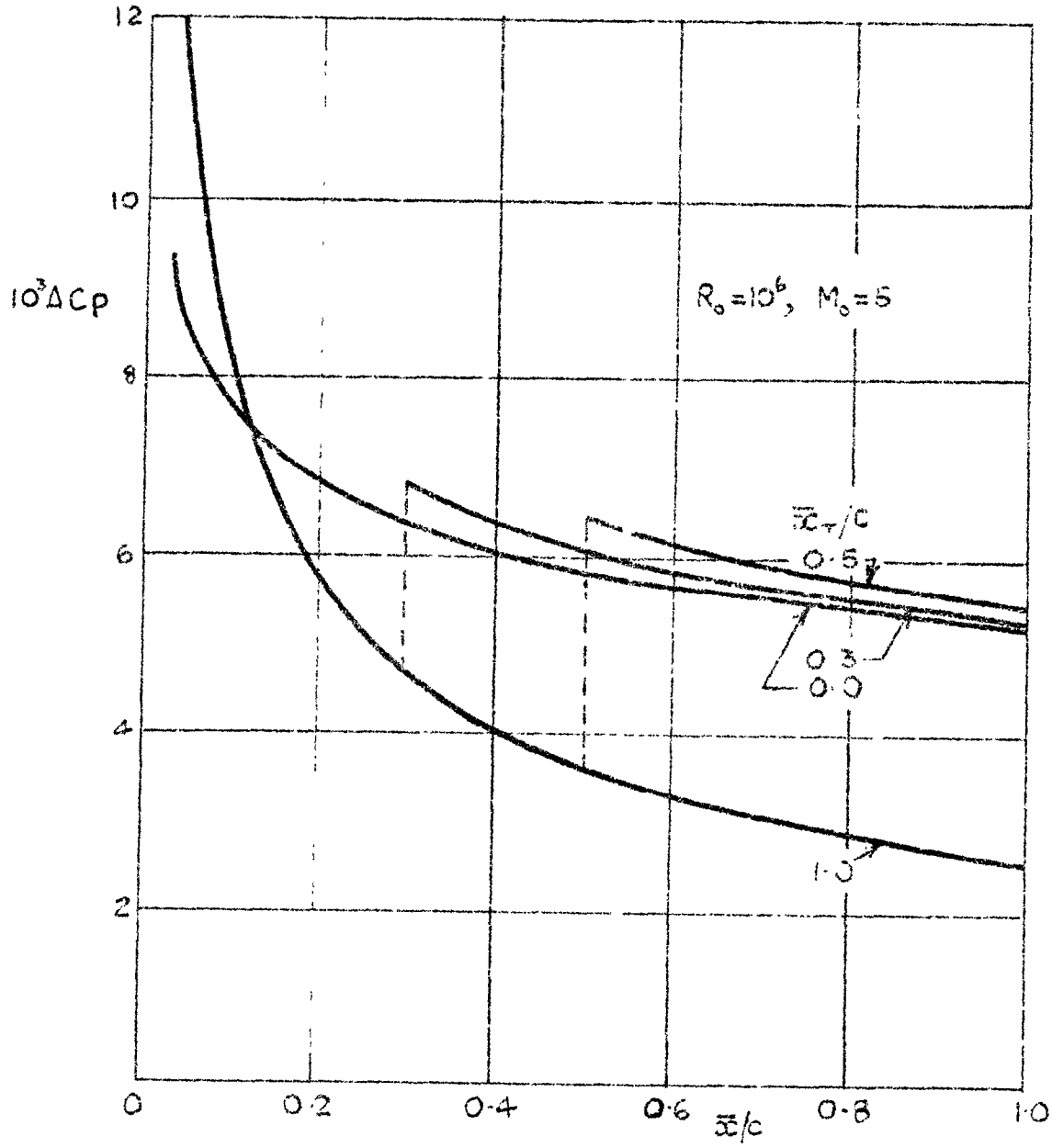

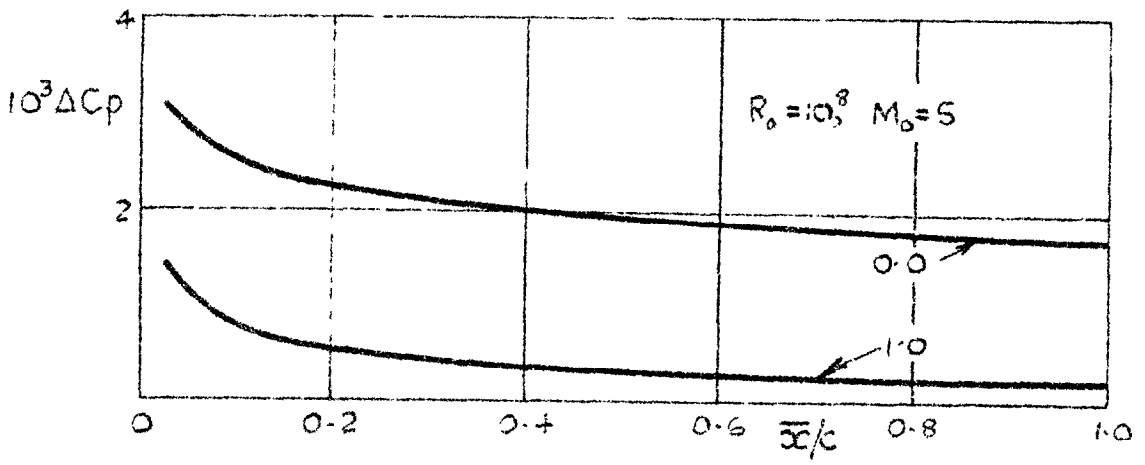

Increment in pressure coefficient on flat plate due to displacement thickness effect at $M_0 = 5$.

FIG 11.

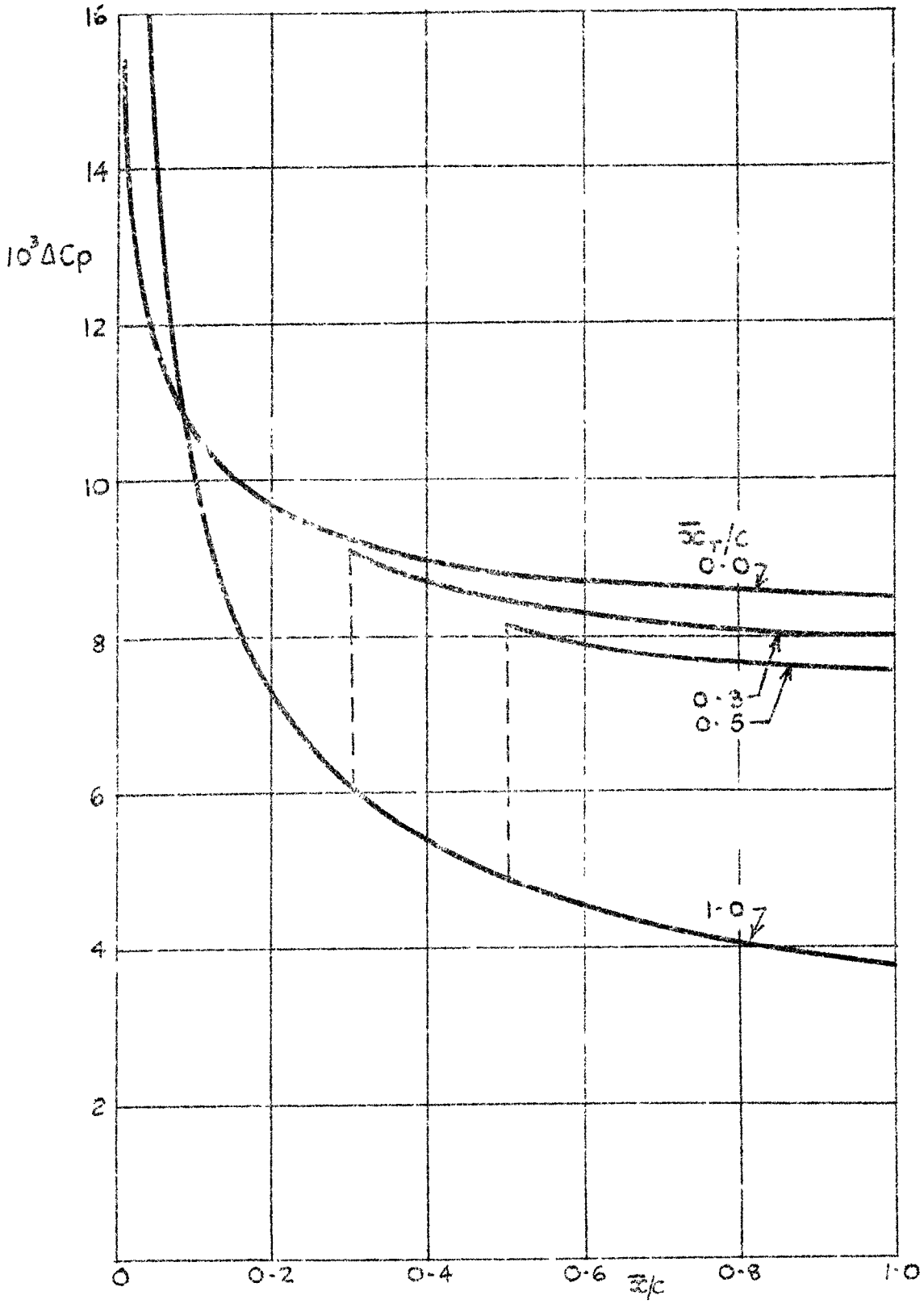

Increment in pressure coefficient on biconvex wing due to displacement thickness effect, t/c=0·05, M_0=5·0, R_0=10^6

FIG. 12.

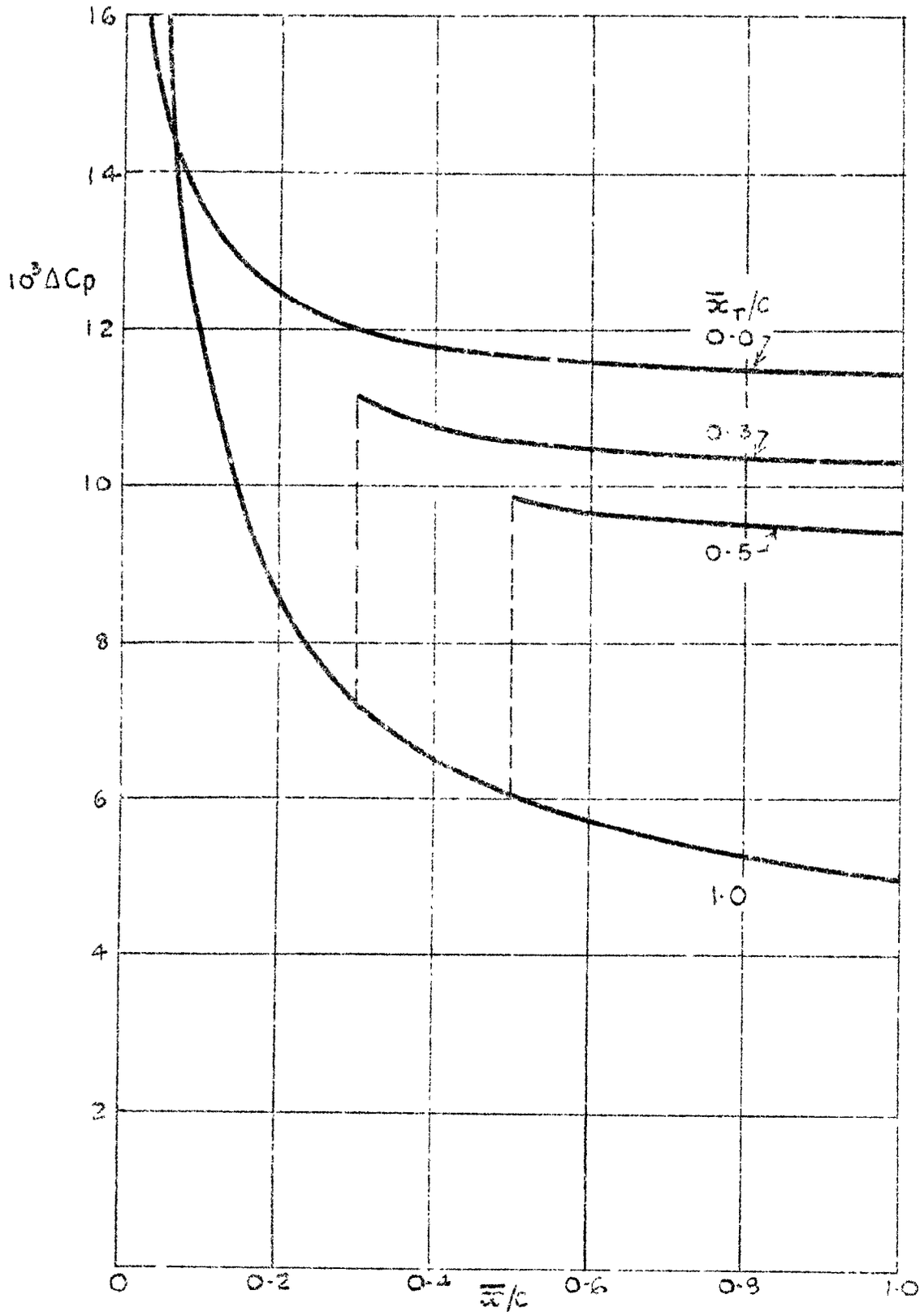

Increment in pressure coefficient on biconvex wing due to displacement thickness effect, $t/c = 0{\cdot}10$, $M_\infty = 5{\cdot}0$, $R_\infty = 10^6$.

FIG. 13.

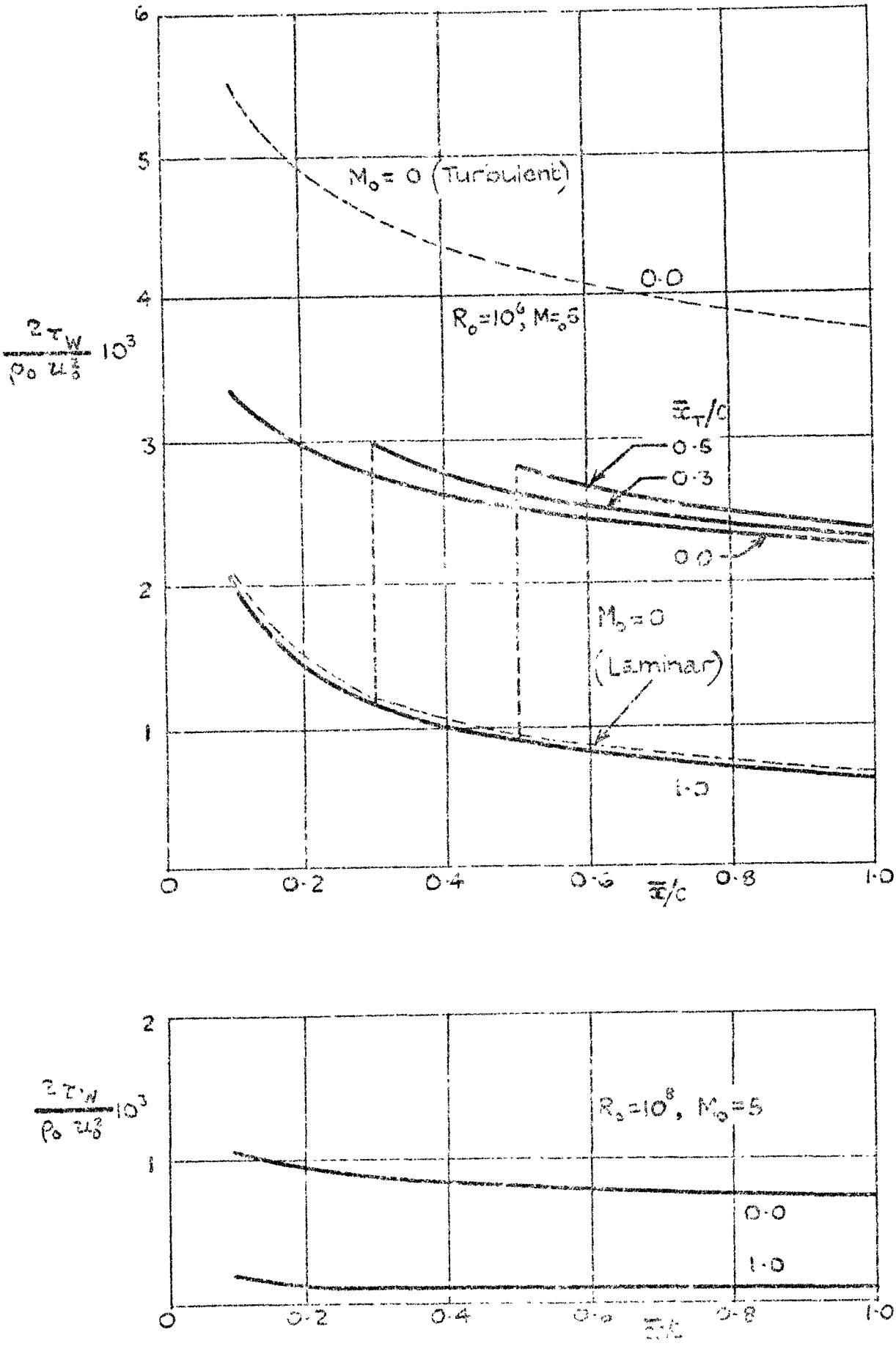

Skin friction distribution for flat plate corrected for displacement thickness effect, $M_\infty = 5$

FIG. 14.

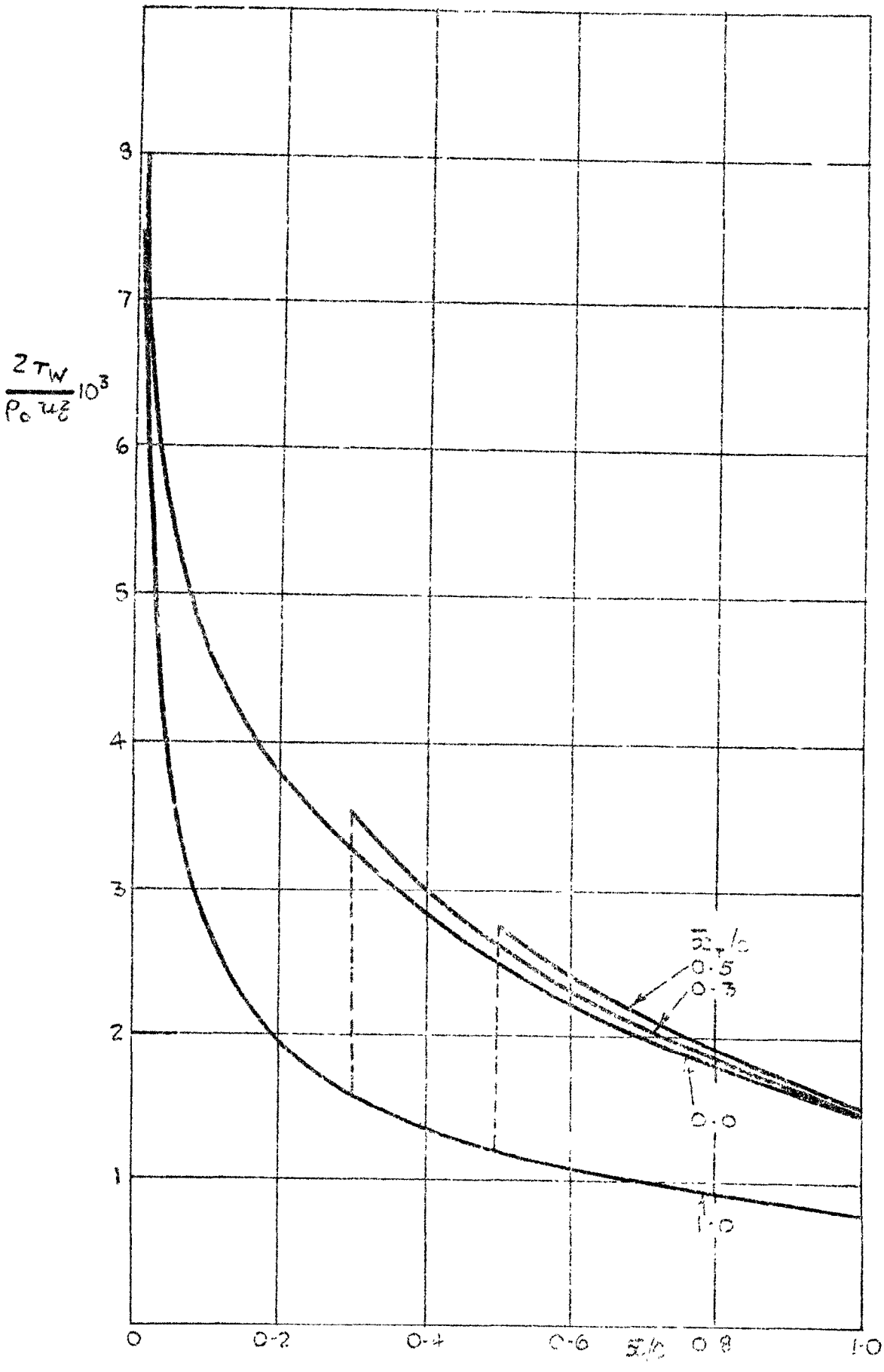

Skin friction distribution for blowing wedge corrected for displacement thickness effect. $\beta_c = 0.05$, $M_0 = 5.0$, $R_0 = 10^6$

FIG. 15

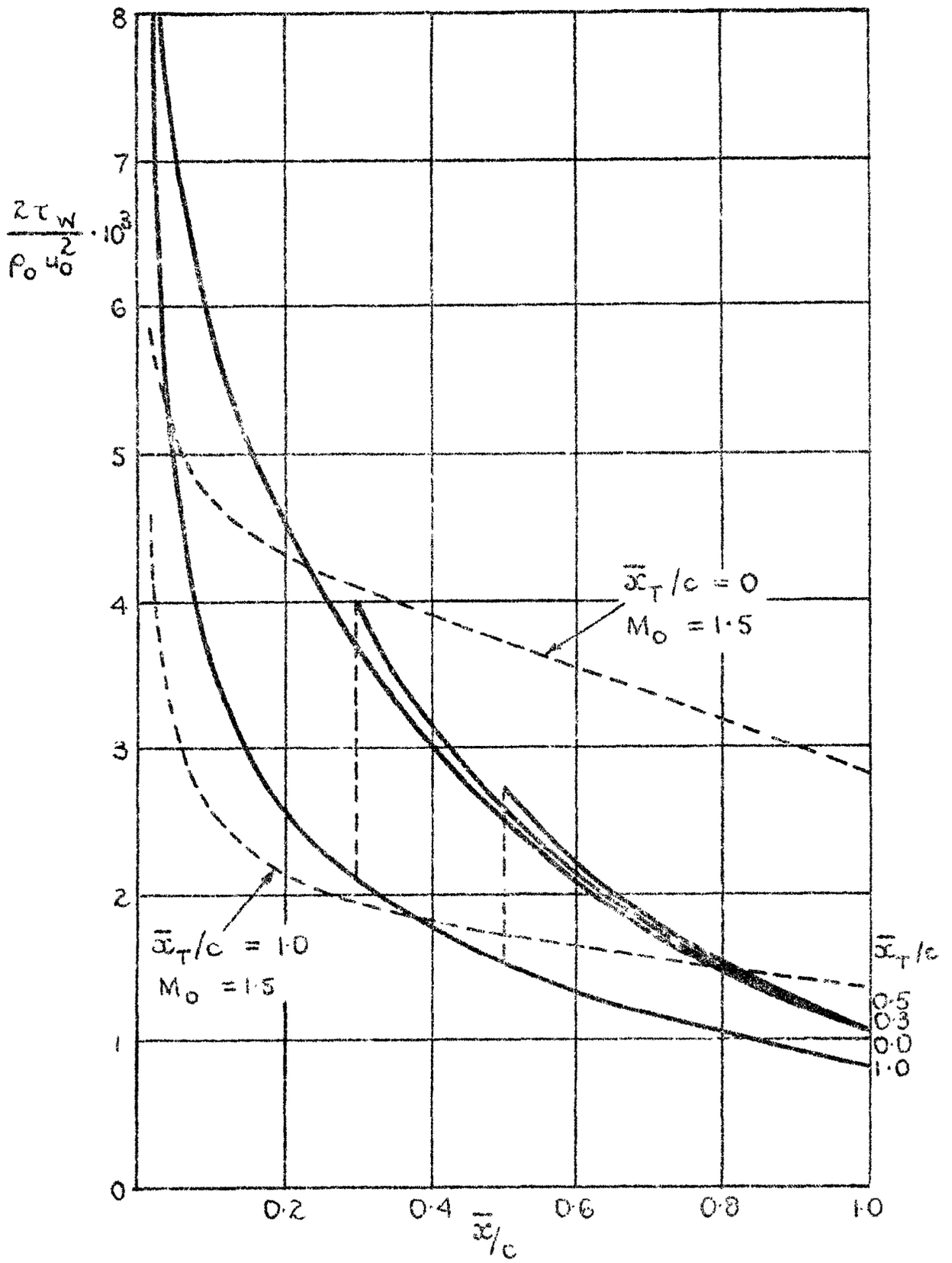

Skin friction distribution for biconvex wings corrected for displacement thickness effect $t/c = 0·10$, $M_0 = 5·0$, $R_0 = 10^6$

Fig 16

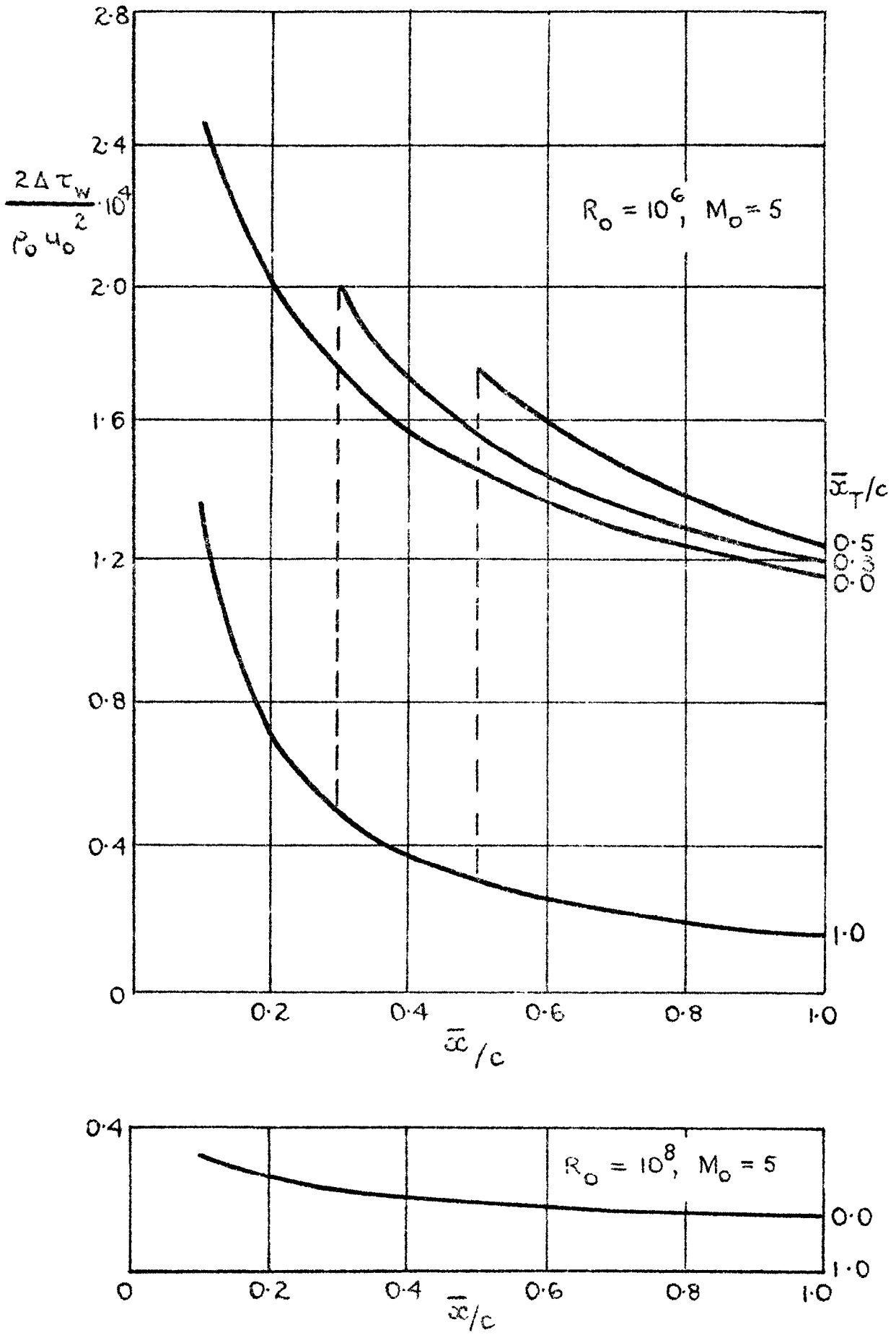

Increment in skin friction coefficient on flat plate due to displacement thickness effect. $M_0 = 5$.

FIG. 17.

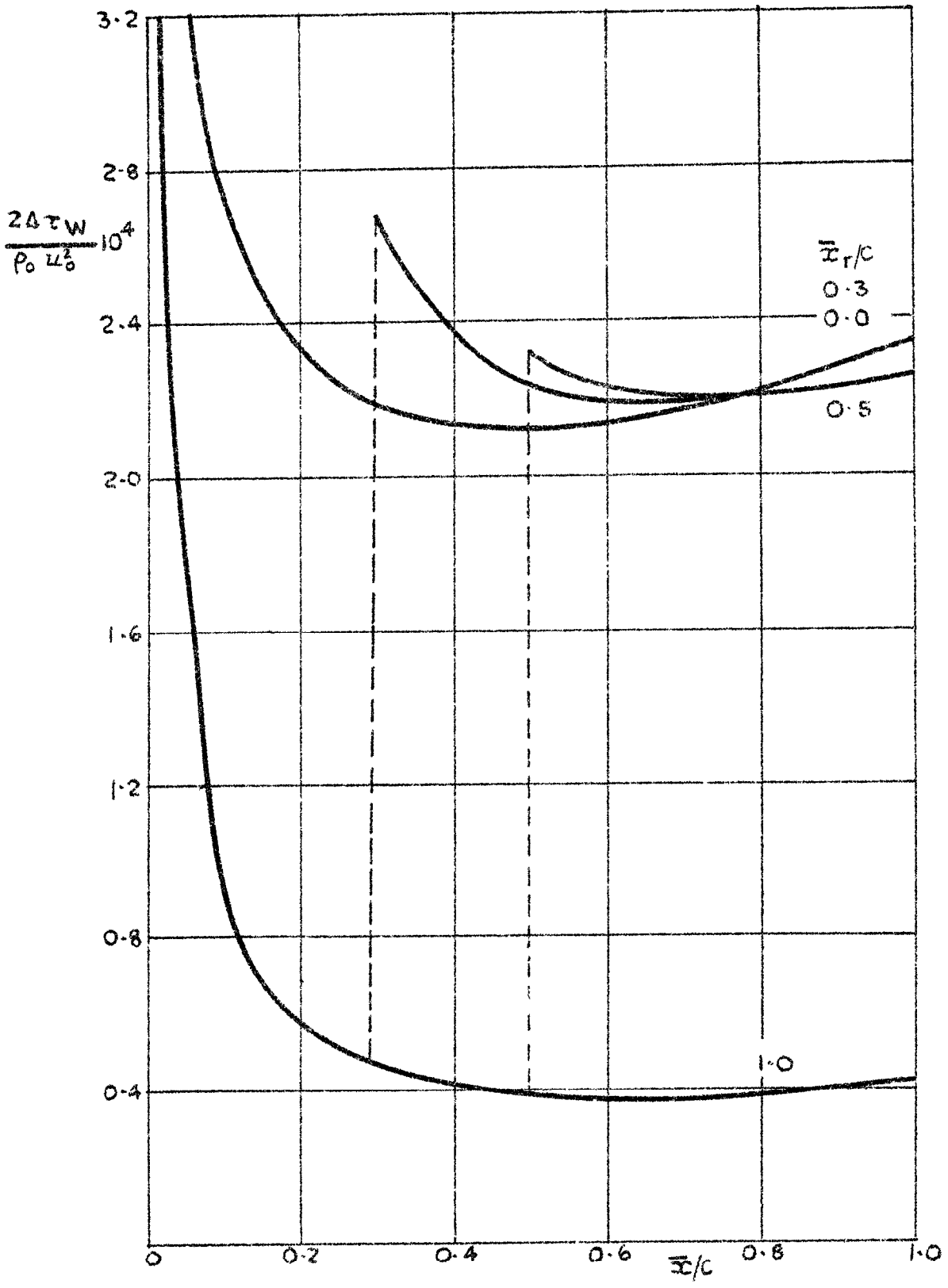

Increment in skin friction coefficient on biconvex wing due to displacement thickness effect, $t/c = 0{\cdot}05$, $M_0 = 5{\cdot}0$, $R_0 = 10^6$.

FIG. 18.

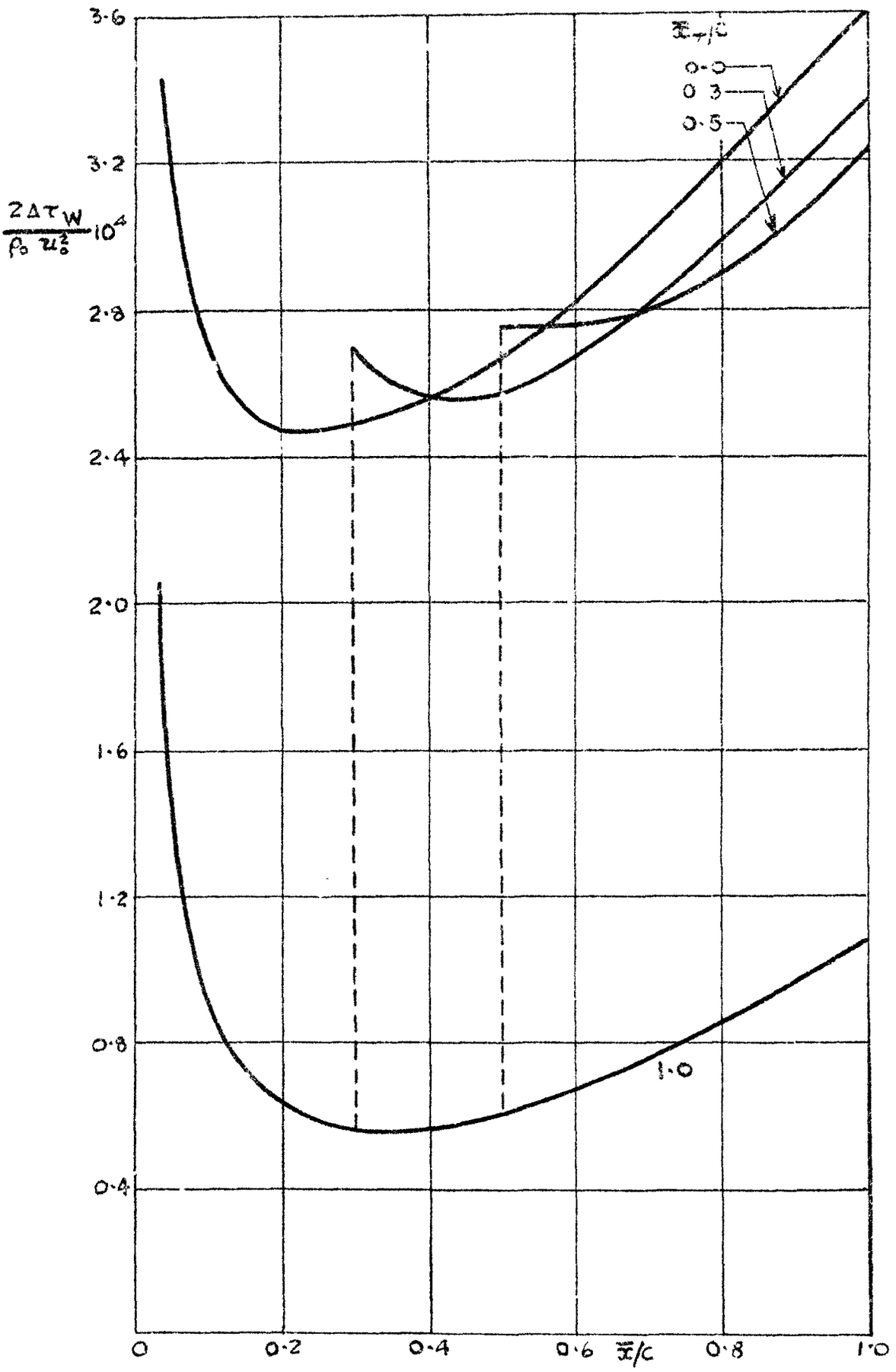

Increment in skin friction coefficient on biconvex wing due to displacement thickness effect, $t/c = 0{\cdot}10$, $M_0 = 5{\cdot}0$, $R_0 = 10^6$

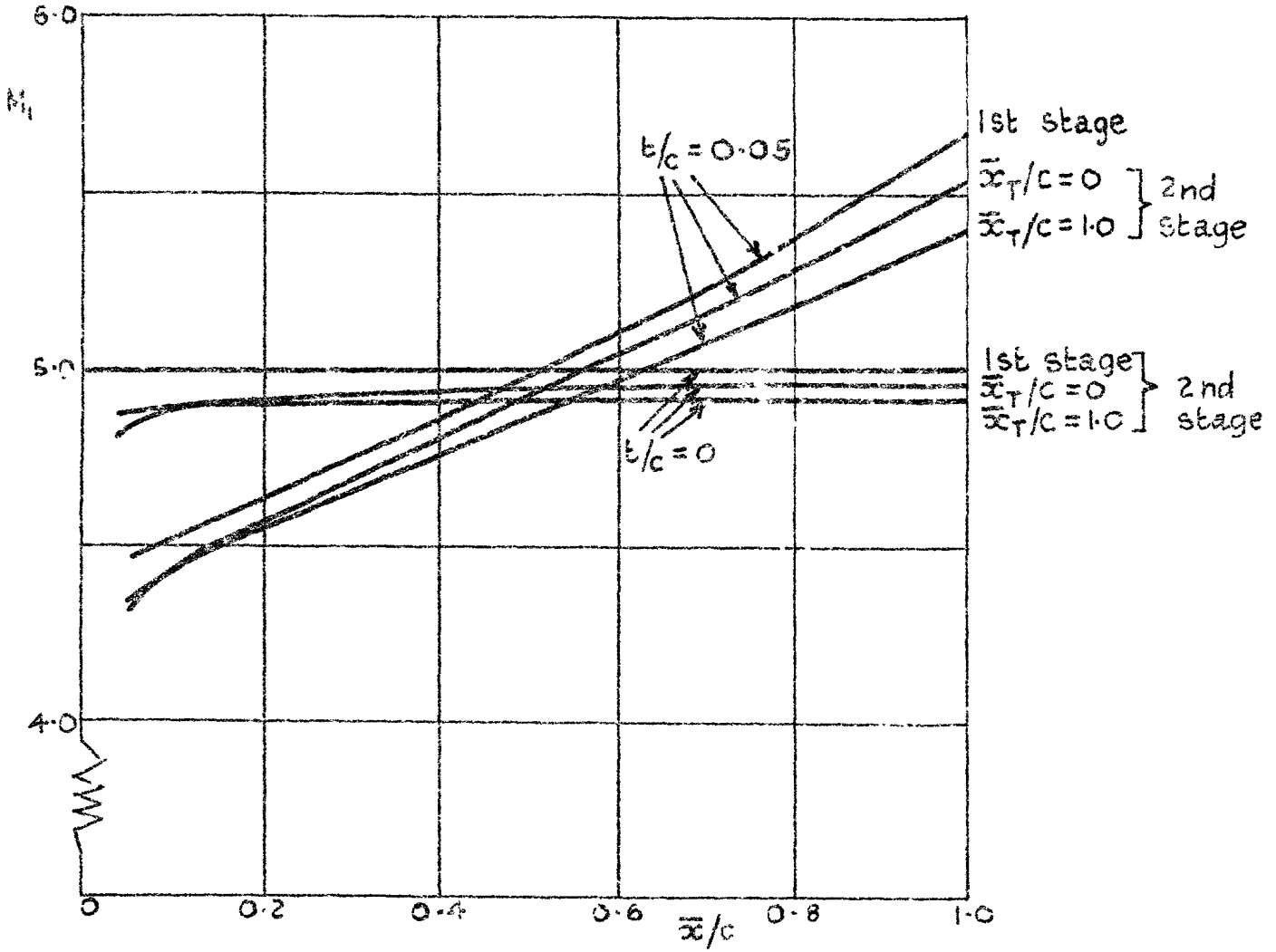

Distribution of Mach number just outside boundary layer on flat plate and biconvex wing of $t/c = 0·05$ ($M_0 = 5·0$, $R_0 = 10^6$).

Fig. 19

FIG. 20.

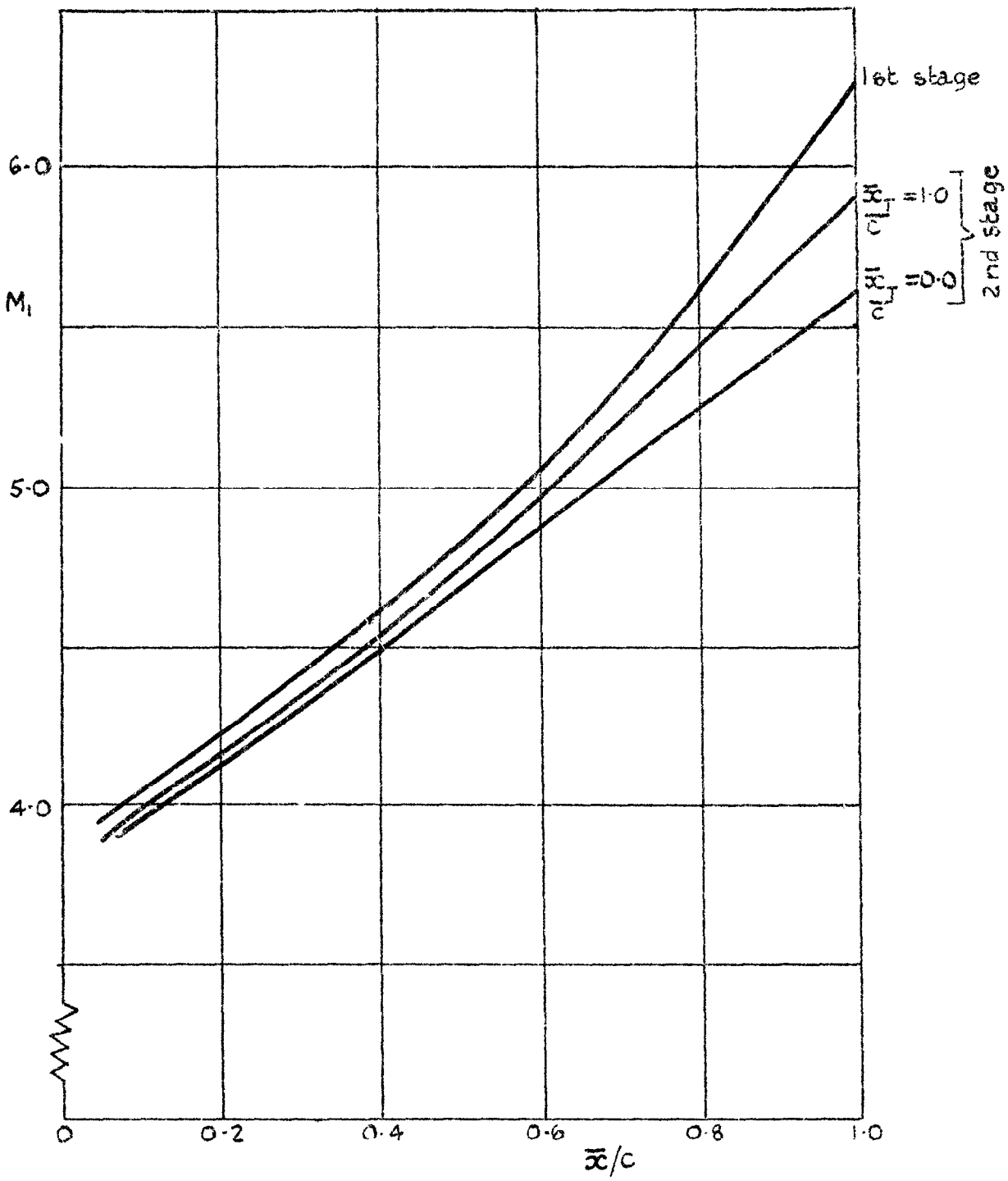

Distribution of Mach number just outside boundary layer on biconvex wing of $t/c = 0.10$ ($M = 5.0$, $R_0 = 10^6$)

FIG 21

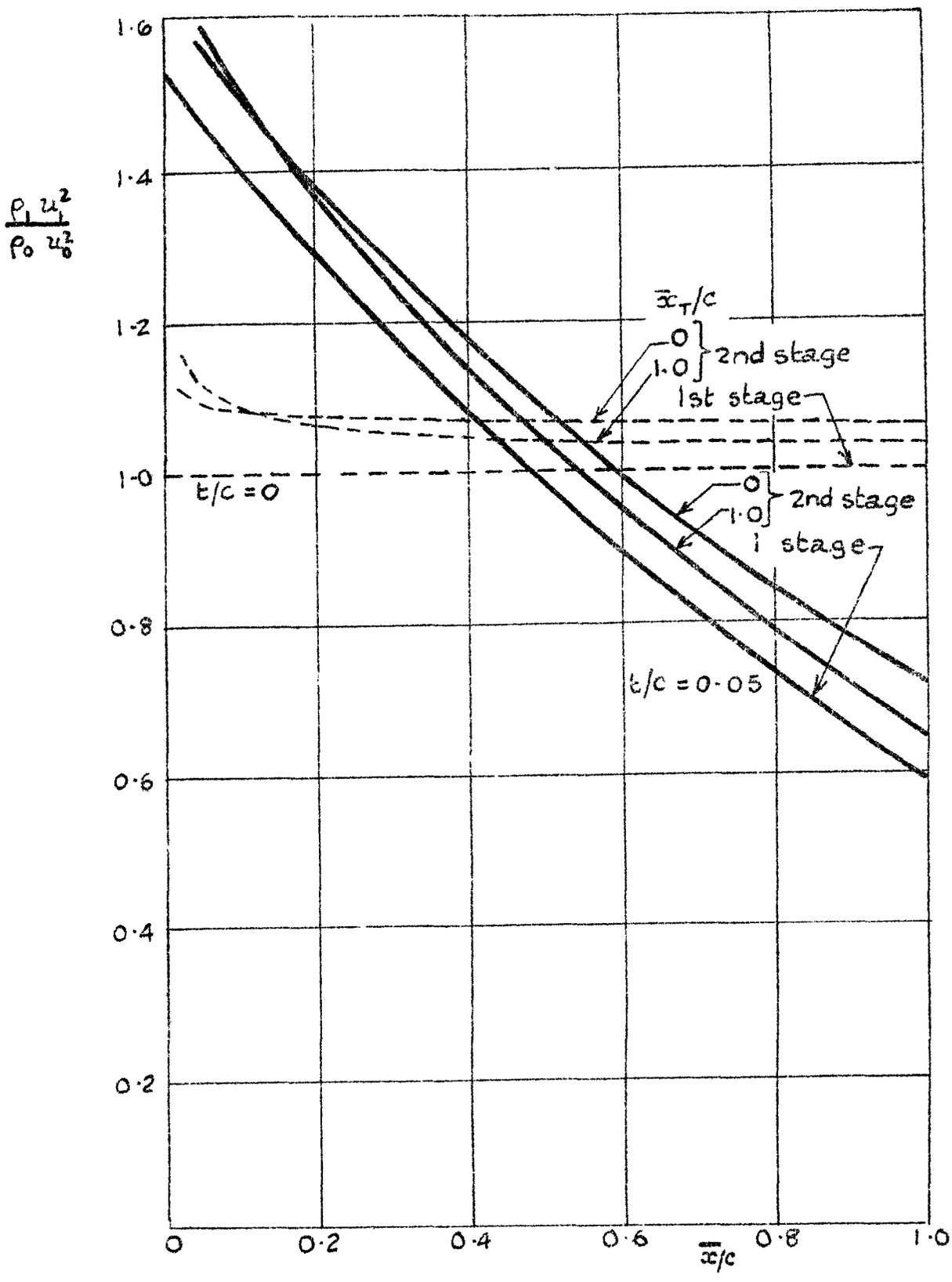

Distribution of $\rho_1 u_1^2 / \rho_0 u_0^2$ on flat plate and biconvex wing of t/c = 0·05 ($M_0 = 5$, $R_0 = 10^6$)

FIG 22.

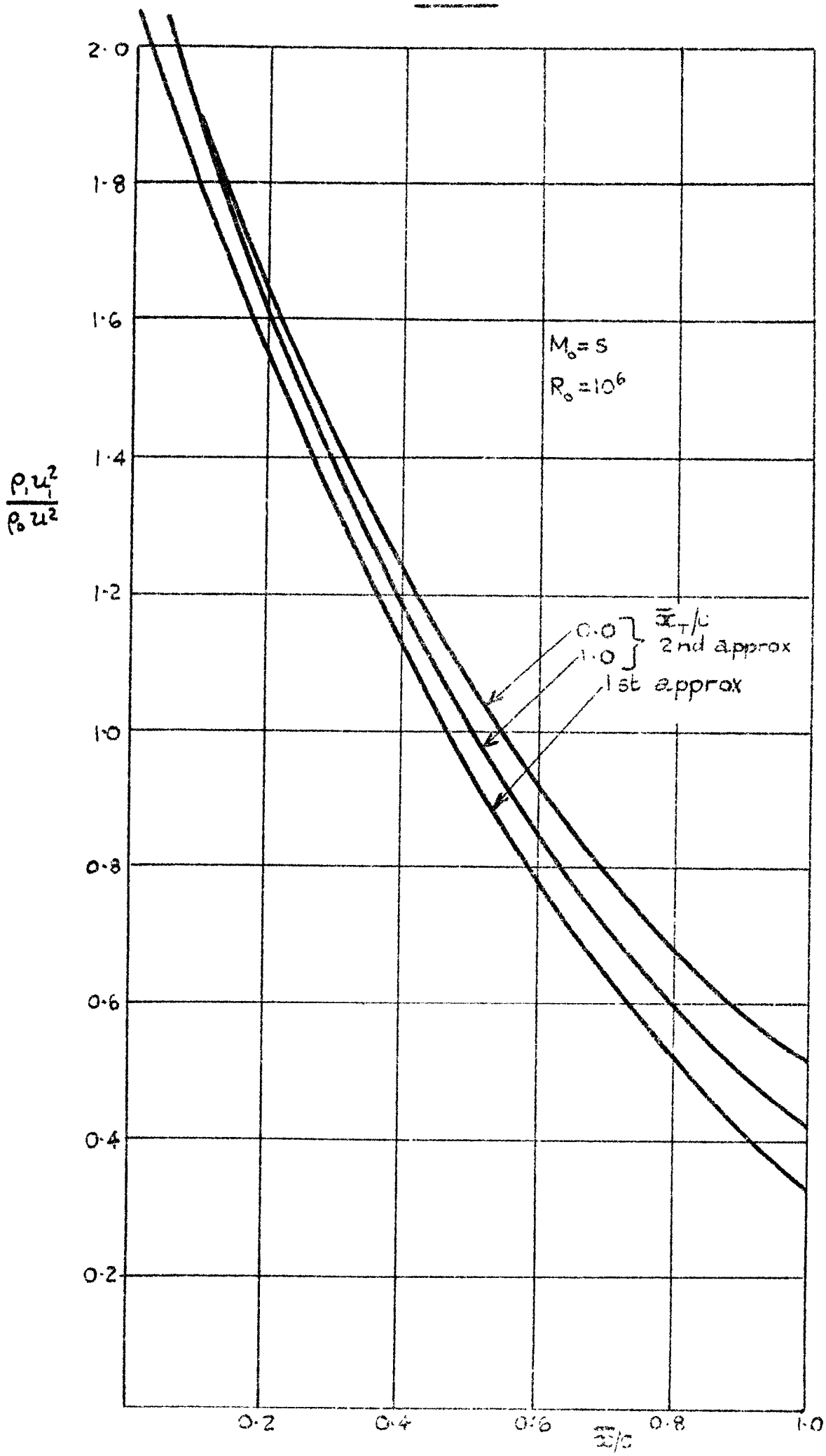

Distribution of $\frac{\rho u_1^2}{\rho_0 u_0^2}$ on biconvex wings of $t/c = 0.10$ $(M_0 = 5.0,\ R_0 = 10^6)$

FIG. 23.

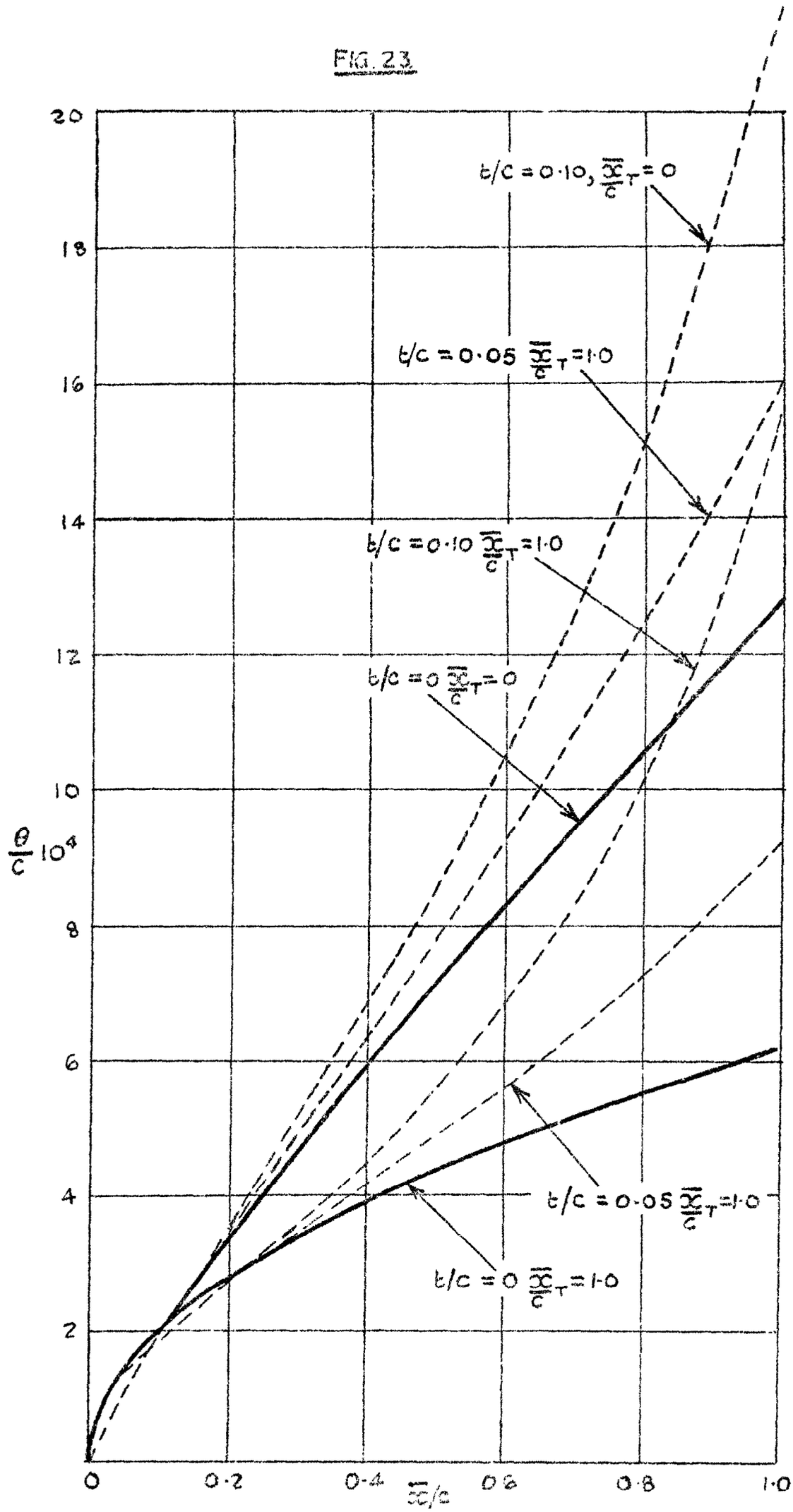

Specimen distributions of θ on flat plate and biconvex wings
($M_0 = 5{\cdot}0$, $R_0 = 10^6$)

FIG. 24

$$\frac{d}{dM}\left(\frac{\rho u^2}{\rho_0 u_0^2}\right)_{M=M_0} = \frac{2-M_0^2}{M_0\left[1+\frac{1}{2}(\gamma-1)M_0^2\right]}$$

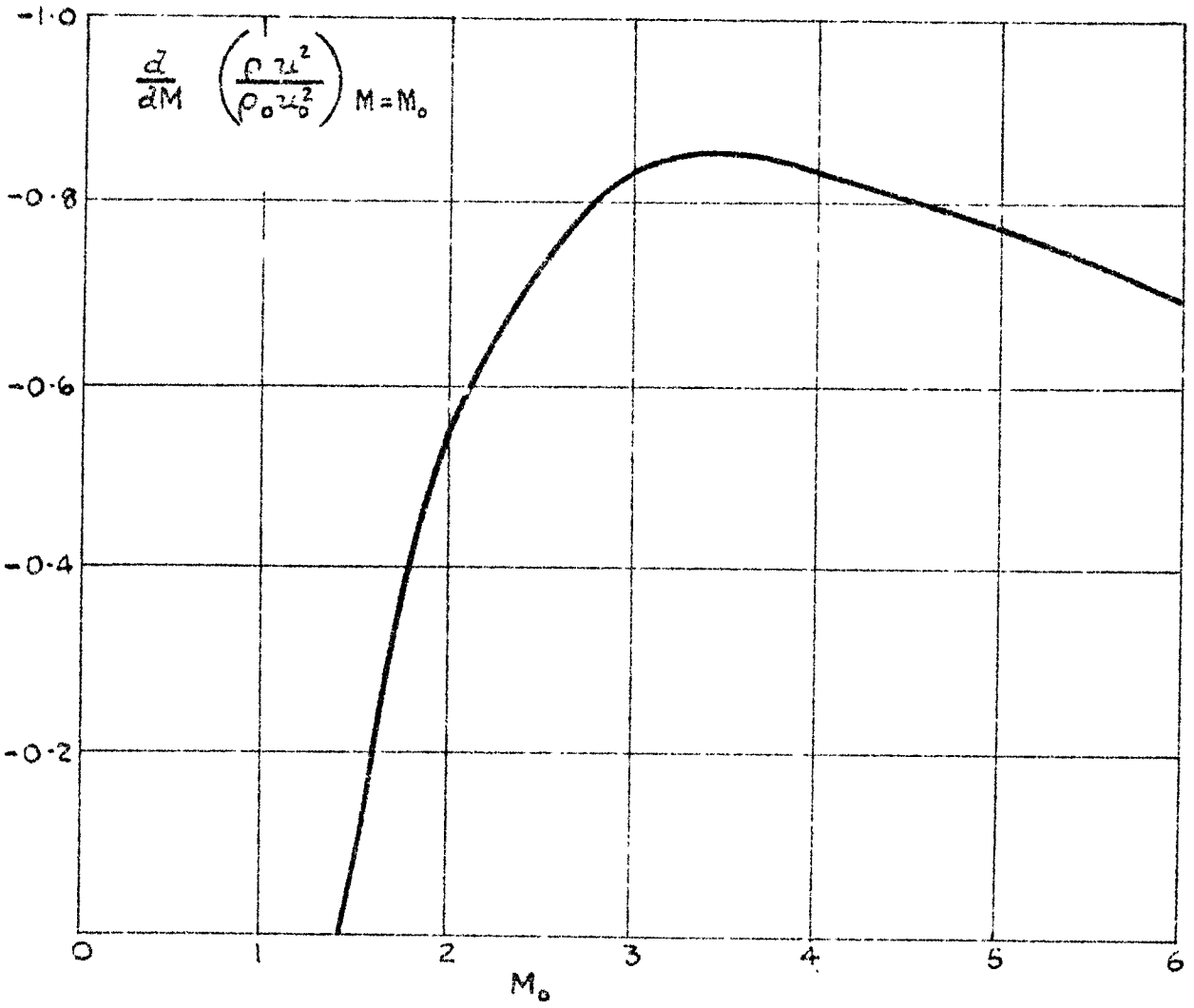

Rate of change of $\rho u^2/\rho_0 u_0^2$ with M near $M=M_0$

FIG. 25.

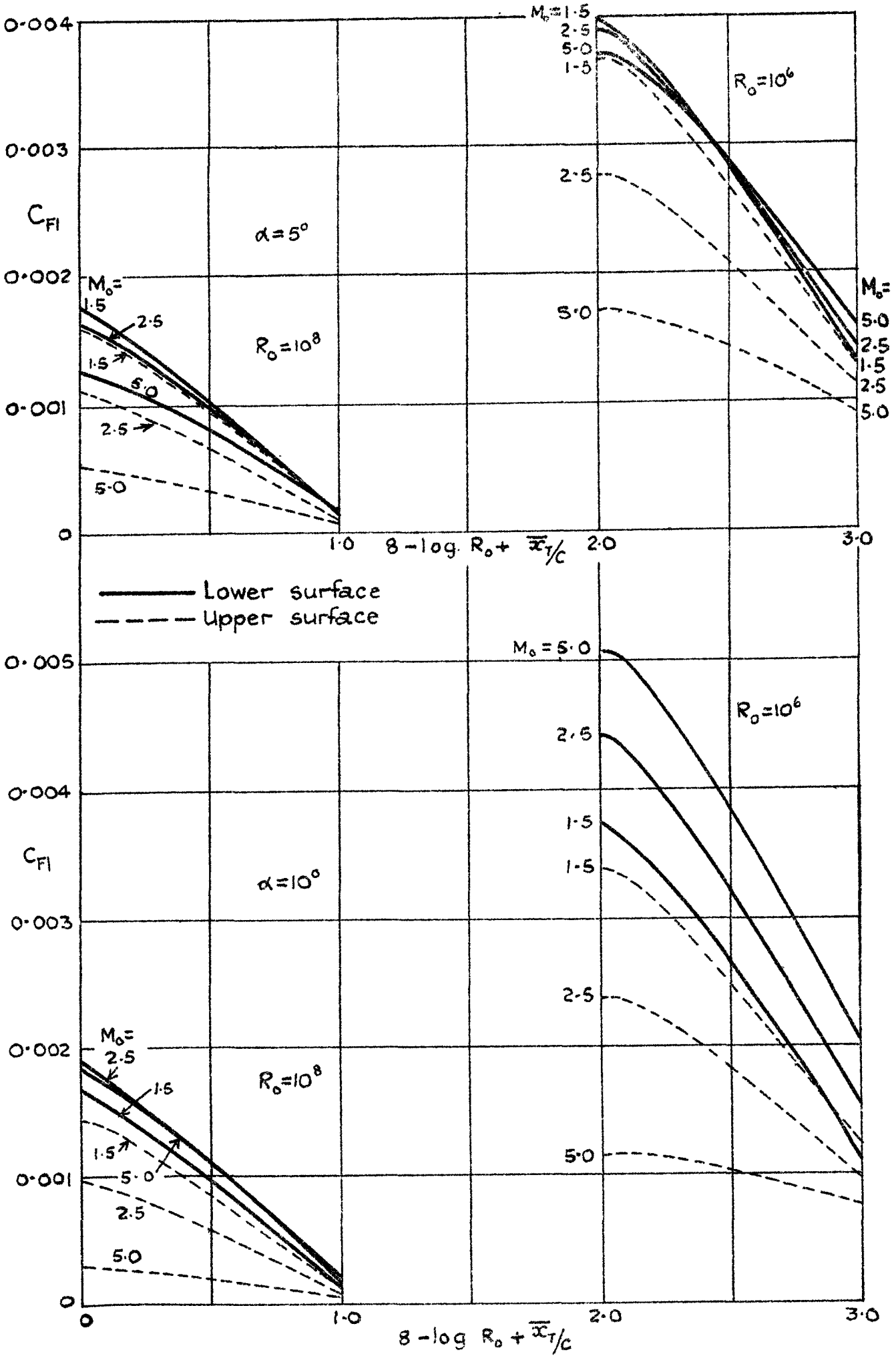

Skin friction coefficient (first stage), C_{Fl}, for upper and lower surfaces of flat plate at incidences of 5° and 10°.

FIG. 26.

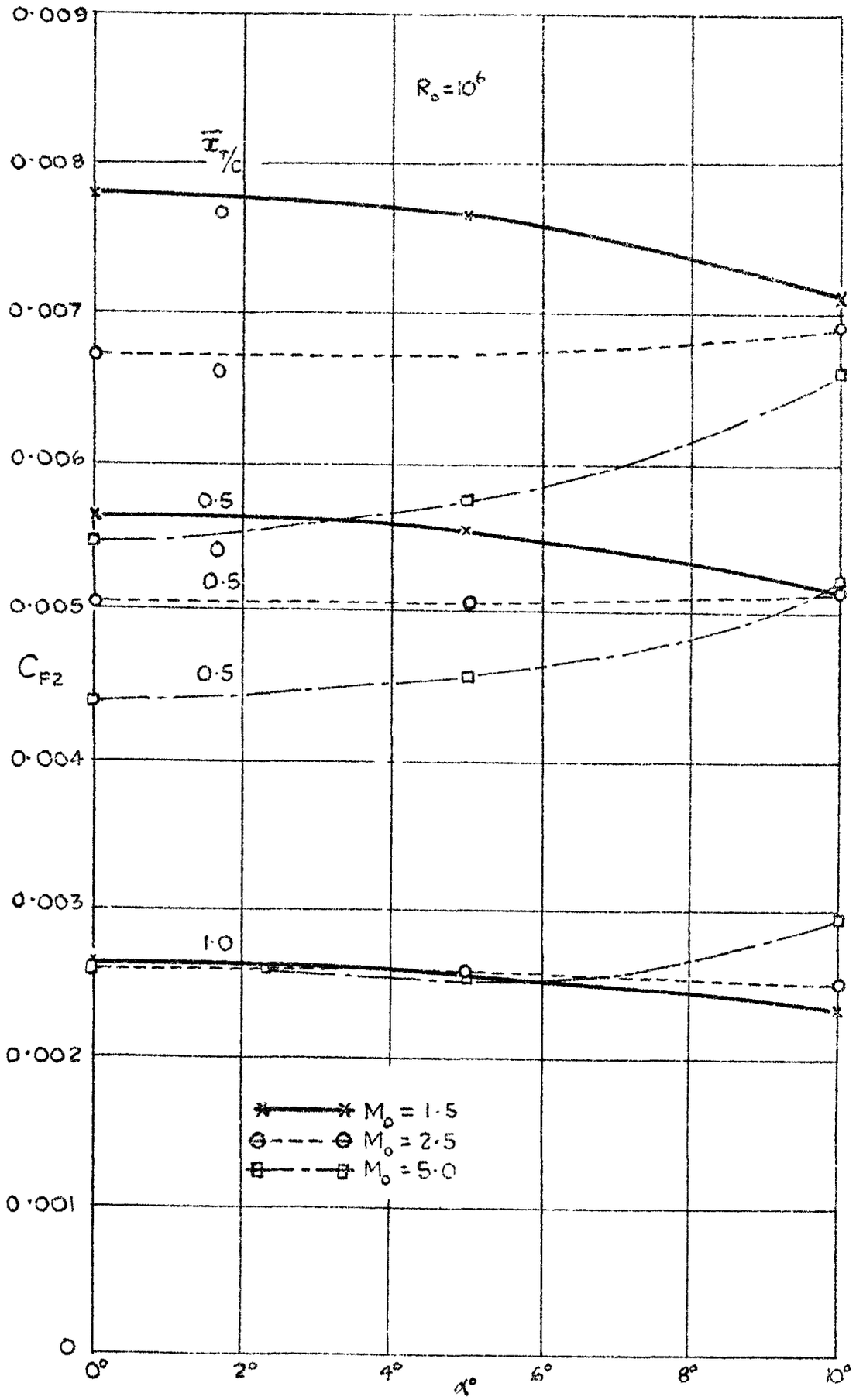

Variation of frictional drag of flat plate with incidence at $R_0 = 10^6$

FIG 27.

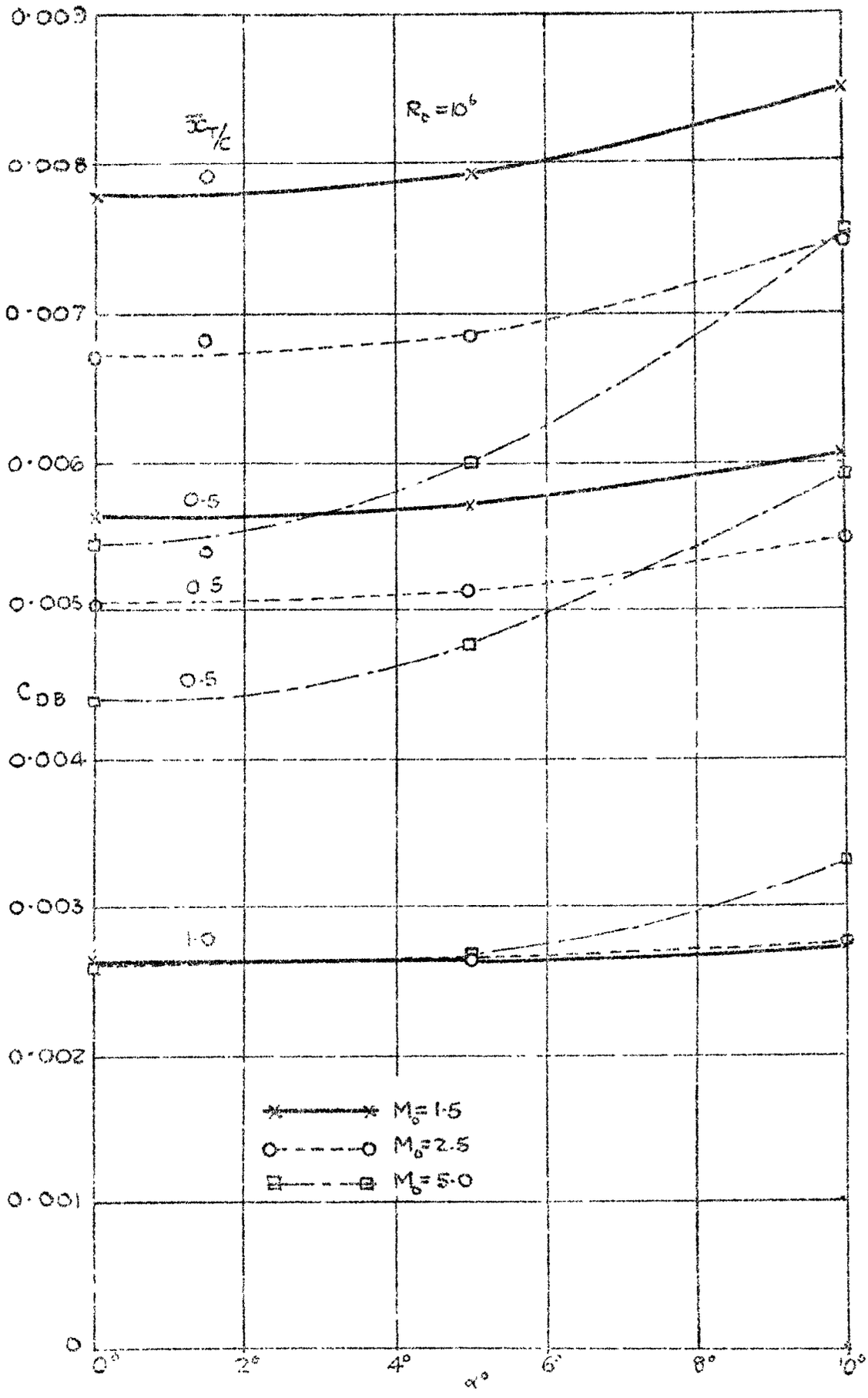

Variation of total boundary layer drag of flat plate with incidence at $R_c = 10^6$

FIG. 28.

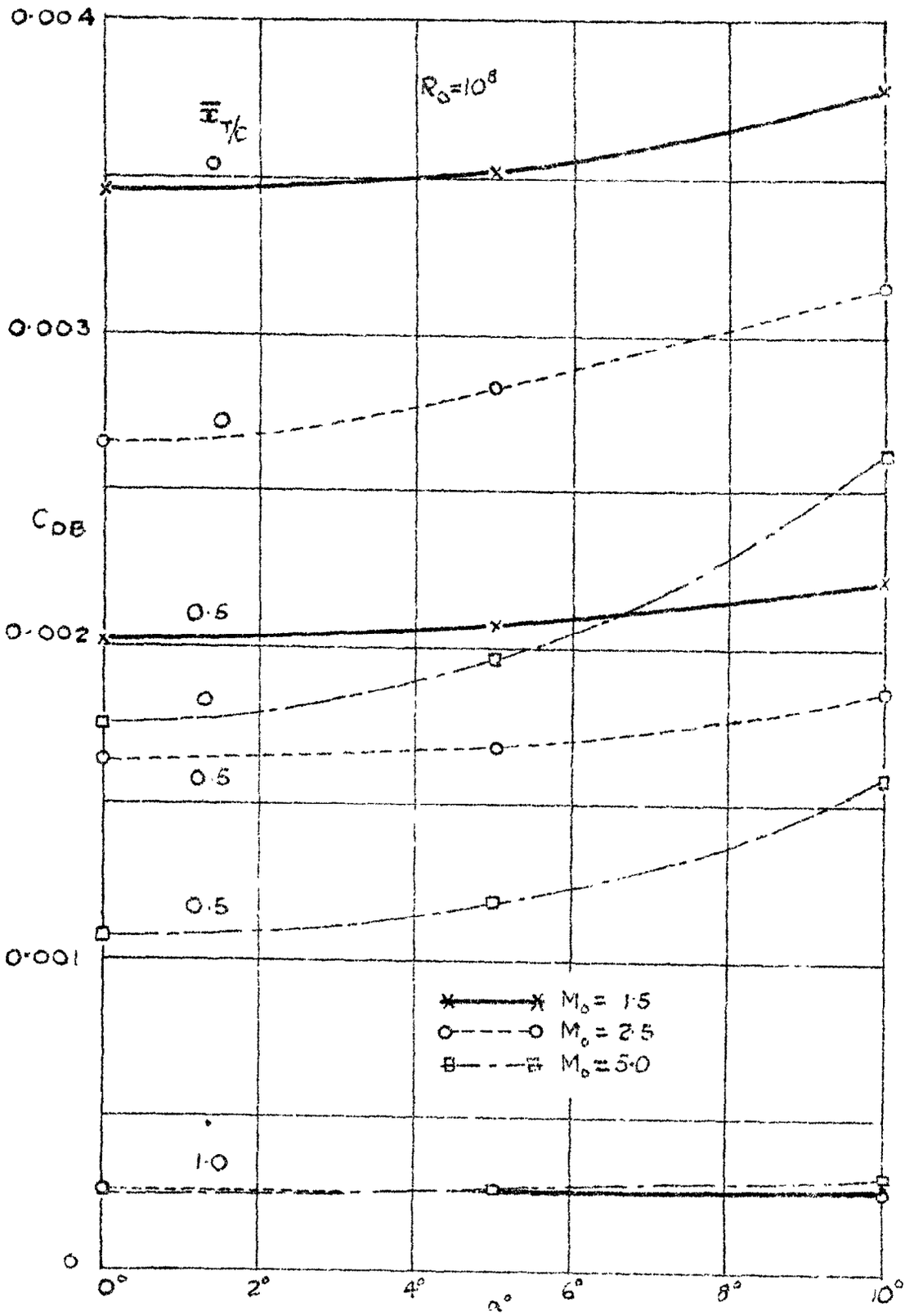

Variation of total boundary layer drag of flat plate with incidence at $R_0=10^8$.

FIG. 29.

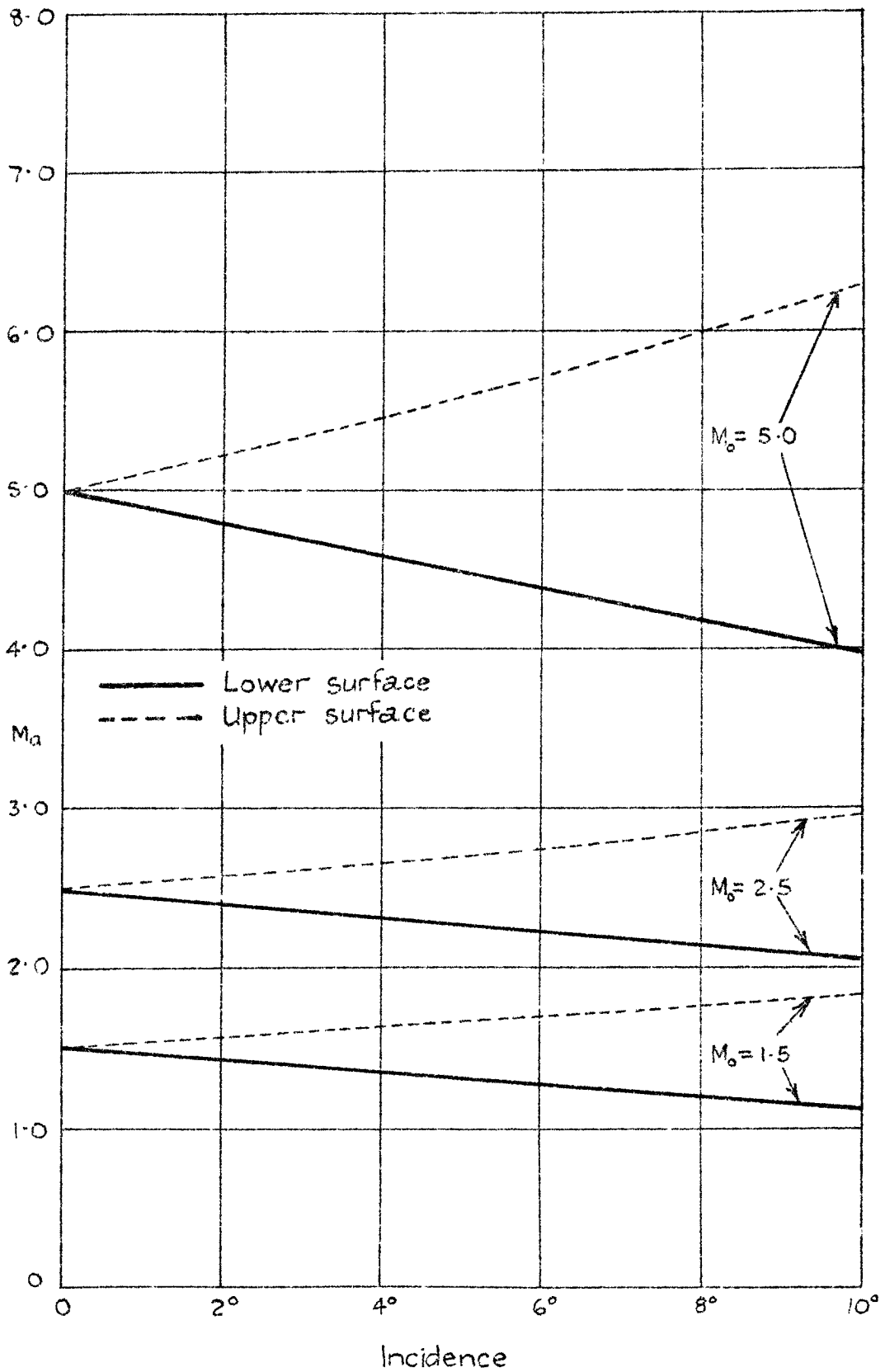

Variation of M_a with incidence and undisturbed stream Mach number (M_o) for flat plate.

FIG. 30.

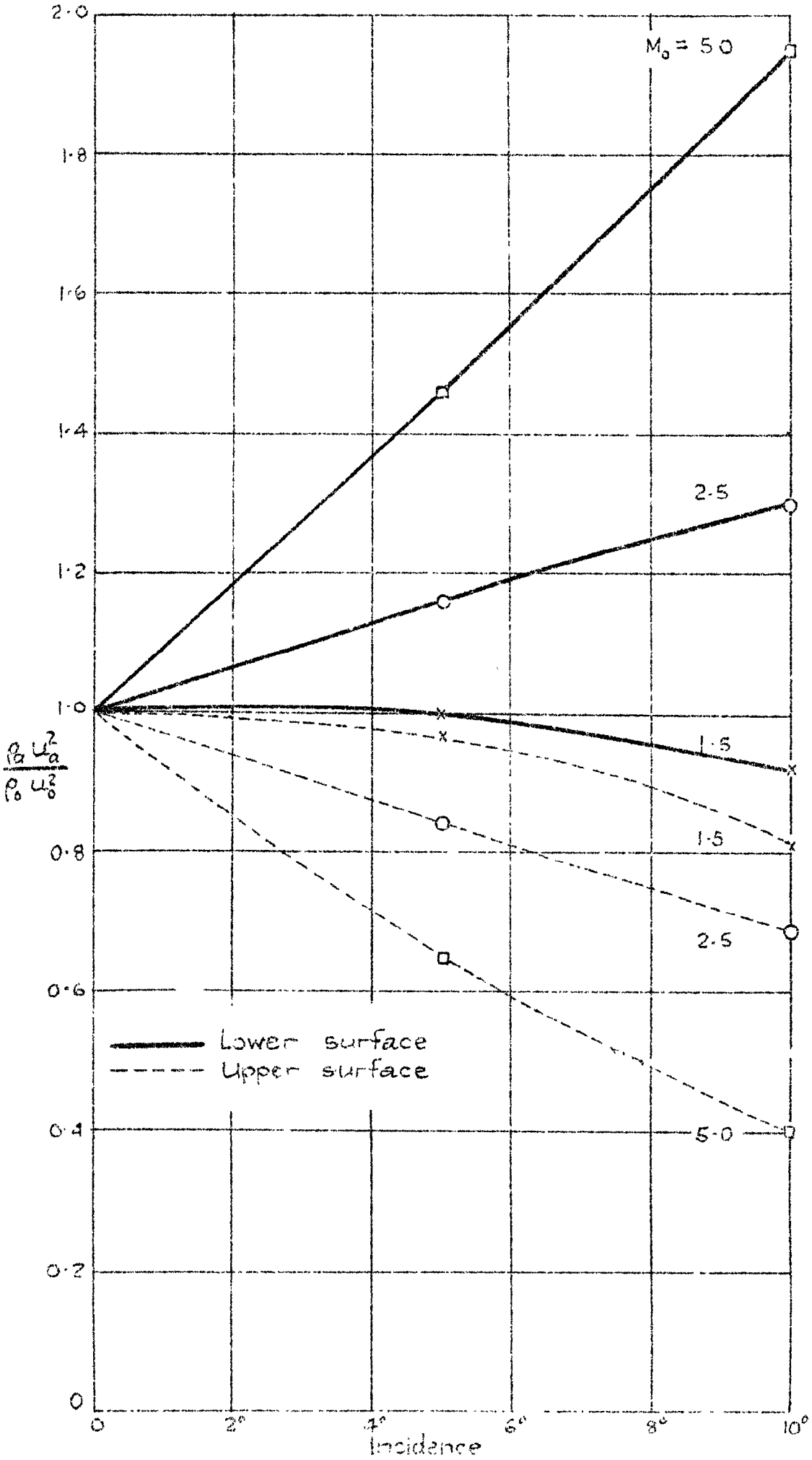

Variation of $\rho_a u_a^2 / \rho_0 u_0^2$ with incidence and undisturbed stream Mach number for flat plate.

FIG. 31.

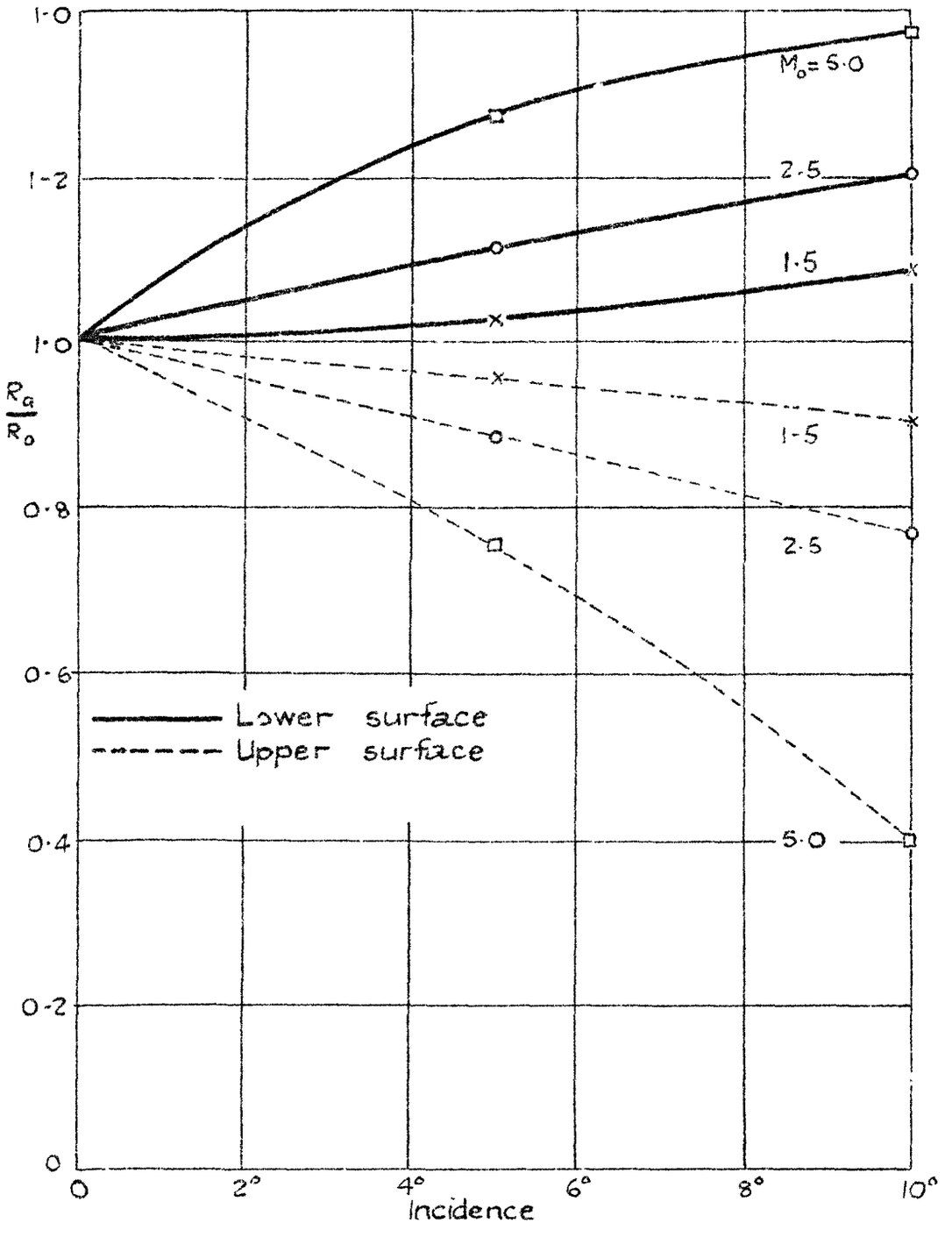

Variation of $\frac{R_a}{R_o}$ with incidence and undisturbed stream Mach number for flat plate.

FIG 32.

□ Completely laminar (full calculation)
Δ Completely laminar (equation A.24)
x Completely turbulent (full calculation)
o Completely turbulent (equation A.37)

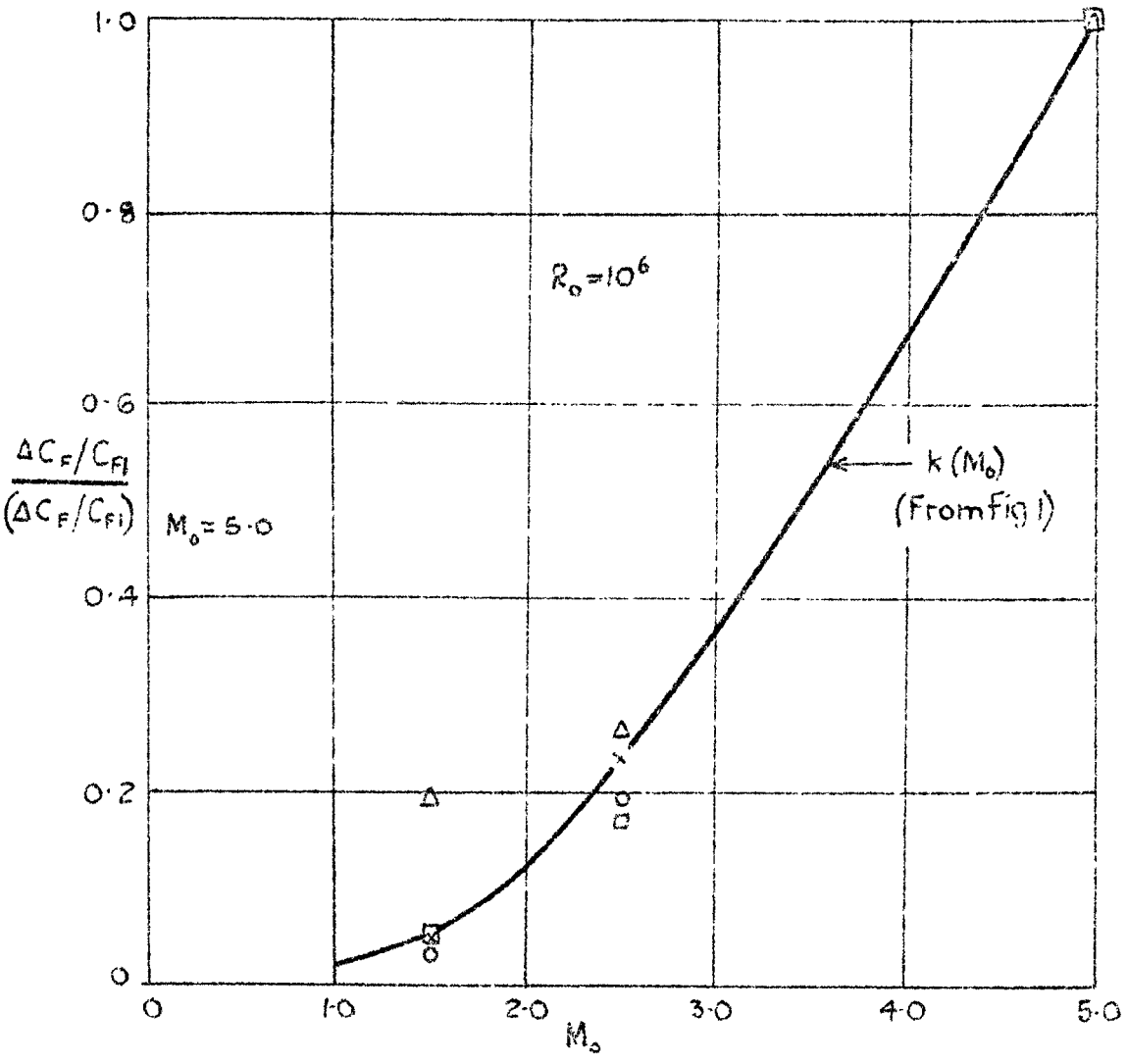

Values of the ratio $\frac{\Delta C_F}{C_{Fi}} \Big/ \left(\frac{\Delta C_F}{C_{Fi}}\right)_{M_0=5\cdot0}$ given by full calculations and by equations A.24. and A.37. for completely laminar and completely turbulent boundary layers on a flat plate at zero incidence.

APPENDIX II.*

Further comments in the light of recent experimental data on the flow in the region of the leading edge and the possible errors involved in the assumed pressure distribution there (Para. 2.3).

---

1. Effects of Leading Edge-Thickness

It may be argued that since leading edges must always have some degree of bluntness it is unrealistic to consider a case where the effects of leading-edge bluntness on the surface pressure distributions and hence on the skin friction distributions are assumed to be negligible.

Certainly the experiments by Bogdonoff and Hammitt[9,10] at Mach numbers between 11 and 15 have demonstrated that at these Mach numbers a leading-edge thickness t for which the Reynolds number $u_1 t/\nu_1$ is much greater than about 100 may have a significant effect on the pressure distribution as far downstream as 10,000 t. This effect has been isolated in the later experiments by Hammitt[11] and it is clearly dominated by the inviscid flow field induced by the separation bubbles that form at the sharp corners of the blunt leading edges tested. However, both analysis and experiment indicate that this effect is reduced in extent and possibly in intensity with reduction in Mach number. Thus, Bertram[12] and Kendall[13] find that at Mach numbers of 5.8, 6.8 and 9.6 leading-edge thicknesses of the order of 0.001 in. ($u_1 t/\nu \approx O(50)$) or less had no effect on the pressure distributions that they measured on plates of some inches chord. Their foremost pressure holes were about 100 leading-edge thicknesses downstream of the leading edge. This implies that it is readily possible in practice to achieve conditions where leading-edge effects can be ignored at least beyond such a distance from the leading edge for the Mach number range considered in the present paper. Closer to the leading edge the matter requires further consideration and we shall return to it later. However it can be contended that the case considered here, in which the leading-edge bluntness is assumed to be sufficiently small not to affect the main surface pressure distribution away from the neighbourhood of the leading edge, is a valuable basic reference case readily realised and worth considering in its own light.

This is not to deny that in many practical instances leading-edge thicknesses and shapes may be such that their effects are bound to be important, but for such cases leading-edge shape like section thickness and incidence is a parameter that requires separate consideration.

2. Pressure Changes Induced by the Boundary Layer Away from the Leading Edge

The experimental investigations of Kendall[13] and Bertram[12] at hypersonic Mach numbers have shown that where the leading-edge thickness is sufficiently small for its effect on the local pressure distribution to be negligible the pressure increment on a flat plate is closely given by the linear relation

$$\Delta p/p_o = 0.45\chi \qquad \ldots(1)$$

where χ is the parameter $M_o^3\sqrt{C}/(R_o x)^{\frac{1}{2}}$, C being the constant in the assumed linear viscosity-temperature relation, and the chord length on which R_o is based is taken as unity. The range of values of over which (1) holds is large, it is within about 4% of the experimental data for $0<\chi<4.0$.

The/

---

* Added August, 1959.

The validity of this relation at supersonic as distinct from hypersonic Mach numbers is open to investigation but we may note that equation A.5 of the Appendix of this paper can readily be transformed to the form

$$\Delta p/p_o = \frac{\gamma H_o}{M_o B_o f_o^{\frac{1}{2}}} \cdot \frac{\chi}{\sqrt{C}},$$

and if we take $M_o = 5.0$ and the insulated plate case this becomes

$$\Delta p/p_o = 0.44\chi.$$

We can therefore infer that the pressure distributions predicted for $x>0.04$ are in good agreement with experiment.

3. Pressure Increments and Associated Skin Friction near the Leading Edge

The extrapolation used in this paper of a constant pressure gradient for $x<0.04$ was admittedly adopted mainly for its convenience in helping to keep the heavy programme of computing down to a minimum. With regard to the possible errors that may result the following points and figures are worth noting.

There is at present no completely satisfactory theory predicting the flow conditions in the region of the leading edge. It is in this region at least that thickness effects must become of some importance even for leading edges of the thinnest practicable thickness, and if a leading edge of zero thickness is considered then slip flow effects must become evident in its neighbourhood and the boundary-layer approximations become suspect. Further the interaction of the boundary layer with the shock wave associated with the leading edge or directly induced by the displacement effect of the boundary layer must effect the flow development in the region of the leading edge. The direct effect of finite leading-edge thickness would presumably be to cause the boundary layer to start at a stagnation point on the forward face of the leading edge, and the infinite skin friction and rate of change of displacement thickness of classical boundary-layer theory would not occur there (see Hammitt[11]). Slip flow effects would presumably also tend to reduce the frictional drag below that predicted by classical boundary-layer theory. Any strengthening of the leading-edge shock due to the boundary layer would increase the drag, but the local reduction in dynamic head would reduce the skin friction, whilst the vorticity introduced by the shock in the flow behind it might also be a factor of some significance[14].

These considerations lead one to conclude that although it would have been possible to have developed a more sophisticated approach to this problem than that adopted in this paper the resulting complexity might not have been justified by any obvious improvement in accuracy, particularly bearing in mind the relatively low Mach numbers considered and the overall aims of the investigation. The fact that for first-stage calculations classical boundary-layer theory with its leading-edge singularity has been found to work so well, at least for Mach numbers other than hypersonic, is an indication of the relative insensitivity of the boundary layer to its past history. This supports the thesis that for the second stage calculation any plausible assumption not clearly inconsistent with available experimental data and which avoids the manifest absurdities associated with that singularity is likely to lead to results of acceptable

accuracy./

accuracy. In the light of these comments let us examine the probable order of magnitude of the errors associated with the pressure distribution assumed for these calculations. The case considered in this paper that would involve the greatest error from this point of view is that of the flat plate at Mach number 5 and Reynolds number 10^6. The experiments of Hammitt[11] on plates with blunt leading edges at a Mach number of 11.4 showed that the pressure coefficient due to the bluntness rose slightly with distance downstream from the leading edge to a value of about 0.1 in a distance of some two leading-edge thicknesses and it then fell to zero in about 1000 leading-edge thicknesses. From equation (1) above a value of C_p of 0.1 would be induced by the boundary layer at about 0.0008c aft of the leading edge for $M_o = 5$ and a Reynolds number of 10^6. If, on the basis of Bertram's[12] and Kendall's[13] results, it is argued that the effect of a small but finite leading edge would be evident for a distance up to 100 leading-edge thicknesses then this thickness would have to be less than about 10^{-5}c for its effect to be negligible at 0.0008c. This would imply a value of t, for example, less than 0.001 in. on a wing of 10 ft. chord. This suggests that if we take account of the possible limitations of making fine leading edges in practice it can be inferred that the pressure distribution at $M_o = 5$ and $R_o = 10^6$ will be such as to have a nearly constant value of C_p of 0.1 back to about 0.0008c and from then on it would fall according to equation (1). It may be noted that in none of the experiments made to date, extending up to Mach numbers of 15, have pressure coefficients greater than about 0.1 been measured. As already remarked, if we do not take such considerations into account then in any case slip flow effects may be expected to be significant within the first 0.001c with associated departures from the predictions of normal boundary-layer theory.

If, therefore, instead of the pressure distribution adopted in the paper we adopt that suggested above then we find that it results in the following increments in skin friction coefficient (ΔC_F) and pressure drag coefficient (ΔC_{D_p}) above the values quoted in the paper:-

	M_o	R_o	ΔC_F	ΔC_{D_p}
Flat plate, all transition positions	5.0	10^6	0.00008	-
Biconvex wing, t/c = 0.05, all transition positions	5.0	10^6	0.00005	0.0001
Biconvex wing, t/c = 0.1, all transition positions	5.0	10^6	0.00004	0.00015

For all the other Mach numbers and Reynolds numbers considered the differences in predicted skin friction coefficients are negligible. The pressure drag coefficient increments vary as $1/\sqrt{R_o}$ and as M_o approximately.

The pressure distribution considered above is suggested as leading to a plausible assessment of the upper limit to the errors incurred by the distribution assumed in the paper. A somewhat less plausible upper limit can be obtained by assuming that Lees' strong interaction theory[15] applies over the first 0.001c after which equation (1) applies. This theory leads

to/

to an infinite pressure at the leading edge. On the basis of this assumption the estimated increments above those quoted in this paper are:-

	M_o	R_o	ΔC_F	ΔC_{D_p}
Flat plate, all transition positions	5.0	10^6	0.00016	-
Biconvex wing, t/c = 0.05, all transition positions	5.0	10^6	0.0001	0.0001
Biconvex wing, t/c = 0.1, all transition positions	5.0	10^6	0.00008	0.0002

Again, for all the other Mach numbers and Reynolds numbers considered the corresponding skin friction increments above those quoted in the paper are negligible, whilst the increments in pressure drag coefficients vary as $M_o/\sqrt{R_o}$, approximately. These results support the view that the assumptions of the paper regarding the pressure distribution in the region of the leading edge are unlikely to lead to errors of serious practical significance. Further support is afforded by the following comparison with experimental results.

4. Comparison with Experimental Results

The only readily available experimental data for comparison are the results of the experiments of Bertram[12] and Kendall[13]. Since these experiments were made at higher Mach numbers than those covered in this paper, the results of the latter have been extrapolated by means of equation A.24 of Appendix I. The experimental data are presented on very small scale diagrams and relevant figures are difficult to extract from the diagrams with adequate accuracy. In each case the figures presented have been corrected for leading-edge wave drag estimated by the authors concerned. The comparison may be summarised as follows:-

				Estimated from the results of this paper						
Reference	t/c	M_o	R_o	C_{F_1}	ΔC_F	C_{F_2}	C_{D_W}	ΔC_{D_p}	C_D	C_D (Measured)
Kendall	0	5.8	3.5×10^5	0.0021	0.0003	0.0024	-	-	0.0024	0.0024
Kendall	0	5.8	1.8×10^4	0.0089	0.0057	0.0146	-	-	0.0146	0.0140
Bertram	0.01	6.8	10^6	0.0024	0.0003	0.0027	0.0003	-	0.0030	0.0029[5]

In addition Bertram[12] made some measurements on a double wedge section of 5% thickness-chord ratio. A comparison for this case is less reliable, however, since the measured pressure drag coefficient was about 0.0012 whilst the calculated inviscid wave drag coefficient was 0.0015. This indicates that there was some separation induced over the rear of the wing by the trailing-edge shock waves. Assuming this extended over the rear 20% of the wing an

estimate/

estimate of the drag can be made as follows:-

For $R_o = 10^6$, $M_o = 6.8$, then based on earlier calculations for a double wedge section, $t/c = 0.05$,	C_{F_1}	$= 0.0029$.
Deduction for separation over rear 20%		$= -0.0001\frac{5}{}$.
Displacement thickness increment, ΔC_F		$= 0.0004$.
Measured pressure drag coefficient		$= 0.0012$.
Final estimated value of C_D		$= 0.0043\frac{5}{}$.
Measured value		$= 0.0045$.

It will be seen that the results of the calculations of this paper are in good accord with experiment, although the number of cases compared are too few and the parameters involved too limited in range for the evidence to be regarded as conclusive. However, it can be inferred that the results of this paper do not appear to display any consistent error arising from the assumptions made regarding the pressure distribution in the region of the leading edge. It would seem that for the purpose of predicting drag for performance needs the errors involved in this paper are likely to be within the order of current experimental inaccuracies.

References

No.	Authors	Title, etc.
9	S. M. Bogdonoff and A. G. Hammitt	Fluid dynamic effects at speeds from M = 11 to 15. J. Aero. Sc. 23, 108 (1956).
10	A. G. Hammitt and S. M. Bogdonoff	Hypersonic studies of the leading edge effect on the flow over a flat plate. J. Amer. Rocket Soc. 26, 241 (1956).
11	A. G. Hammitt	The hypersonic viscous effect on a flat plate. J. Fluid Mech. 5, Part 2. 242 (Feb. 1959).
12	M. Bertram	Boundary Layer displacement effects in air at Mach numbers of 6.8 and 9.6. NACA TN. No.4133 (1958).
13	J. M. Kendall	An experimental investigation of leading edge shock wave boundary layer interaction at Mach 5.8. J. Aero. Sc. 24, No.1, 47 (Jan. 1957).
14	L. Lees	Influence of the leading edge shock wave on the laminar boundary layer at hypersonic speeds. J. Aero. Sc. 23, No.6, 594 (June, 1956).
15	L. Lees	Hypersonic Flow. Fifth International Aeronautical Conference (Los Angeles, Calif. June 1955). Inst. Aero. Sci. Inc., 241 (1955).

C.P. No. 451
(20,572)
A.R.C. Technical Report

Printed and published by
HER MAJESTY'S STATIONERY OFFICE

To be purchased from
York House, Kingsway, London W.C.2
423 Oxford Street, London W.1
13A Castle Street, Edinburgh 2
109 St Mary Street, Cardiff
39 King Street, Manchester 2
Tower Lane, Bristol 1
2 Edmund Street, Birmingham 3
80 Chichester Street, Belfast
or through any bookseller

Printed in England

S.O. Code No. 23-9011-51

C.P. No. 451